# On the pathways of the return flow of the meridional overturning circulation in the tropical Atlantic

by

*Markus Jochum*

M.Sc., University of Kiel, 1997

Submitted in partial fulfillment of the requirements for the degree of
Doctor of Philosophy
at the
MASSACHUSETTS INSTITUTE OF TECHNOLOGY
and the
WOODS HOLE OCEANOGRAPHIC INSTITUTION
June 2002

©2002 Markus Jochum
All rights reserved
The author hereby grants MIT and WHOI permission to reproduce paper and electronic copies of this thesis in whole or in part and to distribute them publicly.

Signature of Author .....

Joint Program in Physical Oceanography
Massachusetts Institute of Technology
and Woods Hole Oceanographic Institution
June 2002

Certified by .....

Paola Malanotte-Rizzoli
Thesis Supervisor

Accepted by .....

Carl Wunsch
Chair, Joint Committee for Physical Oceanography
Massachusetts Institute of Technology
and Woods Hole Oceanographic Institution

# On the pathways of the return flow of the meridional overturning circulation in the tropical Atlantic.

by

Markus Jochum

Submitted in partial fulfillment of the requirements for the degree of
Doctor of Philosophy at the Massachusetts Institute of Technology and the
Woods Hole Oceanographic Institution
April 15, 2002

**Abstract**

A numerical model of the tropical Atlantic ocean is used to investigate the upper layer pathways of the Meridional Overturning Circulation (MOC) in the tropical Atlantic. The main focus of this thesis is on those parts of the tropical circulation that are thought to be important for the MOC return flow, but whose dynamics have not been understood yet.

It is shown how the particular structure of the tropical gyre and the MOC act to inhibit the flow of North Atlantic water into the equatorial thermocline. As a result, the upper layers of the tropical Atlantic are mainly fed by water from the South Atlantic. The processes that carry the South Atlantic water across the tropical Atlantic into the North Atlantic as part of the MOC are described here, and three processes that were hitherto not understood are explained as follows:

The North Brazil Current rings are created as the result of the reflection of Rossby waves at the South American coast. These Rossby waves are generated by the barotropically unstable North Equatorial Countercurrent. The deep structure of the rings can be explained by merger of the wave's anticyclones with the deeper intermediate eddies that are generated as the intermediate western boundary current crosses the equator.

The bands of strong zonal velocity in intermediate depths along the equator have hitherto been explained as intermediate currents. Here, an alternative interpretation of the observations is offered: The Eulerian mean flow along the equator is negligible and the observations are the signature of strong seasonal Rossby waves. The previous interpretation of the observations can then be explained as aliasing of the tropical wave field.

The Tsuchyia Jets are driven by the Eliassen-Palm flux of the tropical instability waves. The equatorial current system with its strong shears is unstable and generates tropical instability waves. These waves cause a poleward temperature flux which steepens the isotherms which in turn generates are geostrophically balanced zonal flow. In the eastern part of the basin this zonal flow feeds the southeastward flow of the equatorial gyre.

Thesis supervisor: Paola Malanotte-Rizzoli Title: Professor, Department of Earth, Atmospheric and Planetary Sciences, Massachusetts Institute of Technology

Acknowledgments

Looking back the last five years, I am stunned when I realize how many people it takes to create a thesis. Further reflection helps to blur the distinction between me as a creator of a thesis, and me as a saucepan that converts lots of love, ideas and money into a new idea. Each of these three ingredients are necessary, none of them is sufficient. Some people give a little bit of everything, some a lot of one ingredient, and of course there are also nonlinear interactions to be taken into account. This makes it almost impossible to acknowledge everybody in due manner (except for NASA and ONR who generously funded me with their respective grants NAG5-7194 and N00014-98-10881).

Clearly, this thesis could not have been written without the love and support of my parents Ilona and Alois and my wife Elizabeth. Being Catholic, my family is of course more numerous than that and I am grateful to all of them for their support during the different stages of my life.

My committee members Tony Busalacchi, Glenn Flierl, Breck Owens and Mike Spall are thanked for their seemingly endless doubts and their knowledgeable advice. This gratitude extends towards the student body of MIT and WHOI, and to Dave Fratantoni who let me see and touch a *real* North Brazil Current ring.

My advisor Paola Malanotte-Rizzoli is more difficult to place; depending on the time of the day and geographical location she makes a valuable contribution to each of the three aforementioned categories. This magic potion is probably the most important ingredient of any, and especially my thesis.

And then there is Raghu Murtugudde who told me always to mention him in the acknowledgments. I suspect not without reason.

*From a certain Chinese encyclopedia:*

*Animals are divided into:*
*a) belonging to the Emperor*
*b) embalmed*
*c) tame*
*d) sucking pigs*
*e) sirens*
*f) fabulous*
*g) stray dogs*
*h) included in the present classification*
*i) frenzied*
*j) innumerable*
*k) drawn with a very fine camelhair brush*
*l)* et cetera
*m) having just broken the water pitcher*
*n) that from a long way off look like flies.*

(Jorge Luis Borges)

# Contents

**1 Introduction** **8**

**2 The influence of the MOC** **15**

2.1 Introduction . . . . . 15

2.2 The model and the experiments . . . . . 16

2.3 The flow field . . . . . 19

2.4 The tropical-subtropical pathways . . . . . 23

**3 Description of the tropical circulation** **29**

3.1 The model configuration . . . . . 29

3.2 Overview of the upper layer circulation in the tropical Atlantic . . . . 37

3.3 Description of the upper layer mean flow in the model . . . . . 46

3.3.1 The thermocline waters . . . . . 54

3.3.2 The surface waters . . . . . 59

**4 North Brazil Current rings** **61**

4.1 Introduction . . . . . 61

4.2 The Ring Shedding . . . . . 62

4.2.1 Rings without wind . . . . . 62

4.2.2 No rings with wind . . . . . 65
4.2.3 The role of Rossby waves . . . . . 66
4.2.4 The unstable NECC . . . . . 72
4.3 The vertical structure, seasonality, and transport of NBC rings . . . . 78

**5 The flow of AAIW along the equator** **88**
5.1 Introduction . . . . . 88
5.2 Observations . . . . . 89
5.3 The AAIW in the model . . . . . 90
5.4 Synthesis of theory and observations . . . . . 97

**6 On the dynamics of the Tsuchyia Jets** **110**
6.1 Introduction . . . . . 110
6.2 The structure of the Tsuchyia Jets in the model . . . . . 113
6.3 Wave-zonal flow interaction . . . . . 117

**7 Summary** **126**

# Chapter 1

# Introduction

During the last five decades, oceanographers have made a considerable effort to estimate and understand the global mean circulation of the world's oceans. Together, the conclusion of the World Ocean Circulation Experiment (WOCE), the systematic use of satellites and the widespread availability of fast computers since the last decade enabled scientists to provide a coherent, albeit vague picture of the global circulation (Ganachaud and Wunsch (2001)). In addition to these developments, there were also advancements in analytical methodology that led to theories about the western boundary currents or the vertical stratification of the ocean (see Pedlosky (1996) for an overview). These developments made clear that in large parts of the ocean the variability of the flow is much stronger than the mean circulation. Therefore the understanding of the ocean's variability is indispensable for the interpretation of observations and the assessment of theories. Furthermore, the ocean forms the lower boundary of the atmosphere and will directly affect its thermal structure and its water content. This implies that the ocean is not passively driven by the atmosphere, but instead the ocean and the atmosphere should be treated as a coupled system. A classical example of a coupled, highly variable ocean-atmosphere system is the equatorial Pacific. Its strong interannual variability ('El Nino - Southern Oscillation (ENSO)') causes a world wide shift in weather patterns and can only be understood by taking into account atmospheric as well as oceanic dynamics. By now, the equatorial Pacific is a well observed system, and it was even possible in recent years to predict the phases of different ENSO cycles (Cane et al. (1986), Chen et al. (1999)).

Although one would expect that the dynamics that control the equatorial Pacific are the same in all equatorial oceans, scientists have been less successful in understanding the climate fluctuations in the tropical Atlantic (see Seager at al. (2001) for a recent analysis). Not only are there very few observations away from the western boundary along the American coast, but matters are complicated further by the more complex dynamics of the Atlantic ocean.

Apart from the seasonal cycle, there are two modes that dominate the tropical Atlantic SST variability. The equatorial mode, which is similar to ENSO, influences the equatorial SST at interannual frequencies (Carton and Huang (1994)). The interhemispheric (or dipole) mode, affects the gradient of the SST between the northern and southern tropics (Servain (1991)) and therefore influences the position of the ITCZ. It has been shown, that these modes are correlated with ENSO (Delecluse et al. (1994) and the North Atlantic Oscillation (NAO, Xie and Tanimoto (1998)). The importance of oceanic processes for these modes is not well know, although it is especially in the tropics where one would expect the SST to influence the atmosphere.

One phenomenon that is capable of affecting the tropical SST is called the subtropical cell (STC). The STCs include all the processes that connect the subtropical ocean to the tropics and thereby determine the water mass structure of the tropical ocean. Within a STC, subduction processes bring surface waters below the mixed layer, where they will be advected towards the eastern Atlantic and the equator. Upwelling then brings these waters to the surface from where Ekman and western boundary flows return it to the subtropics. The source waters of the STCs determine the equatorial stratification and eventually the SST. Therefore, variability in the position of the subduction regions or the strength in the STCs must lead to a change in the tropical SST.

In the Atlantic, an identification of the STC waters and their modes of variability is complicated because of the few available observations. However, observations and models suggest that there is a strong asymmetry between the northern and southern STC. Observations of water mass properties and velocities along the western boundary provide ample evidence for a mean southern STC that feeds the tropical thermocline via the northward North Brazil Current (Schott et al. (1998)). In the northern hemisphere, a set of synoptic cruises (Bourles et al. (1999)) shows that

a small fraction of the subducted water that reaches the western boundary in the North Equatorial Current turns south to feed the North Equatorial Countercurrent. Whether this water continues south towards the equator or recirculates north in the tropical gyre is not clear.

The strong asymmetry between the northern and the southern STC suggest that the Meridional Overturning Circulation (MOC) is important in determining the source waters of the equatorial Atlantic. The MOC can be envisioned as the formation of dense water in the Nordic sea, deep southward displacements along the Atlantic western boundary, circulation within the Antarctic Circumpolar Current, upwelling in the Indian and Pacific oceans and a path back to the North Atlantic (NA) within the upper 1000m (Gordon (1986)). In the Atlantic, the return flow of the MOC is forced to interact with the equatorial wind-driven circulation before it can enter the high latitude sinking regions. It is important to know the path that this relatively cool water takes after it crosses the South Atlantic (SA): if this water upwells along the equator, it will cool the overlying atmosphere and will arrive fresher and warmer in the NA than if it would flow north along the western boundary, shielded from the atmospheric fluxes. Thus, the path that the MOC return flow takes will affect the atmospheric temperature and water content as well as the water mass properties of the NA. It follows that an insight in the dynamics of the crosshemispheric paths of the MOC return flow and the associated heat and freshwater fluxes is a prerequisite for the understanding of the climate fluctuations in the Atlantic. This thesis is an investigation of the dynamics that control the path of the MOC return flow from the SA across the equator into the NA. As such, it constitutes only a small but indispensable step towards the understanding of the fully coupled Atlantic ocean-atmosphere system.

On its way into the northern subtropical gyre, the MOC return flow crosses different dynamical regimes which have traditionally been treated separately. Only recently have the connections between the tropics and the subtropics received significant attention. Pedlosky (1987) was the first who studied the dynamical aspects of the tropical-subtropical connections as an extension of the ventilated thermocline theory (Luyten et al. (1983)). His results suggest that the strength of this connection is directly related to the zonal wind stress at the equatorward boundary of the subtropical gyres (the zero wind curl line). At this line, the meridional Sverdrup

transport is zero by definition. This means that the poleward Ekman flow across this line has to be compensated for by an equatorward flow in the thermocline. This equatorward flow continues towards the equator where it forms the Equatorial UnderCurrent (EUC) by converting planetary vorticity into relative vorticity. Pedlosky's theory was subsequently extended to include diapycnal upwelling and Ekman layer dynamics, both in analytical studies (McCreary and Lu (1994) and Liu (1994)) as well as in highly idealized numerical ones (McCreary and Lu (1994), Liu et al. (1994) and Liu and Philander (1995)). These studies show that some of the subducted subtropical water, after joining the EUC, is forced by the equatorial Ekman divergence to upwell into the equatorial mixed layer and subsequently returns to the subtropics via the Ekman layer. The observational evidence for the tropical-subtropical pathways comes mainly from tracer distributions in the Pacific (Fine et al. (1981) and Fine (1987)). The observations in the Atlantic are more ambiguous because of the smaller data coverage there and the Atlantic's more complex circulation.

The idealized earlier works provide invaluable insight into the dynamics of the tropical-subtropical pathways, but they are too idealized to fully understand the intricacies of the Atlantic equatorial circulation which includes a series of strong zonal jets, an asymmetric wind field and a buoyancy-driven MOC. A next generation of numerical models (Blanke et al. (1999), Fratantoni et al. (2000), Harper (2000) and Malanotte-Rizzoli et al. (2000)) attempted to simulate the Atlantic circulation in all its complexity, but unfortunately they all have slightly different setups and boundary conditions often leading to contrasting results. Neither can the observations alone provide a more accurate picture, since the high phase speed of the equatorial waves and the high variability of the tropical wind field make it difficult to use single hydrographic surveys to estimate the flow (compare the four surveys in Schott et al. (1998)). It seems that the nature of the crosshemispheric flow makes it necessary to bridge the gap between highly idealized studies and very detailed, quantitative studies with an intermediate type of investigation. Its purpose is to understand how the simple concepts of the aforementioned analytical and idealized studies are modified in the presence of strong zonal jets or the MOC. Therefore, the aim of this thesis is to execute and analyze numerical experiments that are more complex than previous ones, while still simple enough to reveal the dynamics of the processes that shape

the crosshemispheric pathways.

This research was begun by first repeating the experiments described in Liu et al. (1994), and then continued by increasing the complexity of the model in two separate steps. The first step featured a more realistic, asymmetric wind field and a basin wide MOC. In the second step, a more realistic basin geometry and an increased horizontal resolution was added. The working hypothesis for the experiments is that the strength of the buoyancy driven MOC is independent of the tropical wind-driven circulation, even though in the real ocean this separation is clearly impossible. This assumption, however, allows us to identify important and basic dynamical mechanisms. A similar approach has been taken towards the atmosphere: There is no feedback between the ocean and the atmosphere, the sea surface temperature will be restored to a fixed value and the salinity is constant in time and space. Thus, the model is driven by fixed boundary conditions that are not affected by the model's dynamics. It was not the intention to create an overly realistic numerical representation of the Atlantic ocean; rather an emphasis was placed on those basic features of the circulation whose existence and dynamics do not depend on the details of the boundary conditions or the parameterizations. It was therefore possible to simulate a circulation of the tropical Atlantic that is consistent with the observations, but which is created with a numerical model that is much less complex than the fully realistic ocean general circulation models.

The first set of experiments focused on the interaction between the MOC and the tropical wind-driven circulation, and they show that the MOC effectively blocks the flow from NA thermocline water to the equator. The results of this study are discussed in the third chapter and are published as well (Jochum and Malanotte-Rizzoli, 2001). During this study a detailed understanding of two of the cross hemispheric pathways by which SA water reaches the NA was gained: one path at intermediate depths along the western boundary and the previously described thermocline-upwelling-Ekman path. Unfortunately, the North Brazil Current (NBC) rings, which were thought to constitute an important third pathway, could not be reproduced in this idealized study. These rings are formed at the retroflection of the NBC and the North Equatorial Countercurrent (NECC), and contain SA water in their core which they transport into the Caribbean Sea. Fratantoni et al. (1995) attribute 30% of the MOC transport across the tropical gyre to the NBC rings, making them worthy of

a more detailed study, especially since such an important pathway might invalidate some of the results of the investigation of Chapter Three. To that end, the fourth chapter of this dissertation gives a detailed account of a series of new experiments that were designed to understand the dynamics involved in creating the NBC rings. After describing the mean circulation in the model in Chapter Five, the sixth chapter provides a new way of looking at the NBC ring generation. Furthermore, the experiments show that NBC rings are probably not an important pathway for the shallow water limb of the MOC.

The setup of the experiments that have been executed to study the NBC rings features a certain degree of realism, and it becomes meaningful to compare the model results with the available observations for that region. It was somewhat surprising to see how close the model matches the observations despite its simplifications. However, no evidence was found for the equatorial intermediate currents as described in Schott et al. (1998) in the model. In trying to explain this discrepancy, it was concluded that the Schott et al. (1998) results are aliased by the strong seasonal cycle of the equatorial circulation, and most likely seasonal Rossby waves were interpreted as currents. The seventh chapter describes how this conclusion was reached.

The observations in the intermediate layer are not the only observations the model reproduced unintentionally. It also reproduced the Tsuchyia jets, a set of narrow subthermocline currents. Their dynamics has long been a matter of debate, and the model solutions help to understand the relevance of the different ideas. The analysis in Chapter Eight rejects the previously published theories and shows how the jets are driven by eddy fluxes.

In light of the above review, we summarize the contributions of this thesis research as follows:

- Clarification of the interaction between the MOC and the wind-driven circulation.
- A quantitative study of the relative contributions of the different cross hemispheric pathways to the warm water limb of the MOC.
- A dynamical explanation for the generation and structure of the NBC rings.

- A new interpretation for the observed flow fields in the intermediate layer of the equatorial Atlantic.
- A theory for the Tsuchyia jets.

The following chapters can each be read independent of one another, with the understanding that the results discussed in Chapters Five to Eight are based on the experiments described in Chapter Four.

# Chapter 2

# The influence of the MOC on the tropical-subtropical pathways

## 2.1 Introduction

For a long time, the subtropical gyres, the tropics and the meridional overturning circulation have been treated independently (see Pedlosky (1996), Philander (1990) and Warren (1981) for reviews). Then Pedlosky (1987) developed a theory for the EUC that shows that the tropics and the subtropics must exchange a significant amount of water (see also Liu (1994) and McCreary and Lu (1994) for a more detailed discussion of the pathways). Evidence for this connection can be found in hydrographic measurements (see Tsuchiya et al. (1989) for the Pacific and Arhan et al. (1998) for the Atlantic). Other measurements indicate that the water of the MOC returns through the upper layers of the tropical Atlantic (Schmitz and McCartney (1993)).

This raises the question, to what extent do those three dynamically very different systems influence each other? The physical mechanisms of the tropical/subtropical exchange are based on conservation of potential vorticity and were first described by Pedlosky (1987) in his adiabatic theory of the EUC. Because of the highly diabatic nature of the tropical upwelling system, it was not possible to close the circulation in the framework of this theory. But idealized numerical studies by Liu et al. (1994) and McCreary and Lu (1994) confirmed Pedlosky's results. Those models were symmetric about the equator and focused on the relation between the strength

of the wind field and the tropical/subtropical exchange (Liu and Philander (1995)). Further up the hierarchy of complexity there are only high resolution OGCM with realistic topography and wind fields. Their complexity makes it difficult to analyze the impact that basin geometry, topography, wind field and the MOC have on the tropical/subtropical circulation. To our knowledge only Fratantoni et al. (2000) ever tried to single out the effect of the MOC on the wind-driven circulation. But they too used a very complex model and focused on equatorial variability.

We tried to fill this gap between highly idealized models and very complex models. We took the experiment of Liu et al. (1994) as a starting point and increased the model complexity step by step. It turned out that the influences of bottom topography and basin geometry are either negligible or easy to be understood compared to the influence that a superimposed MOC has. Thus, we will focus here on the comparison between the the purely wind-driven circulation and the circulation resulting from wind and thermal forcing. The paper is arranged as follows. Section 2 introduces the model and the experiments to be performed; Section 3 briefly discusses the flow fields. In section 4, float trajectories are used to study the pathways between the subtropics and the tropics as well as the cross equatorial pathways. Section 5 analyzes shortcomings and summarizes the results.

## 2.2 The model and the experiments

The model used is the MOM2b code. The domain is an idealized rectangular basin from $40^o S$ to $40^o N$ in latitude and from $0^o$ to $60^o$ in longitude, with a flat bottom at 3000m. The longitudinal resolution is $1^o$; the latitudinal resolution is $1/3^o$ within $6^o$ of the equator and increases linearly to $1^o$ at the domain boundaries at $40^o$. There are 30 levels in the vertical with a 10m resolution in the top 100m. Horizontal mixing is the constant coefficient scheme with the eddy viscosity and diffusivity of 2000 and 1000 $m^2 s^{-1}$ respectively. In two sponge layers poleward of $36^o$, temperature is restored to prescribed values with a restoring timescale of 40 days at $36^o$. This value decreases to 4 days at $40^o$. In the vertical a Richardson number-dependent vertical mixing scheme is used. Unstable temperature gradients are eliminated by mixing heat vertically to a depth that ensures a stable density gradient.

The initial condition is a state of rest. Salinity remains a constant value of 35

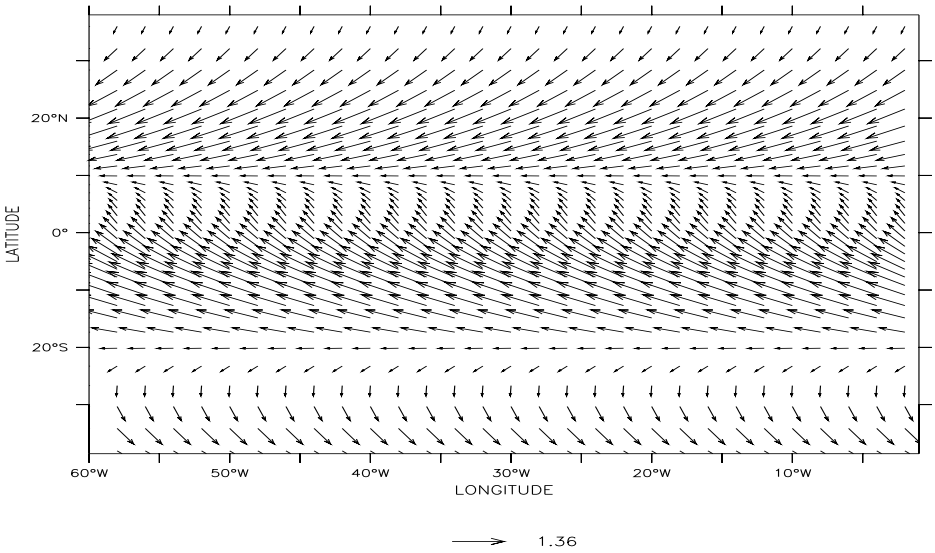


Figure 2.1: The wind stress in $dyn/cm^2$.

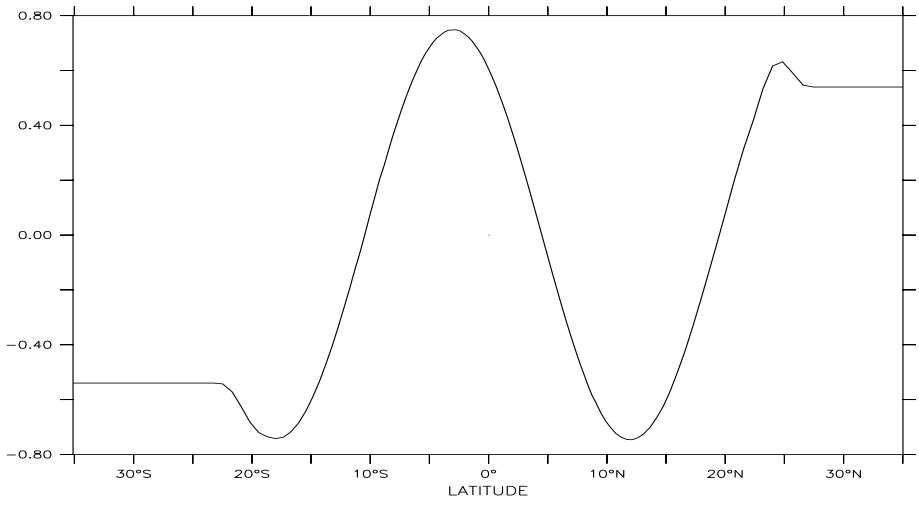


Figure 2.2: The wind curl in $10^{-8} dyn/cm^3$.

psu. The wind stress (Hellerman and Rosenstein, smoothed and averaged in time and longitude) and the wind curl are shown in Figures 2.1 and 2.2. The initial temperature is independent of longitude and shown in Figure 2.3. This profile is also used at the surface to restore the surface temperature with a 40-days relaxation time and as boundary restoring values in the sponge layers (experiment 1). Both experiments were integrated for 18 years before any analysis was performed or floats were injected (for a justification see Liu and Philander (1995)). In the case of the experiment with the superimposed MOC (experiment 2) the sponge layers are replaced by open boundary conditions (OBC). It is known, that OBC render the problem of solving the primitive equations ill posed (Oliger and Sundstrom (1978)). Nevertheless one can make progress if the errors that are introduced by the OBC are small enough and do not grow in time (see Spall and Robinson (1989) for a detailed discussion).

At the open boundaries the temperature and the barotropic streamfunction are specified. With the help of the Sverdrup balance and the thermal wind relation the model calculates the velocity field (Stevens (1990)). The open boundaries were put at $35^o N/S$ to allow the inflow to be in agreement with the Sverdrup balance. The

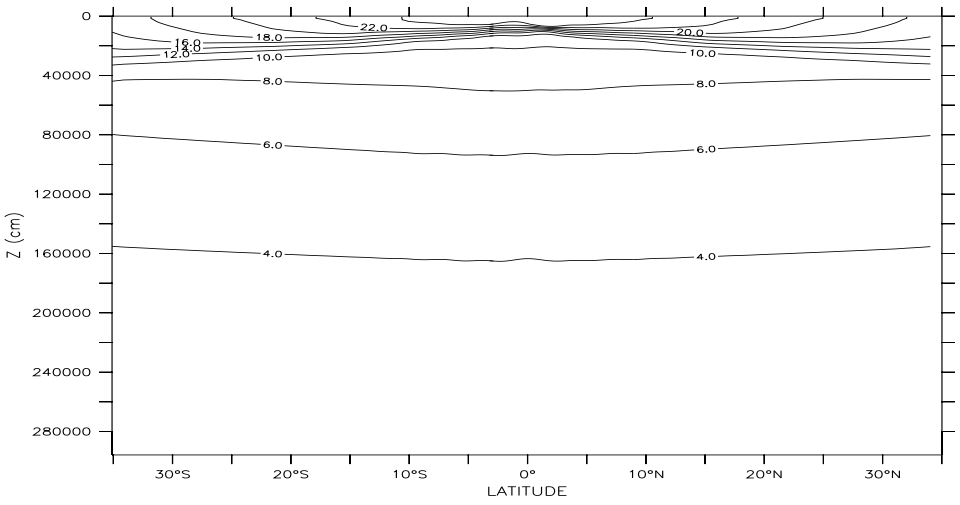


Figure 2.3: The initial stratification T(y,z).

barotropic streamfunction and temperature at $35^oN/S$ are taken from the steady state solution of the purely wind-driven circulation. To simulate the throughflow of the MOC return flow, the barotropic streamfunction is modified so that there are 15 Sv flowing into the South Atlantic all along the southern boundary and leaving the North Atlantic in the northwest corner through a western boundary current. These 15 Sv are roughly consistent with numbers from the literature (Schmitz and McCartney (1993)) and the Sverdrup transport across $35^oS$. The prescribed temperature profile at the southern boundary ensures via the thermal wind relation that the inflow is mainly in the upper 1000m. We did not try to simulate a deep western boundary current because we wanted to focus on the interaction between the thermocline of the tropical Atlantic and the warm water return flow of the MOC.

## 2.3 The flow field

Given the difficulties using OBC, we compared the temperature, velocity and streamfunction fields of the two experiments. The first two fields did not reveal any major differences in the interior so that we will just present the barotropic and the overturning streamfunctions for a comparison. Figures 2.4 and 2.5 show the barotropic streamfunctions for experiments 1 and 2, respectively. In both pictures we can clearly distinguish the subtropical, the tropical and the equatorial gyres which are separated by the zero wind curl lines. The major differences in these two figures are - except for the 15 Sv offset in Figure 2.4 - close to the western boundary. In Exp2 the northward western boundary currents increased their strength by 15 Sv whereas the southward western boundary currents became weaker by the same amount. This was to be expected from a simple linear superposition of the wind-driven flow and the warm water return flow. We do not expect any changes in the interior because the wind field is the same in both experiments. A non-linear effect of this superposition can be seen at $8^oN$ where the North Brazil Current (NBC; for the sake of argument we will name the currents after the corresponding real ocean currents) overshoots its original separation latitude and the North Equatorial Counter Current (NECC) meanders back to the zero wind curl line. Fratantoni (1996) showed that this overshooting is caused by the MOC and is responsible for most of the mesoscale variability in this area.

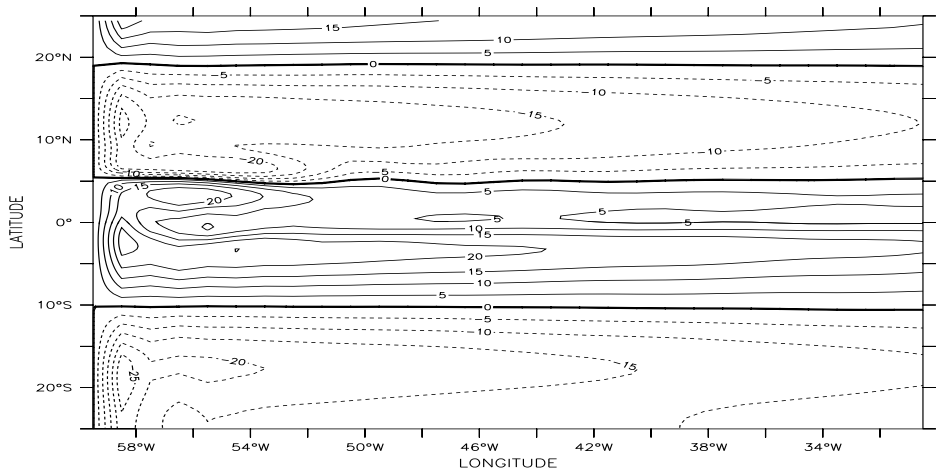


Figure 2.4: Barotropic Streamfunction in the western tropical part of the basin for Exp1.

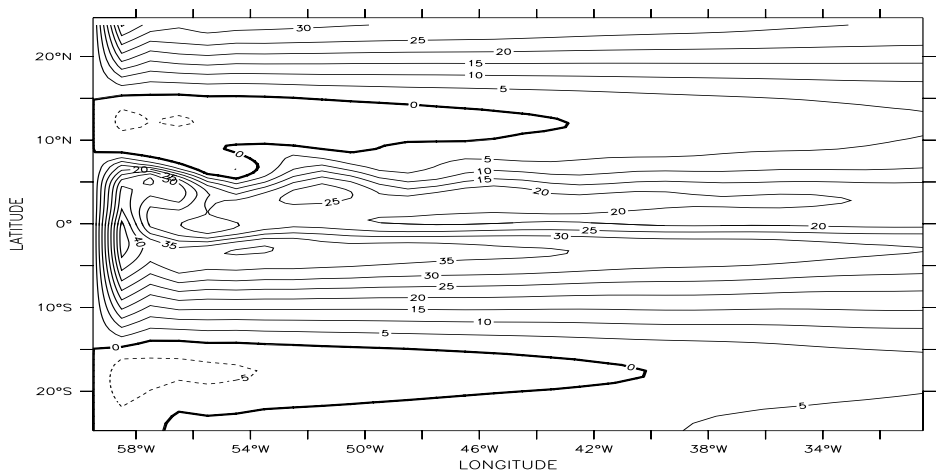


Figure 2.5: As in Figure 2.4 but for Exp2. Note the intensification of the NBC and its overshooting at $8^o N$.

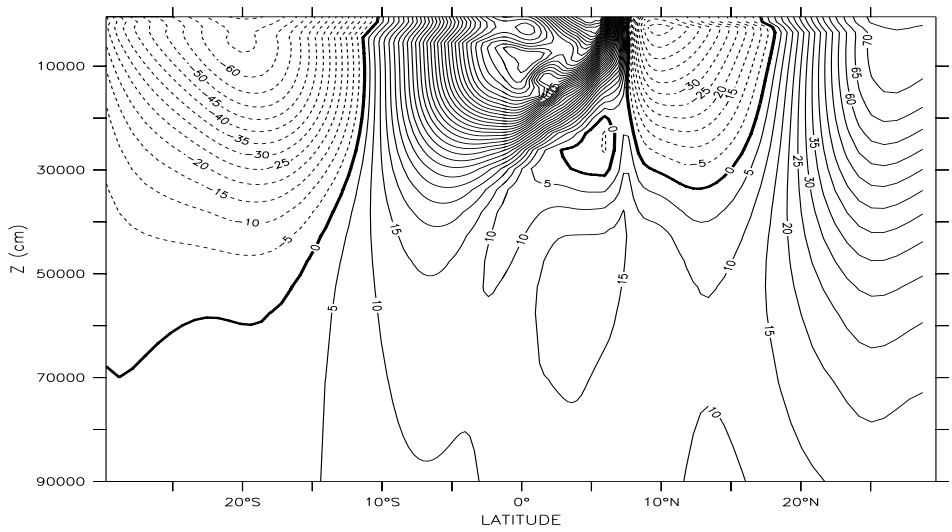


Figure 2.6: Meridional velocity in the upper 900m along the western boundary for Exp2 (contour interval: 5 cm/s). The maximum velocity is reached in the NBC with 200 cm/s at $5^o N$.

Of course, those figures show the barotropic streamfunction and not the velocity, but the NBC and NECC make up most of the transport in that area. The baroclinic structure of the western boundary currents in Exp2 is shown in Figure 2.6. We can see the western boundary currents of the four gyres and a continuous northward flow below 700m. The northward flow in the northern tropics is blocked by the western boundary current of the tropical gyre. As we will see later, this has important implications. Away from the boundaries, the interior velocity fields of the two experiments are almost identical and are not shown here (see Philander (1990) for their description). But there are, however, changes in the transition region between the western boundary and the interior. As an example, the flow field along the boundary between the northern subtropical gyre and the tropical gyre is shown in Figure 2.7. In Exp1 the interior has to feed a southward western boundary current and gains a southward component at the gyre boundaries in the transition region. In Exp2 (broken arrows), the interior feeds a northward western boundary current and therefore has a northward component in the transition region.

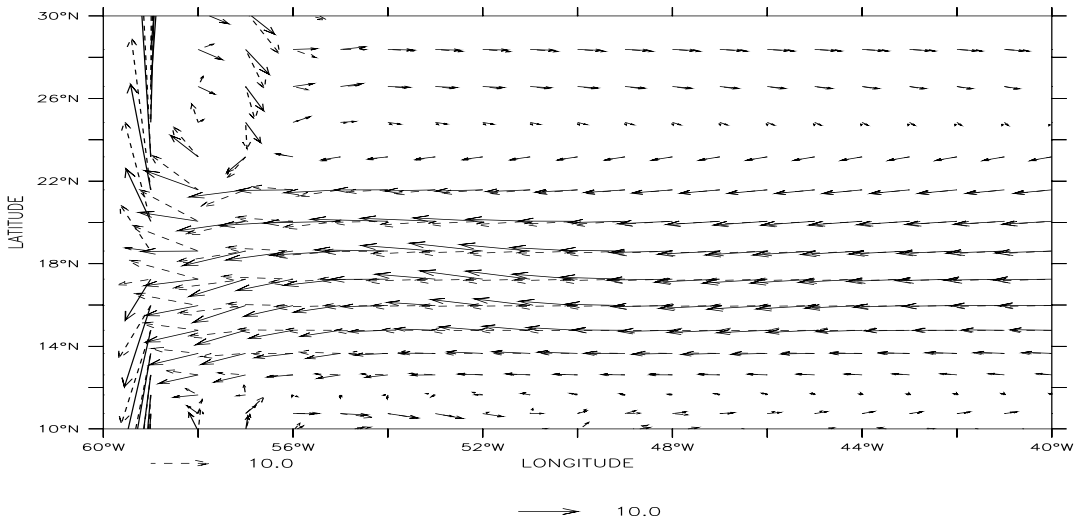


Figure 2.7: Velocity in 100m depth (cm/s). The broken arrows show the velocity field in Exp2, the other ones show the velocity field in Exp1. In most of the shown domain the fields are almost indistinguishable, but where the gyre boundary approaches the western boundary, the field of Exp1 has a southward component, the field of Exp2 has a northward component.

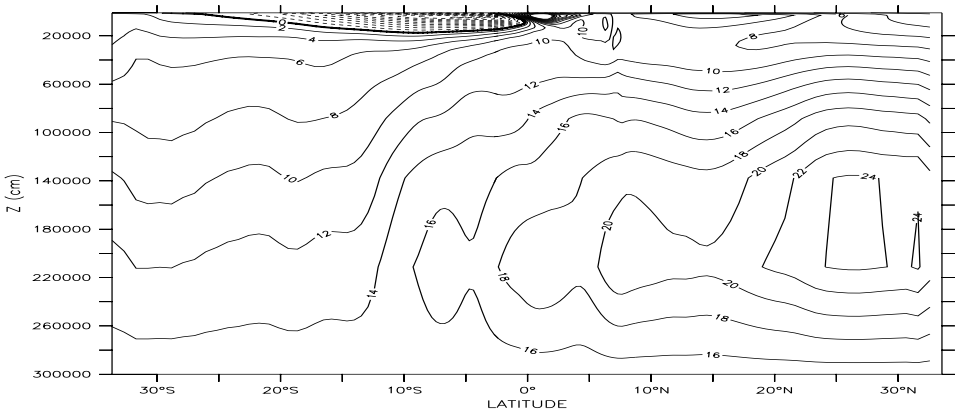


Figure 2.8: Overturning streamfunction for Exp2 in Sv.

The overturning streamfunction (Figure 2.8) indicates that a significant amount of intermediate water is entrained into the equatorial thermocline. It also shows that due to the lack of a deep western boundary current in our model, the return flow of the MOC has a abyssal component in the southern hemisphere and is not restricted to the upper or the intermediate levels as it should be. This spurious deep flow is due to the OBC and we will assume that its only effect is to weaken the upper level return flow in the southern hemisphere. At the equator we can see the two tropical cells that are induced by the Ekman upwelling system at the equator. The cross equatorial winds make them non symmetric. We can also see the southern subtropical cell which merged with the dynamically different southern tropical cell (see Liu et al. (1994) for their dynamics). The northern subtropical cell is barely noticeable, a point which will be discussed in the next section.

## 2.4 The tropical-subtropical pathways

After subduction, water from the subtropical gyres has three different possibilities to continue. The water from the westernmost part of the basin recirculates in the subtropical gyre. Water from regions further east enters the tropics either through the interior or in a lower western boundary current. This water feeds the EUC, becomes entrained in the equatorial mixed layer and returns poleward in the Ekman layer (Pedlosky (1987), Liu et al. (1994)). This complex three dimensional structure of the flow field is best analyzed with floats (virtual particles in our model). We released the floats in different areas of the subtropical gyres. Out of all the resulting trajectories we picked those that highlight the interaction between the MOC and the wind-driven circulation.

Figure 2.9 shows the trajectories of floats in Exp1. The floats were released below the Ekman layer in the eastern part of the northern subtropical gyre (NSG). The first thing to notice is that the Ekman suction in the tropical gyre effectively blocks the interior pathway in the north. After subduction down to about 150m, the water flows west in the North Equatorial Current (NEC), flows south in a lower western boundary current until it leaves the boundary again to flow east in the NECC. From there it flows south to feed the EUC, upwells and makes it poleward again in the Ekman layer. It takes about 8 to 10 years to complete this journey. In

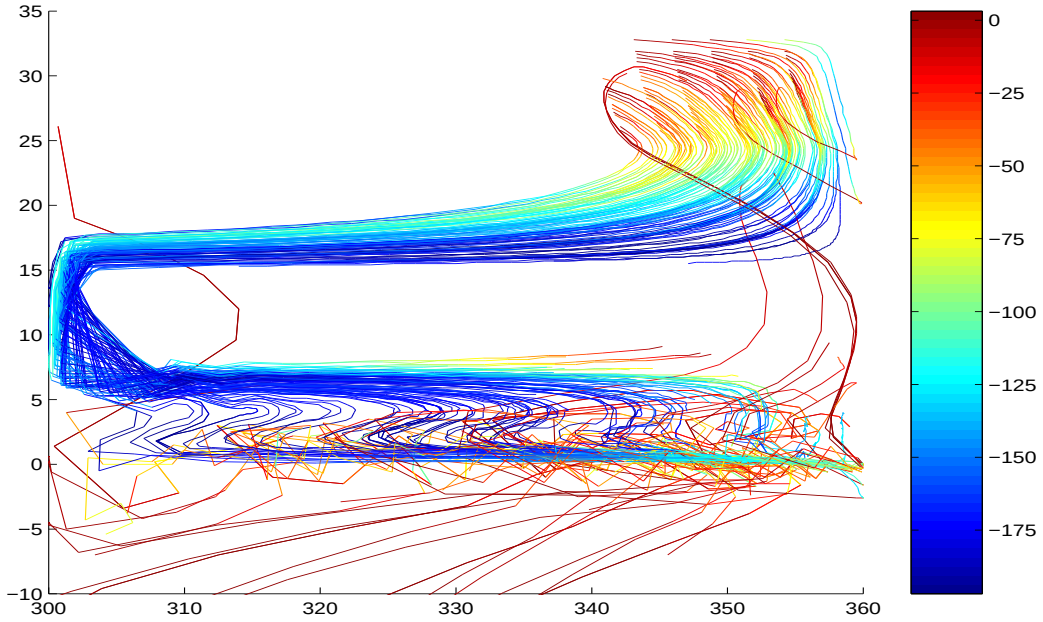


Figure 2.9: Trajectories for floats released below the Ekman layer in the northern subtropical gyre of Exp1 (the colorbar indicates the depth in meters).

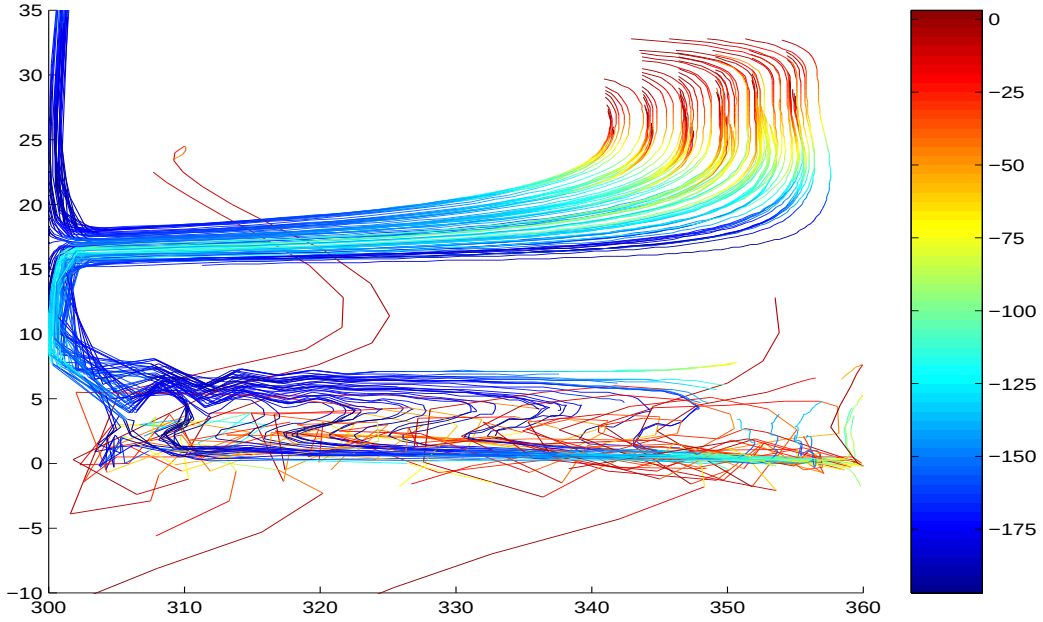


Figure 2.10: As in Figure 2.9 but for Exp2.

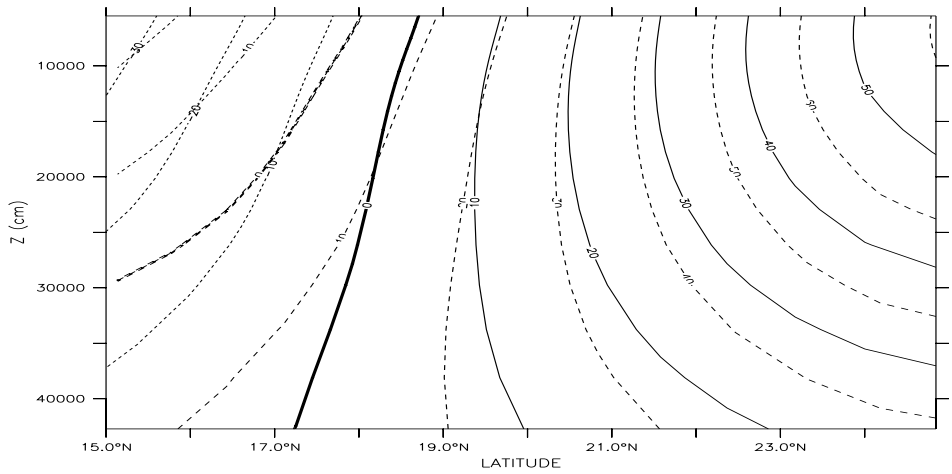


Figure 2.11: Meridional velocities in the area where the floats enter the western boundary currents (in cm/s). The straight zero line indicates the bifurcation latitude for Exp1, the broken zero line the bifurcation latitude for Exp2.

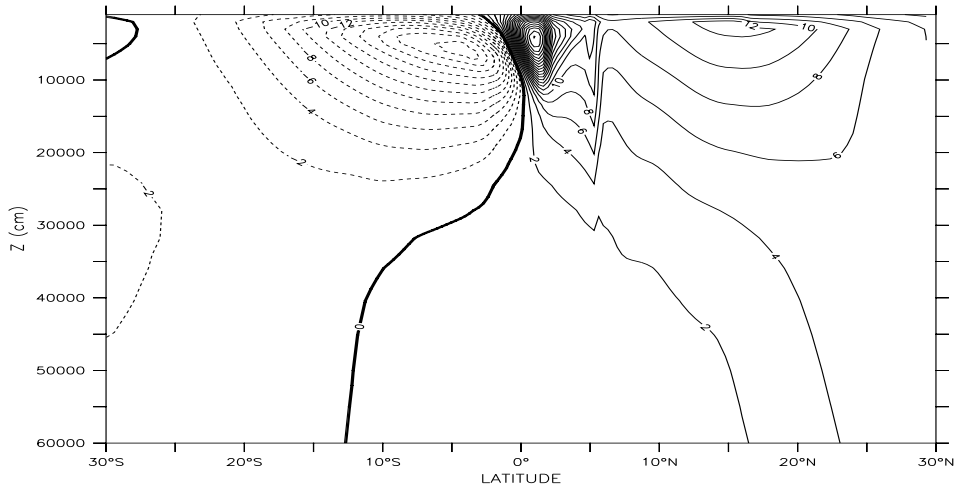


Figure 2.12: Overturning streamfunction for Exp1 in Sv. Just the upper 600m are shown to emphasize the structure in the thermocline.

Exp2 the floats were released in exactly the same area but only a minority of them enter the tropics (Figure 2.10). Most of them recirculate in the subtropical gyre. Apparently the return flow of the MOC changed the flow field at the western boundary in a way to inhibit the connection between the northern subtropical gyre and the tropics. Figure 2.11 shows that the return flow of the MOC shifted the latitude of vanishing meridional velocity (bifurcation latitude) south by approximately 1-2 degrees in the relevant depths (relevant means that a significant amount of subducted water arrives at those depths at the western boundary). Furthermore, as pointed out already in the last section, the MOC does not only change the flow field at the western boundary, but to a lesser degree changes the field within several degrees of it. A comparison of the endpoints of the vectors nearby the bifurcation latitude shows, that this effect is about as big as the effect of shifting the bifurcation latitude. Because the position of the subtropical gyre did not change, this means that some of the water that turned south in Exp1 has to turn north in Exp2. To quantify those changes in the cross equatorial flow, it is easiest to look at the overturning streamfunction in both experiments. As Figure 2.12 shows, there are 17 Sv of water upwelling into the equatorial thermocline from the southern subtropical gyre and

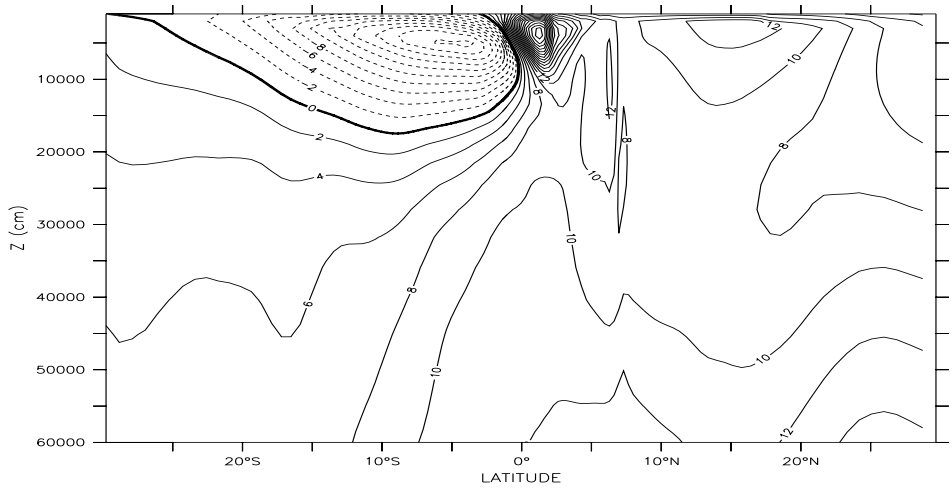


Figure 2.13: As in Figure 2.12 but for Exp2.

10 Sv from the northern subtropical gyre. This asymmetry is due to the wind field. By looking at Figure 2.13 we see that in Exp2 25 Sv come from the southern and only 2 Sv from the northern subtropical gyre (the equatorward gyre boundaries are at $10^oS$ and at $18^oN$ respectively).

What are the exact pathways of the MOC return flow? The analysis of float trajectories shows that there are just two possiblities in our model. The first one is a flow along the western boundary in intermediate layers (Figure 2.14). The second one is a complicated journey through the thermocline and Ekman layers of the equator. Because the thermocline waters flow south in the equatorial gyre, the water has to flow north either in the Ekman layer or along the western boundary to reach the northern midlatitudes. Two typical trajectories are displayed in Figure 2.15. The water subducts in the southern subtropical gyre to about 200m, enters the NBC which feeds the EUC. The EUC transports the water east where it upwells into the mixed layer. After another upwelling and downwelling cycle in the equatorial upwelling system it finally escapes north in the Ekman layer.

Without tracers it is difficult to tell exactly how much of the MOC return flow passes through the Ekman layer or the intermediate western boundary current (IWBC). So we carried out an additional run that was identical to Exp2 but without

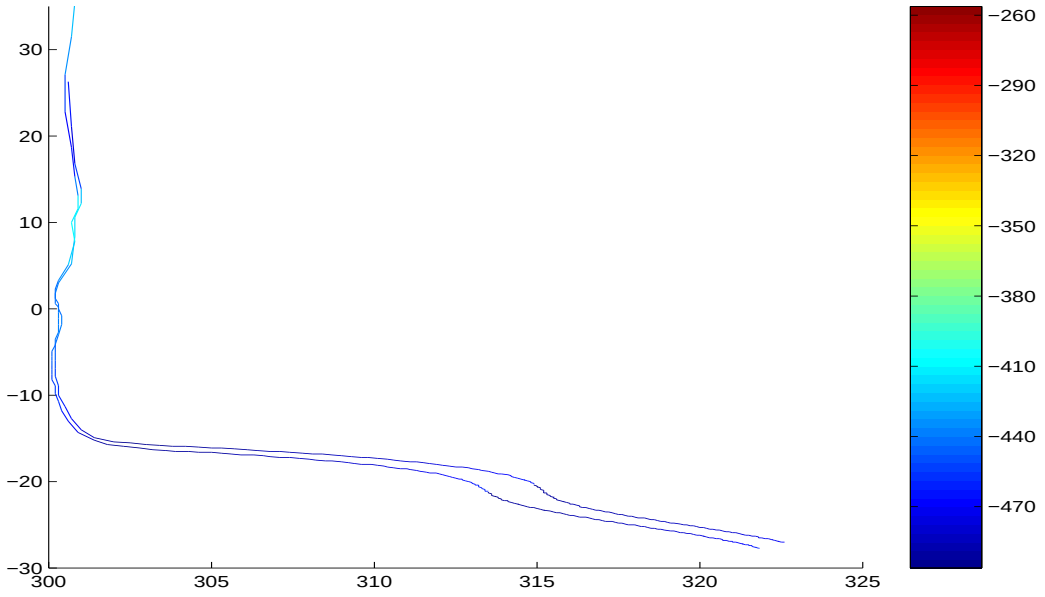


Figure 2.14: Float trajectories in the intermediate level.

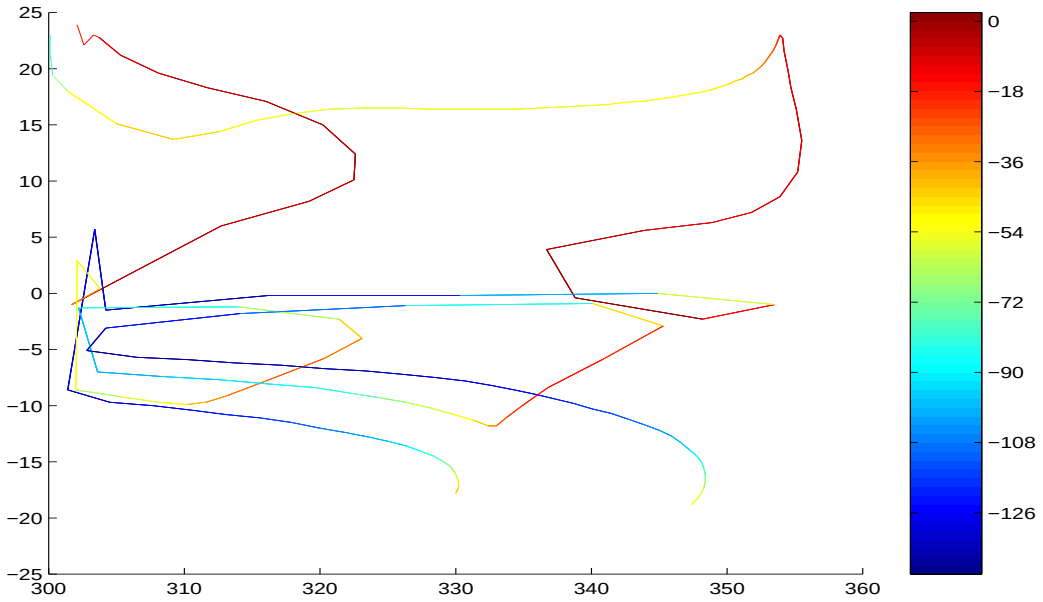


Figure 2.15: Two floats that take the surface path to the north. They move to the EUC, join the tropical cell and after another upwelling/downwelling cycle they escape to the North in the Ekman layer.

wind. Apart from the nonlinear overshoot region of the NBC/NECC the results in the flow field were almost identical to the difference of Exp2 and Exp1 (not shown). Below the thermocline and above the abyss, we interpret this as the intermediate layer (400m to 1500m) return flow of the MOC which is constrained to the western boundary. An integration of the flow at the western boundary yields an IWBC transport of about 7 Sv across the equator and next to nothing in the abyss. Due to lateral influx and upwelling of abyssal waters at the western boundary, the IWBC increases its transport to about 11 Sv at $20^o N$. Thus, we can estimate that about one half of the MOC return flow is carried by the IWBC, the other half has to pass through the Ekman layer.

# Chapter 3

# Overview of the circulation in the tropical Atlantic

The previous chapter described experiments in a simple model to illuminate the role of the MOC in determining the source waters of the tropical Atlantic. Unfortunately, the NBC rings, which were thought to be a major link in the connection between the tropics and subtropics, could not be reproduced. Therefore, we decided on a series of new experiments with a more realistic configuration that allows for the representation of NBC rings. The present chapter is not the focus of this thesis, it provides merely a framework within which to understand the following three chapters. The first section describes the model and is followed by an overview of the circulation of the tropical Atlantic. In the third section, model results are used to illustrate the pathways of the warm water return flow and to provide a picture of the mean circulation in the tropical Atlantic.

## 3.1 The model configuration

The model used is the MOM2b code. The domain is an idealized basin from $25^oS$ to $30^oN$ in latitude and from $70^oW$ to $15^oE$ in longitude, with a flat bottom at 3000m. The resolution is $1/4^o$ by $1/4^o$ at the western boundary between the equator and $12^oN$ and becomes coarser towards the eastern, northern and southern boundaries: the latitudinal resolution is reduced from $1/4^o$ to $1^o$ at the meridional boundaries,

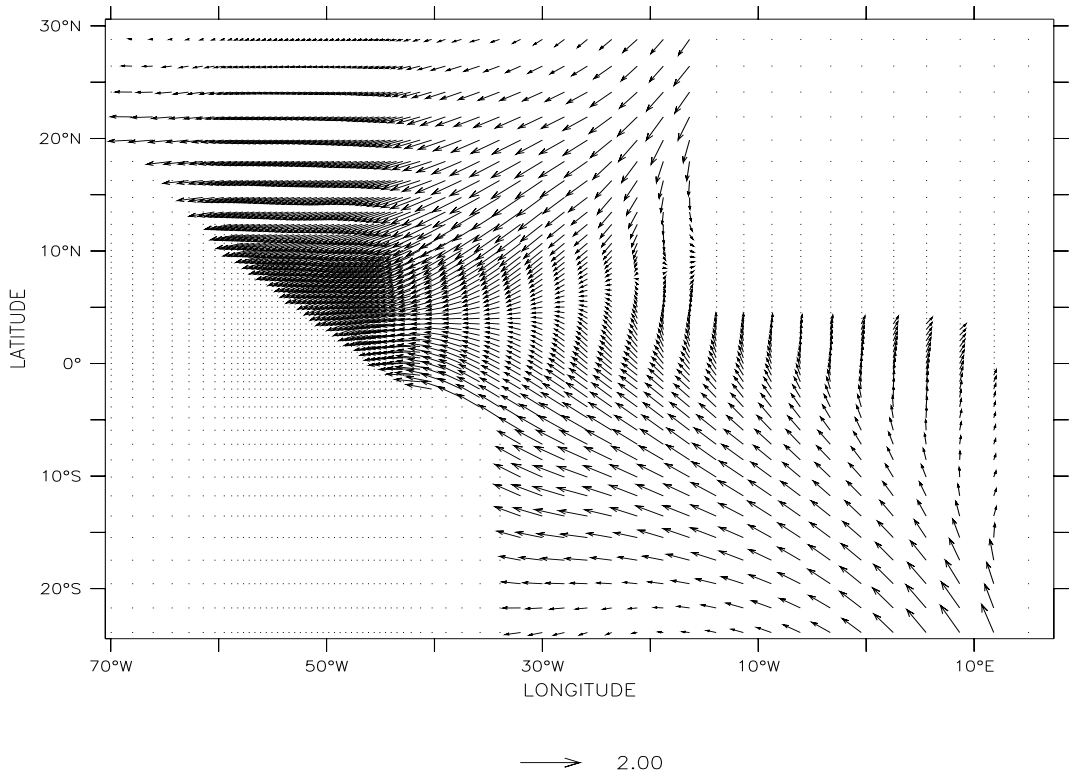


Figure 3.1: The yearly mean wind stress over the domain. This figure furthermore shows the high resolution along the Brazilian coast and the equator (for the sake of clarity only every fourth gridpoint is shown). The Caribbean Sea is not part of the model domain.

the longitudinal resolution is reduced from $1/4^o$ to $1.5^o$ at the zonal boundaries (see Figure 3.1 for an illustration of the resolution). There are 30 levels in the vertical with a 10m resolution in the top 100m.

Horizontal mixing is done by a Laplacian scheme with the eddy viscosity and diffusivity being linearly dependent on the resolution: from $200m^2s^{-1}$ for $1/4^o$ to $2000m^2s^{-1}$ for $1^o$ resolution. In the vertical, a Richardson number-dependent vertical mixing scheme is used. Unstable temperature gradients are eliminated by mixing heat vertically to a depth that ensures a stable density gradient.

The initial condition is a state of rest. Salinity remains constant in time and space

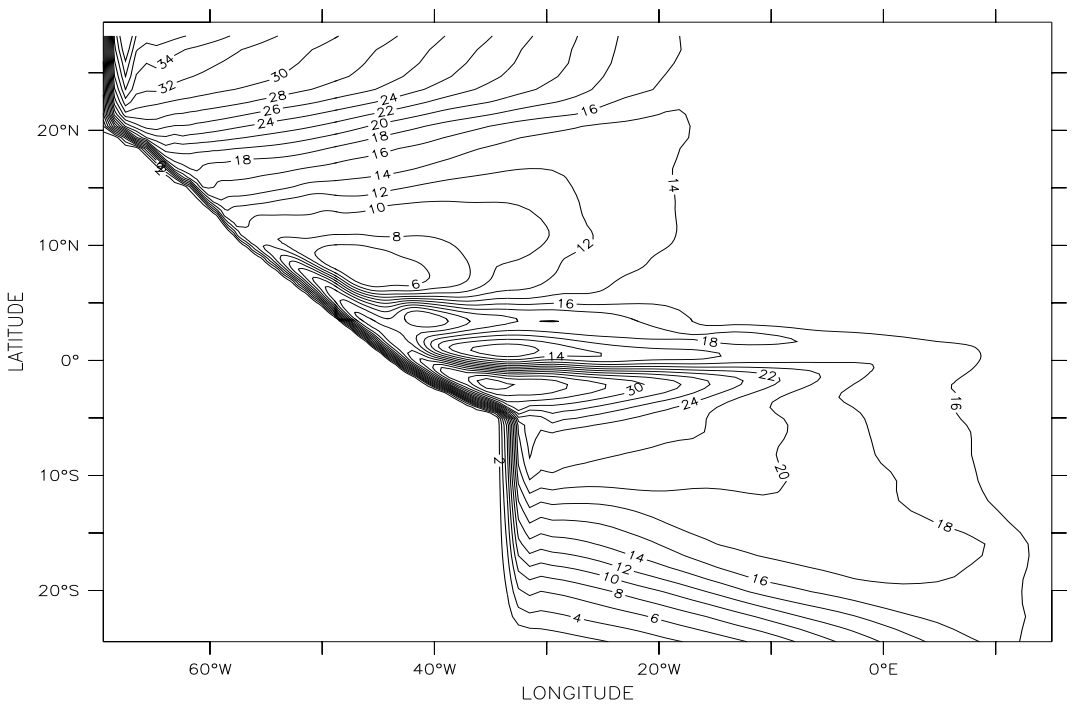


Figure 3.2: The time mean depth integrated transport (in Sv). The anticyclonic circulations north of $18^0N$ and south of $10^oS$ will be referred to as northern and southern subtropical gyres (STGs). The cyclonic circulation between $5^oN$ and $18^oN$ will be called tropical gyre (TG) and the equatorial gyre (EG) is between $10^oS$ and $5^oN$.

at a value of 35 psu. The wind stress (Hellerman and Rosenstein (1983)) and the resulting depth integrated circulation are shown in Figure 3.1 and Figure 3.2. The initial temperature distribution is symmetric about the equator and is essentially a zonally averaged, idealized climatology (as shown in Fig. 2.3). This profile is also used at the surface to restore the surface temperature with a 40-days relaxation time. The experiment was integrated for 18 years before any analysis was performed or floats and tracer were injected (because of the fast tropical adjustment and the initial stratification this a sufficient spinup time - see Liu and Philander (1995)). The

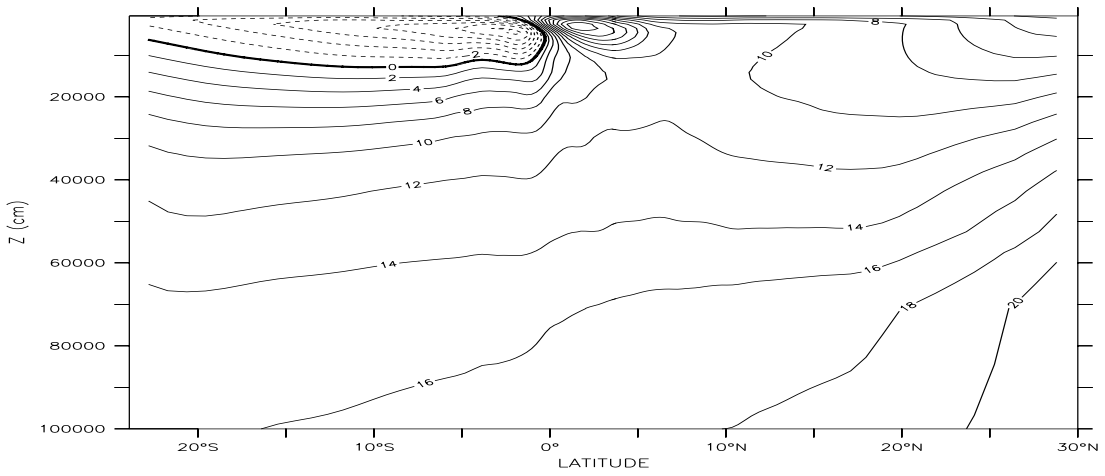


Figure 3.3: The time mean zonally integrated transport in the upper 1000m of the water column (contour interval: 2 Sv). The dashed lines indicate counterclockwise circulation. We can see the southern subtropical cell in the Southern Hemisphere, the strong wind-induced equatorial cell at the equator and the throughflow of intermediate water below the thermocline.

effect of the global MOC was represented by open boundary conditions (OBC). It is known, that OBC render the problem of solving the primitive equations ill posed (Oliger and Sundstrom (1978)). Nevertheless one can make progress if the errors that are introduced by the OBC are small enough and do not grow in time (see Spall and Robinson (1989) for a detailed discussion).

At the open boundaries the temperature and the barotropic streamfunction are specified. Using the Sverdrup balance and geostrophy, the model calculates the velocity field (Stevens (1990)). The barotropic streamfunction and temperature at the meridional boundaries are taken from the steady state solution of the purely wind-driven circulation. The basin for the purely wind-driven circulation extended from $40^oS$ to $40^oN$. To simulate the throughflow of the MOC return flow, the barotropic streamfunction is modified so that 15 Sv flow into the South Atlantic all along the southern boundary and leave the North Atlantic in the northwest corner through a western boundary current (see Figures 3.2 and 3.3). These 15 Sv enter the domain across the southern boundary in the upper 1000m of the water column, their

exact spatial distribution depends on the specification of the temperature field at the southern boundary. The total inflow is roughly consistent with numbers from the literature (Schmitz and McCartney (1993)) and the Sverdrup transport across $25^oS$. We did not attempt to simulate a deep western boundary current because we wanted to focus on the warm water return flow of the MOC and its interaction with the wind-driven circulation.

To support the analysis of the model results we included virtual Lagrangian floats in our numerical experiments. When attempting to extract Lagrangian information from an Eulerian dataset, care must be taken that computational errors remain small compared to the amplitude of the flow field. To compute the particle trajectories the equation:

$$d\vec{x}/dt = \vec{u}(\vec{x}, t) \tag{3.1}$$

has to be integrated. Two problems exist in applying this equation to the Eulerian velocity field of the model. The velocity must be established at a point in space and time which is, in general, positioned between available data points. Second, the time integral must be evaluated accurately. The first problem asks for a optimal interpolation scheme to determine the velocity of the particle between grid points. An obvious choice (chosen here) is linear interpolation between the eight surrounding gridpoints. However, one may argue that a given gridpoint velocity represents the velocity at all points within its grid box. Fortunately, Boening and Cox (1988) were able to show in a comparative particle study that there is no significant difference between the results of these two methods.

There are various ways to perform the time integral of the Lagrangian velocities, ranging from the simple Euler timestepping (chosen here) to more complex schemes. However, the simpler schemes can be made accurate as well by using a smaller timestep. The important parameter to study is the relation between grid size and product of velocity and timestep:

$$N = \Delta x/(v\Delta t) \tag{3.2}$$

If the velocities or the timestep are too large, it is possible that a virtual particle can cross a front and end up in a regime where it should not be. Boening and Cox (1988) and later Kroeger (2001) studied how the numerical dispersion depends on this parameter N. Especially the study by Kroeger (2001) is interesting as it is done

with an eddy permitting GCM of the tropical Atlantic. He shows that even in the turbulent regions of the NBC/NECC retroflection values of N beyond 100 give almost identical results. For qualitative purposes, to illustrate pathways, values of N between 1 and 10 are sufficient.

In the present study, the particle positions are calculated online at every timestep (=3000 seconds). For a grid size of 30km, N is estimated to be O(10) for the turbulent NBC/NECC retroflection region ( $u \approx 1m/s$) and O(100) for the intermediate layers ($u \approx 0.1m/s$). This enables us to use the virtual particles (floats from now on) in this study to understand the three dimensional structure of the flow in the thermocline. In the quieter intermediate layer we can use the floats for a quantitative study of the Lagrangian flow.

To gain some confidence in the model's performance, the model results were

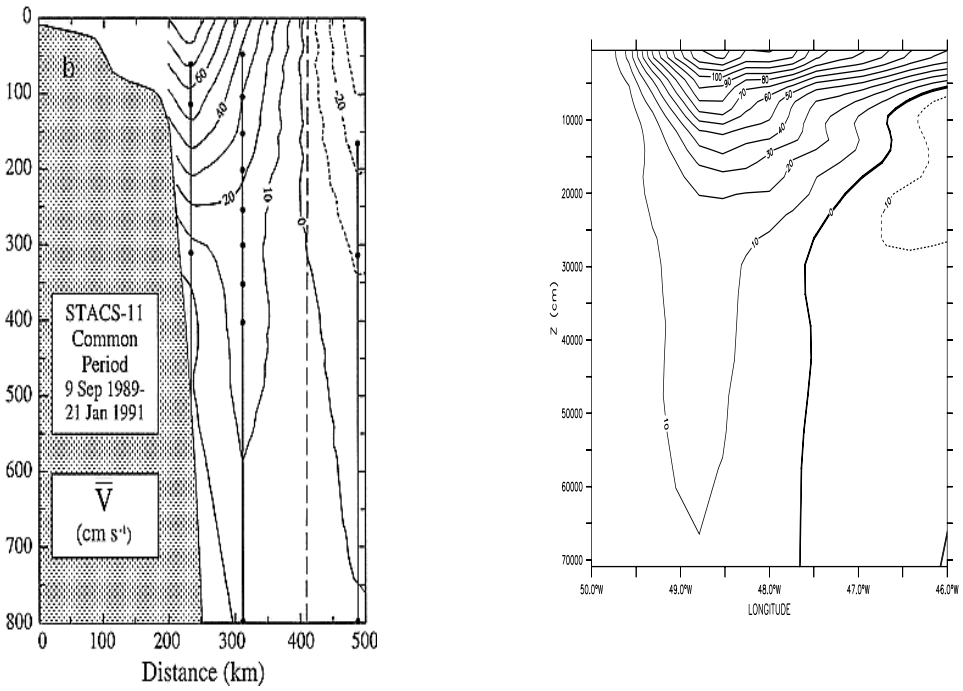


Figure 3.4: The alongshore velocity at 4N averaged over 16 months as measured by Johns et al. (1998, left) and in the model for the same period (right, in cm/s).

compared with available observations. The right side of Figure 3.4 shows the mean alongshore velocity at $4^oN$ for the period starting September to the January 16

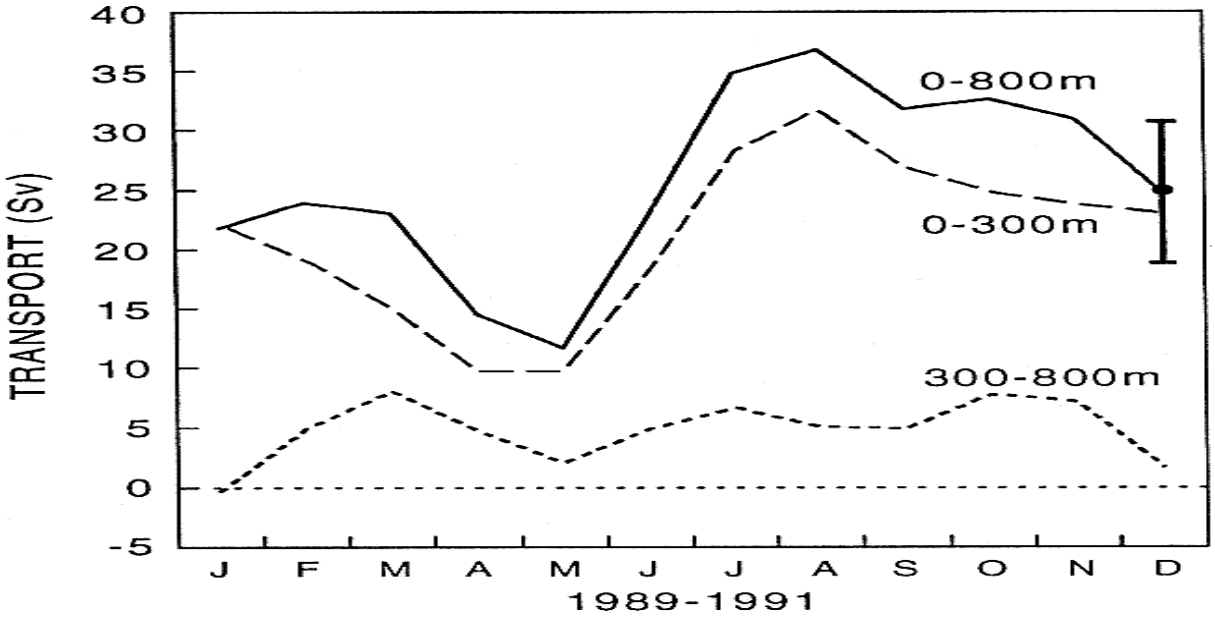


Figure 3.5: The seasonal cycles of meridional NBC transport at 4N for the upper 300m (dashed line), for the depth range 300m-800m (dotted line) and the upper 800m (solid line) as observed by Johns et al. (1998). These values were obtained after a 90 days low pass filtering.

months later. The structure of the flow is very similar to that inferred by Johns et al. (1998) from their current meter moorings (shown on the left side of Figure 3.4). The NBC transport at this latitude varies from 17 Sv in March to 35 Sv in August and November which again compares reasonably well with the observations of Johns et al. (1998, compare Figure 3.5 with Figure 3.6). These figures show, that the model is able to reproduce the steep increase of transport in spring and the peak transport in August. In the observations, however, the transport minimum is in May whereas the model indicates a minimum in March. Moreover, the model generates a maximum transport in November which is not observed by Johns et al. (1998). Although one might argue that the model values are mostly within the uncertainties of the observations ( $\pm 6$ Sv), it is interesting to note that the Fratantoni et al. (2000) solution uses the same wind field and has similar shortcomings - the early minimum in March and the second maximum in November. This suggests that the differences in transport are due to shortcomings in the wind product.

The NECC transport has a similar cycle at 38W with no transport from April

to May and a maximum of 28 Sv in September, similar to the observations as discussed in Katz (1987). However, the model results suggest that the NECC exists throughout the year. The position of its core can vary between 4N and 8N and in the spring the flow in the Ekman layer is westward. This makes it difficult to calculate a timeseries of the NECC transport as apparently the NECC seems to vanish during part of the year. For example, in May the NECC has a maximum velocity of 12 cm/s (at 38W), but the above calculation yields a zero transport, because the transport is integrated from 3N to 9N over the upper 300m (to be able to compare it with Katz's (1993) data).

The NBC rings also compare well with the description given in Fratantoni et al. (1995): At 8.5N the observed average maximum swirl velocity is 85cm/s at the surface and the average penetration depth is 650m $\pm$ 50m (Fratantoni et al. (1995) defined penetration depth as the maximum depth of the 10cm/s isotach). The NBC rings in our simulation seem to be slightly stronger and deeper than the ones generated in the simulation of Fratantoni et al. (1995). We attribute this to the higher

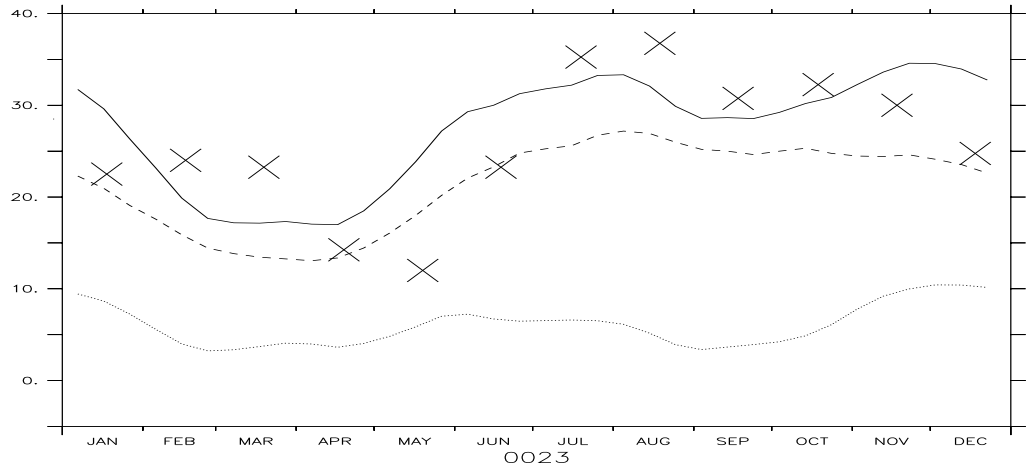


Figure 3.6: Like the previous figure, but for the model results. It shows the NBC transport at 4N for the upper 300m (dashed line), for the depth range 300m-800m (dotted line) and the upper 800m (solid line). The crosses indicate the observations for the total transport by Johns et al. (1998) as shown in the previous figure.

vertical resolution in our model and a lower viscosity. Goni and Johns (2000) published a census of NBC rings based on altimeter data. They found that on the average there are six NBC rings shed every year with no apparent seasonal signal. We find a similar statistics in our experiment: Every 50 days a new NBC ring is generated, independent of the season.

The above discussion is by no means a detailed comparison between observations and our results. Its purpose is solely to demonstrate that our model, even though idealized, is able to reproduce reasonably well those features of the tropical circulation which are thought to be relevant for the generation of NBC rings. Three different experiments were performed: Exp1 is the experiment conducted with seasonal varying wind, Exp2 the experiment with steady winds and Exp3 is done without any wind at all. For illustrative purposes we injected a passive tracer at the southern boundary of Exp1. We did not integrate the model long enough to use this tracer for a quantitative analysis of the transports but on a few occasions we will use the tracer fields to illustrate pathways.

## 3.2 Overview of the upper layer circulation in the tropical Atlantic

Before describing the detailed pathways of the upper layer SA water through the tropics, a brief introduction is given into the annual mean structure of the tropical current system. The upper layer flow in the tropical Atlantic is characterized by a series of alternating zonal currents that are connected at the western boundary with the NBC, and in the interior by a strong Ekman drift at the surface and a weak meridional flow below it. Apart from connecting the zonal currents, the NBC brings SA water into the tropics. How this SA water makes its way into the northern subtropical gyre across the tropics will be discussed in the following sections. The intermediate layer flow (between the thermocline and the NADW) in the tropical Atlantic is one of the research topics in this thesis and will be discussed in Chapter Five. In this section we mainly discuss what is known about the surface and thermocline currents in the tropical Atlantic and provide the phenomenological background.

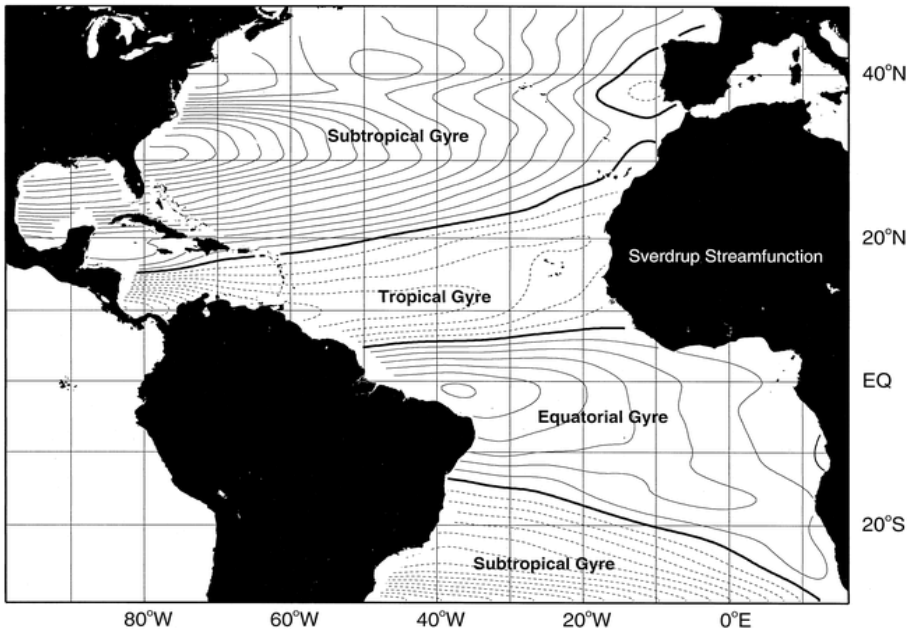


Figure 3.7: The barotropic streamfunction based on Sverdrup balance and Hellerman-Rosenstein winds (Fratantoni et al. (2000), every contour line represents 2 Sv). The tropical and the equatorial gyres are separated by the NECC which feeds the interior circulation of both gyres.

The large-scale wind field is dominated by the southeast and northeast trade winds and results in four large gyres that are shown in Figure 3.7. This figure reflects the assumption of a pointwise balance between the input of vorticity by the wind and stretching (or squeezing) of the water columns. To conserve mass, these interior gyres are closed at their western end by western boundary currents (from south to north): the southward Brazil Current, the northward NBC, the (hypothetical) southward Guyana Current and the northward Gulfstream. It was seen in the previous chapter, that the presence of a MOC will amplify the northward western boundary currents and weaken (or possibly reverse in the case of the weak Guyana Current) the southward western boundary currents. This description of the tropical circulation is very basic and unlikely to be accurate, even if the wind field would be known perfectly well. The real ocean is in parts very nonlinear and can have a surprisingly rich vertical structure. Below we will discuss observations, model results and theoretical ideas to outline the circulation in the tropical Atlantic. This outline will be the background for the actual thesis research that is presented in later chap-

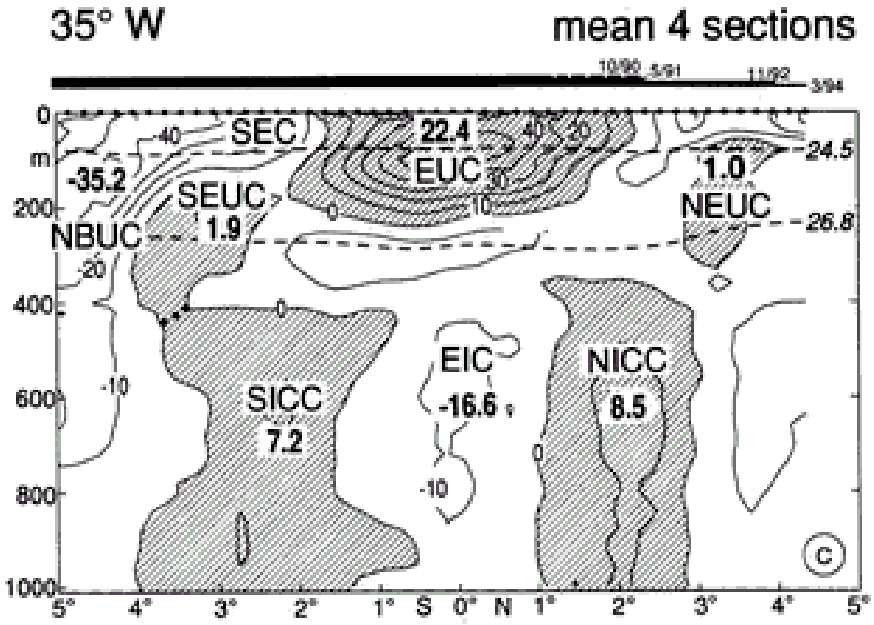


Figure 3.8: The zonal velocity across 35W as estimated by Schott et al. (1998). The NBUC is identical with the NBC, the SEUC and NEUC will be referred to as southern and northern Tsuchyia jets. The structures below 400m depth will be discussed in chapter 5. Eastward flow is shaded and the numbers indicate the transport in Sverdrup computed from four different LADCP and shipboard ADCP sections. Unfortunately the sections do not cover the latitudes north of 5N, so the NECC was not captured in these measurements. See, however, a model realization of a section at 30W in the next figure.

ters.

Measurements of water mass properties and velocities by Schott et al. (1998) show that the NBC not only feeds the NECC (as indicated in Figure 3.7) but also the subsurface EUC. They find that approximately 12 Sv enter the equatorial gyre at 10S above the thermocline in the NBC (based on two hydrographic sections). While approaching the equator the NBC increases its strength to 24 (3) Sv due to the contribution of the SEC (based on current meter moorings, the number in brackets is the standard deviation). Johns et al. (1998) find at 4N a NBC transport of 21 (8) Sv (based on current meter moorings). The strength of the zonal currents is far more difficult to measure because of their proximity to each other (see Figures 3.8 and 3.9). Adding to the problem is that the position of the currents changes with the position of ITZC. However, Schott et al. (1998) estimate the strength of

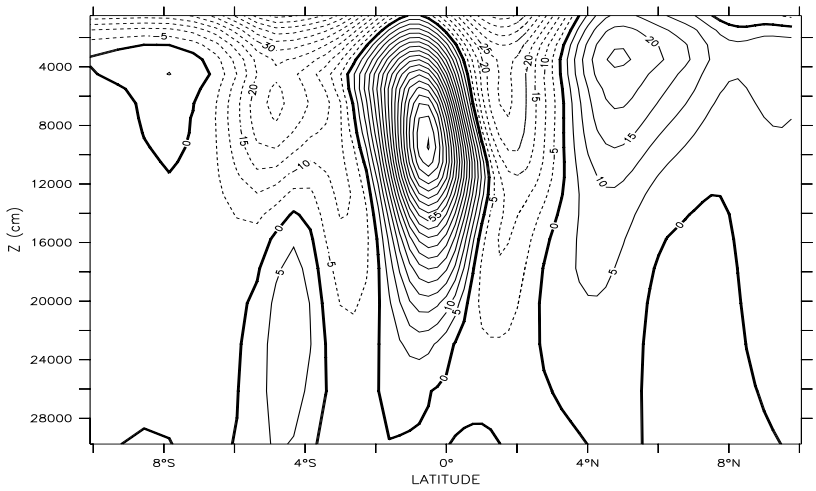


Figure 3.9: The annual mean of the zonal velocity across 30W in Exp1. Contour interval is 5 cm/s. The bands of westward velocity at 4S/2N constitute the SEC, the EUC can be seen at 1S and the NECC is centered at 5N. The southern and northern Tsuchyia Jets (sTJ and nTJ, respectively) can be seen as the bands of eastward velocity below 150m depth at 5S and 4N. Their dynamics will be investigated as part of this thesis in Chapter Seven.

the EUC to be approximately 22 Sv (at 35W), and Katz (1991) finds the annual mean of the NECC to be 14 Sv (almost 7 years of inverted echo sounder data). These figures are reported to broadly access the relative strength of the equatorial currents. The corresponding intensities of the simulated currents are: 13 Sv for the NECC, 25 Sv for the EUC, 23 (3) Sv for the NBC at the equator and 20 (7) Sv for the NBC at 4N. From the strength of the NBC in relation to the NECC and the EUC it is clear that a substantial amount of water must be recirculating between the EUC, the NECC and the SEC. The weak meridional and vertical flows that are required for this recirculation are almost impossible to measure, and only recently Johnson et al. (2001) were able to produce a (rather noisy) map for these velocities in the Pacific.

Figure 3.10 shows the MOC in the upper 300m of the tropics as modeled in Exp1. We see the strong Ekman divergence at the equator and the downwelling

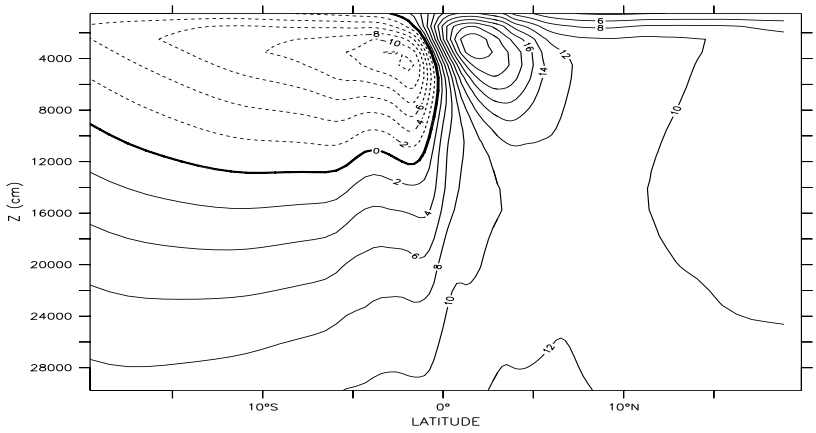


Figure 3.10: The zonally integrated circulation in Sverdrups. The equatorial cells can be identified by the strong upwelling at the equator and the adjacent downwelling polewards of it. The southern subtropical cell merges with the southern equatorial cell but reaches beyond the southern limits of the equatorial gyre (10S).

to the north and the south of it. These strong recirculations are called equatorial cells (ECs). It is important to distinguish them from the subtropical cells (STCs). The STCs connect the subtropics with the equator, whereas the the ECs recirculate water within the equatorial gyre. Figure 3.10 suggests that there is no STC but a strong EC in the NA. On the other hand, the SA has a STC but only a weak EC. Of course, the distinctions between these different cells are not exact because they are based on a zonally integrated flow field. Thus, the EUC and SEC are constantly exchanging water and the EUC consists to a good part of water that does not come directly from the SA, but is recirculating between the SEC and EUC (this statement will be quantified in the next section). The ECs are a central part of the equatorial circulation and their strength influences the SST, the shape of the thermocline and therefore the strength of the zonal currents. Unfortunately the Ekman theory breaks down at the equator as the Coriolis force approaches zero. Thus, the strength of the modeled ECs depends on the parameterizations for mixing. Blanke and Delecluse (1993) compare two different mixing schemes in a numerical simulation of the Atlantic circulation and find differences in the strength of the ECs of 30%. This leads

to SST differences of $1^oC$ and differences in the EUC and NECC strength of up to 30%. To complicate matters further, Bryan et al. (1995) find that the ECs are very sensitive to the intensity of the crossequatorial wind. For Hellerman and Rosenstein (1983) winds, they find a total strength of the ECs of 53 Sv, whereas ECMWF winds lead to an EC of 38 Sv (in this model, Hellerman and Rosenstein winds lead to an EC of 34 Sv). Luckily, the numerical experiments of Liu et al. (1994) show that the strength of the connection between the tropics and the subtropics is unaffected by the details of the ECs. Therefore we conclude that, while important for climate studies, the exact strength of the ECs is not overly important for the present purpose.

South of the equator there is the wind-driven STC (Figure 3.10), which connects the tropics to the subtropical SA. Its dynamics and its relationship to the thermally driven MOC has been discussed in an idealized configuration in the second chapter. Figure 3.10 shows that roughly 14 Sv of SA water flow north across 15S in the upper 300m. Approximately 4 Sv of this water return south in the Ekman layer and 10 Sv continue north as part of the warm water limb of the MOC. The details of this flow will be discussed in the next section.

Each one of the currents in Figure 3.8 is connected to the NBC, but is governed by different dynamics which we will now briefly discuss. The SEC can most easily be understood by considering a $1\frac{1}{2}$-layer model with steady easterly winds. The governing equations for the linear momentum balance are:

$$u_t - fv + g'\eta_x = \tau^x/H \tag{3.3}$$

$$v_t + fu + g'\eta_y = 0 \tag{3.4}$$

Assuming no meridional boundaries ($\eta_x = 0$) and an initial state of rest, one finds at the equator:

$$u_t = \tau^x/H \tag{3.5}$$

Thus, in the absence of friction and meridional boundaries, easterly winds will generate a steadily accelerating westward surface current. Away from the equator $u_t$, will eventually be smaller than $fu$, and the winds will establish a poleward Ekman transport. This off-equatorial Ekman drift will create a minimum of sea surface height at the equator and geostrophy (equation 2, $v_t/fu \ll 1$), will support the zonal current

poleward of the equator. Yoshida (1959) investigates the transitional region between the equator (accelerating jet) and the regions far away from the equator (Ekman drift) but the above description gives the basic dynamics of the equatorial jet. Including the advection of momentum in the balance above will render the problem too complicated for an analytical treatment. Philander (1990), however, shows in a numerical study how the equatorial jet as described above is changed into the SEC seen in the observations. He finds that upwelling transports eastward momentum from the underlying EUC to the SEC, and the poleward and downward flow that is forced by the wind field (the ECs) leads to advection of westward momentum away from the equator and below the mixed layer. This creates the characteristic shape of the SEC velocity profile in Figure 3.9. Of course, the actual ocean does have boundaries: At its eastern and western boundaries the normal flow must vanish. This can only be achieved by generating a Rossby wave front at the eastern boundary and a Kelvin wave front at the western boundary. The waves carry the boundary information into the interior and set up a zonal pressure gradient that will eventually balance the wind stress.

To understand the EUC one has to abandon the $1\frac{1}{2}$-layer model and study a higher mode model or a continuously stratified system. The boundary conditions are then satisfied by a set of waves that project on the structure of the equatorial jet. In the equatorial Atlantic, the surface jet projects mainly on the second baroclinc mode (Philander (1990)), but other modes will be excited as well. In an inviscid ocean the waves will carry the boundary information into the interior and build a pressure gradient to balance the wind stress. However, in the presence of dissipation, only the gravest modes will be able to propagate throughout the basin. The higher modes will dissipate and a residual circulation will remain. The EUC is the resulting residual circulation in the equatorial Atlantic. Figure 3.11 provides a simple sketch for this process. McCreary (1981) was able to find an analytical solution for the EUC based on these mechanisms. The beauty of this linear theory lies in its description of the spinup of the equatorial currents. The major drawbacks of the study are first that it cannot explain the thermal structure of the equatorial thermocline, second that the wave-induced spin-up pattern does not account for mass transport in the EUC and finally that the observed EUC is highly nonlinear.

Pedlosky (1987) developed an extension of the LPS theory (Luyten et al. (1983))

to include the equator. He finds that PV conservation forces some of the streamlines that originate in the subtropical subduction regions to continue towards the equator. By this mechanism the equatorial thermocline is supplied with cold subtropical waters and the EUC is formed by converting planetary vorticity into relative vorticity. For all the elegance of this theory, it is not closed and it depends on the a priori knowledge of the bifurcation latitude. Its position determines whether a streamline that is approaching the western boundary from the northeast will return north in a western boundary current or continue south towards the equator. Liu (1994) argues that the vanishing wind stress line is an adequate approximation for the bifurcation latitude.

However, neither the linear nor the nonlinear theory can incorporate the dissipative processes or the upwelling that eventually terminate the EUC. Wacogne (1990) used a numerical model to study the dynamical balances within the EUC. Her findings support Pedlosky's nonlinear theory west of 30W below the mixed layer. Everywhere else dissipation and the vertical flux of momentum are important terms in the momentum balance. If the linear theory may explain the set-up of the EUC, it is the nonlinear theory that explains its structure and transport. Mixing and upwelling as parameterized in numerical models and expressed in the ECs, that

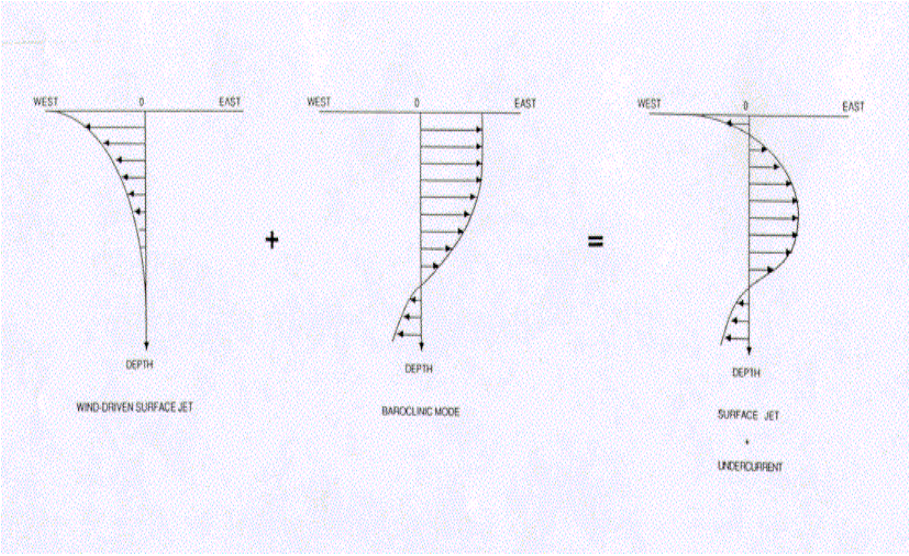


Figure 3.11: Sketch to illustrate how the superposition of the surface jet and the second baroclinc mode lead to the EUC (Philander (1990)).

determine the amount of recirculation between EUC and SEC, help to understand how the circulation is closed by returning the EUC water to the subtropics in the Ekman layer.

A review of the published literature reveals that less work has been conducted

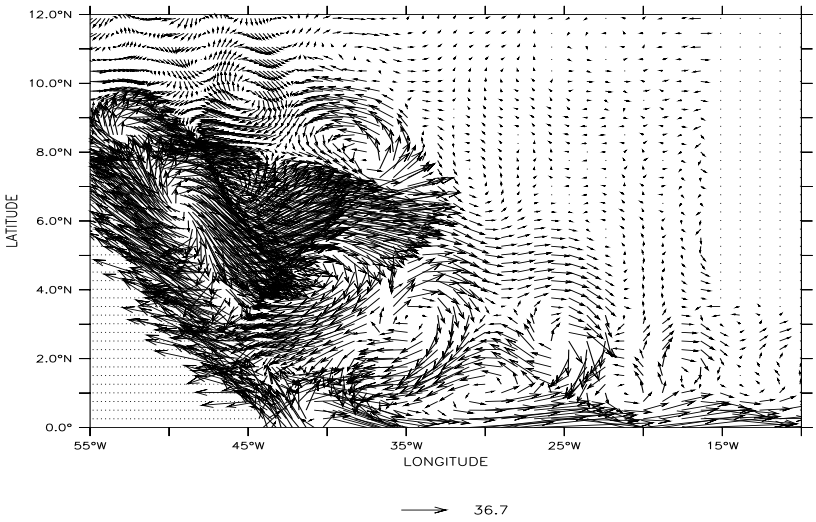


Figure 3.12: Snapshot of velocity in 100m depth. Note the highly turbulent flow west of 30W that does not resemble at all a steady, zonal current.

to understand the NECC than to understand the EUC. Sverdrup (1947) used the NECC in the Pacific ocean to prove the validity of the Sverdrup balance. This work is still quoted in textbooks (Pond and Pickard (1983)) although Leetmaa at al. (1981) pointed out that the agreement between the observed zonal transports and the predictions obtained from the Sverdrup balance are rather accidental. Garzoli and Katz (1983) used observations to evaluate the vorticity balance of the NECC. They found that only in the range between 42W and 22W, the NECC structure can be explained by Rossby waves and local Ekman suction. Philander (1990) points out that even this is controversial. Seasonal Rossby waves should be deflected towards the equator in the presence of an eastward current and leave the NECC in a shadow zone that is only influenced by local Ekman suction. A look at Figure 3.12 makes clear that the NECC would be more accurately described as a nonlinear, turbulent flow that cannot be described by linear dynamics. The North Brazil Current rings

and the instabilities are one aspect of the NECC and will be discussed in great detail in the next chapter. However, this is only a part of the NECC and its dynamics still needs further investigation. Based on current research and numerical studies, it can only be stated that the NECC connects the interior with the NBC and supplies the tropical and equatorial gyres with water for their respective wind-driven flow. Even though this may indicate a Sverdrup balance, Figures 3.10 and 3.12 show that a significant amount of vertical and horizontal recirculation contributes to the NECC transport (similar to the EUC).

## 3.3 Description of the upper layer mean flow in the model

The surface and thermocline pathways through the tropics are arguably among the most complicated ones because they involve western boundary current dynamics, diabatic upwelling and intense mixing through waves and eddies. Therefore a detailed account of the origin, path and destination of the water can only be accomplished with a model that features tracers for different water masses and is run into equilibrium (see Cox (1989) for the method). Unfortunately the computational resources did not allow for this method. Nevertheless, the high temporal and spatial coverage of the model should further expound on the understanding gained from observations and also reveal details of the circulation that are not yet accessible by the existing datasets.

In the following section virtual particles (floats) and a passive tracer were used together with the four year mean of Exp1 to infer how the South Atlantic (SA) water reaches the North Atlantic (NA). Fortunately, the mean pathways and the mean transports in the Atlantic do not differ significantly for studies with constant or seasonal winds (Inui et al. (2001)). To validate the model results, they should be compared with the available observations, but because of the strong temporal and spatial variability a quantitative comparison with far-from-synoptic observations would not be meaningful. As an example, the only quasi-synoptic set of observations that tries to determine the inflow of NA water into the equatorial gyre (Wilson et al. (1994)) does so at a time when the inflow of NA water is at its maxi-

mum (see the analysis of Anderson and Corry (1985)). Instead, the model results of this study were compared with available long term current meter mooring data and the comparison was favorable. This suggest that the model is also able to reproduce other areas reasonably well.

The only other numerical study which our results can be compared to is the one by Fratantoni et al. (2000). Unfortunately these authors mainly discuss how the total mass transport is changed by the MOC and do not analyze the pathways that the SA water takes into the northern hemisphere. Other numerical studies that focus on the cross hemispheric transport have either an insignificant MOC transport or too coarse a resolution.

For analysis purposes we will define SA water as water which originates in the SA and is colder than 23C (see the map in Figure 3.13). Water that is warmer than 23C has been produced in the equatorial (EG) or tropical gyre (TG). The SA water with a temperature between 5.5C and 13.5C will be called AAIW and was discussed in the previous chapter. For the present purposes it is convenient to split the upper water into lower thermocline water (LTW, 13.5C-17C, its upper boundary is shown in Figure 3.14, its lower boundary in Figure 3.15), thermocline water (UTW, 17C-

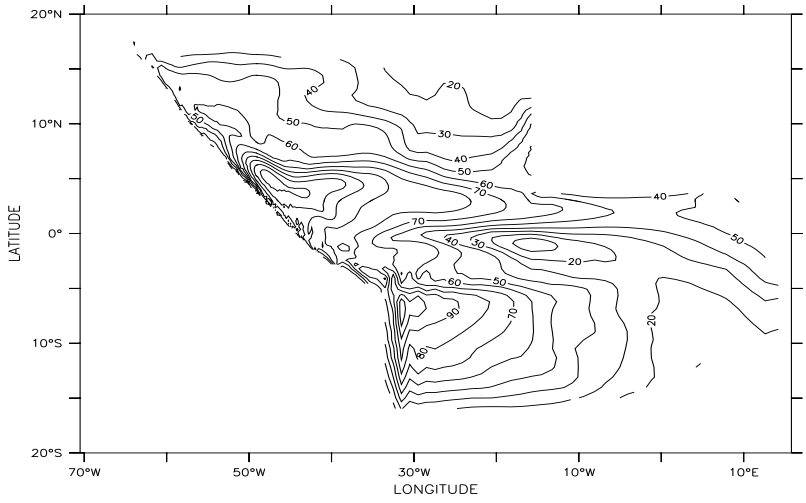


Figure 3.13: Depth of the 23C isotherm in meters.

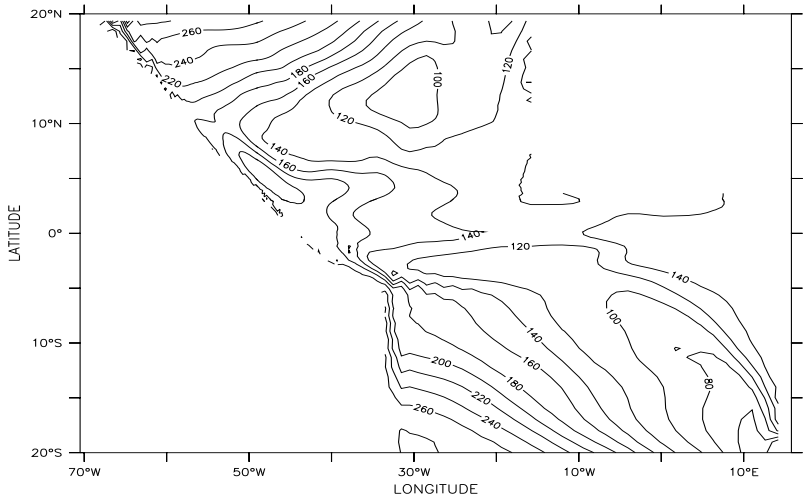


Figure 3.14: Depth of the 17C isotherm in meters.

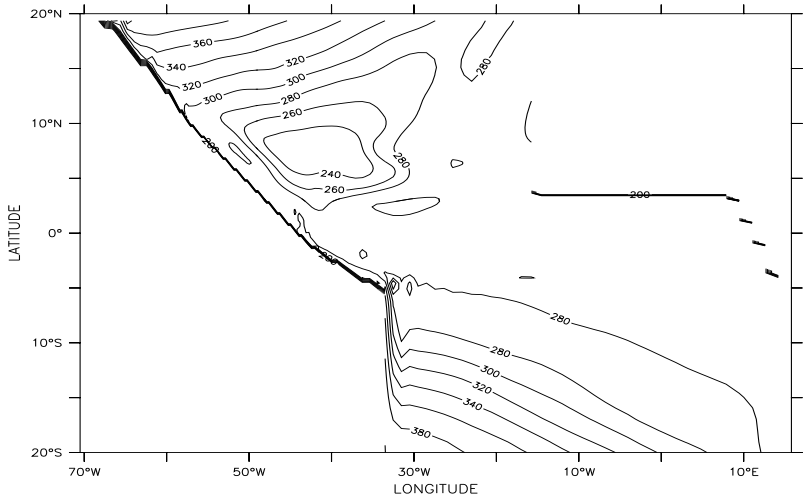


Figure 3.15: Depth of the 13.5C isotherm in meters.

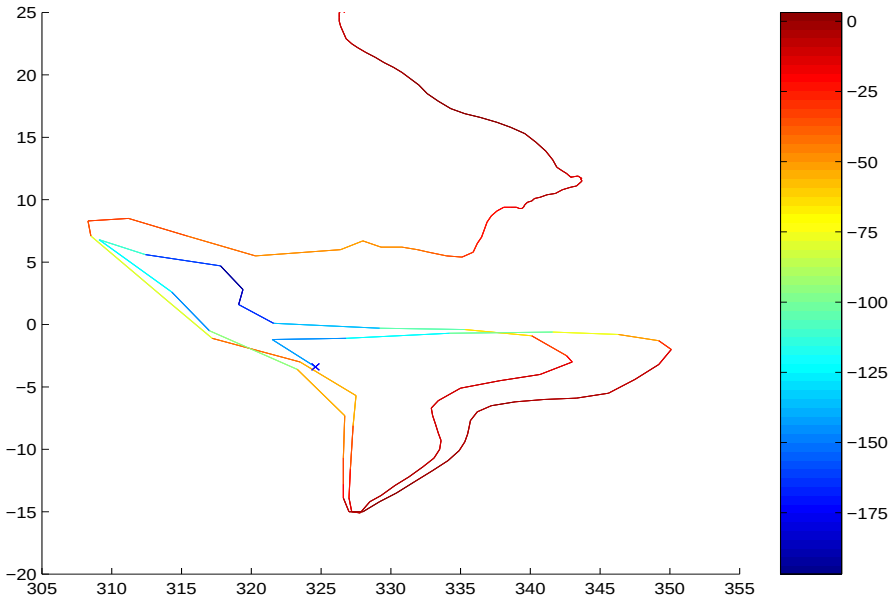


Figure 3.16: The typical path of a float that followed the surface route to the north, the color indicates the depth of the float. After its launch in the UTW, the float enters the EUC, upwells there, recirculates a couple of times in the SEC/EUC system before returning to the NBC in the SW. From there, it retroflects into the NECC and continues its way north in the Ekman layer. 24 out of 50 floats followed this path.

23C) and surface water (SW, >23C).

In the first analysis floats are used to identify pathways. The floats were released between 6S and 8S at the LTW and UTW level and tracked for four years. 104 floats were launched in the UTW and 101 of them entered the EUC, the other 3 moving north in a NBC ring. Out of the 50 floats that left the equatorial gyre within four years, 24 upwelled into the SEC slightly south of the equator, returned to the western boundary to re-enter the NBC (but this time in the SW), then retroflected into the NECC and from there turned north in the Ekman layer (see Figure 3.16 for a typical path). 11 other floats took a similar path, but instead of joining the NECC they were trapped in a NBC ring and traveled north in its core. 15 out of 101 floats upwelled in the SEC but returned south in the Ekman layer. No float was observed to upwell north of the equator and continue north directly in the Ekman layer. This can be explained by the asymmetry of the equatorial wind field: The strongest wind divergence is slightly south of the equator and there is a strong Ekman convergence

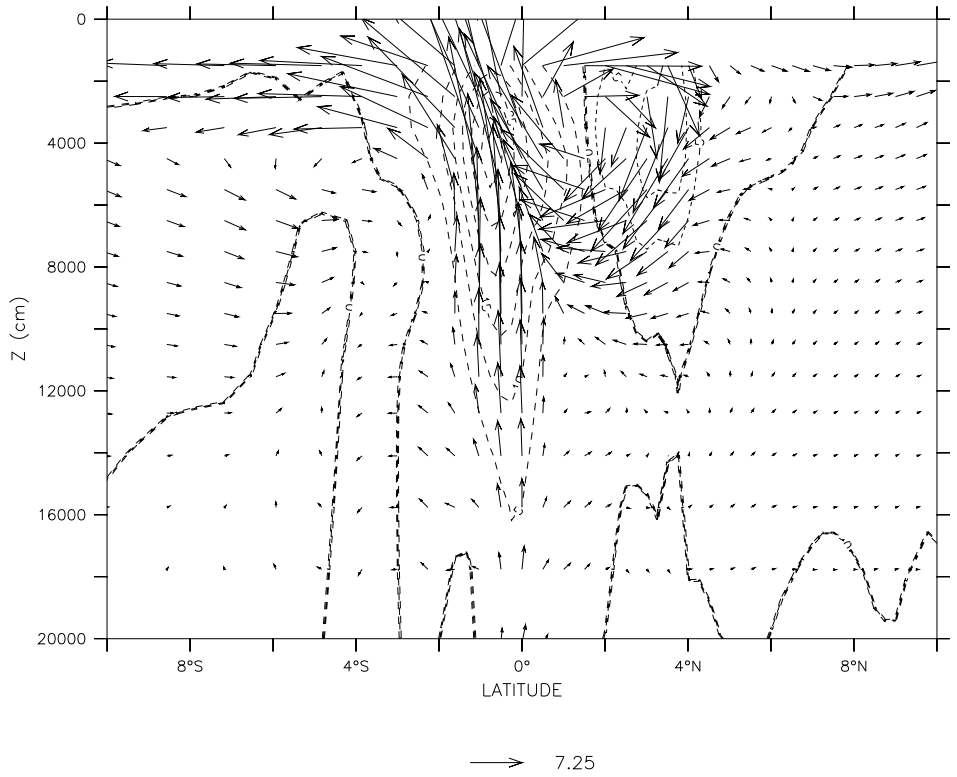


Figure 3.17: The equatorial upwelling cells along the equator, averaged over 4 years from 30W to 20W. The contour lines indicate the strength of the upwelling (contour lines in 5e-6 m/s). Noteworthy is how the center of upwelling is slightly south of the equator and how most of the water north of the equator is downwelled again at 4N, because of the Ekman convergence south of the ITCZ.

at 4N. This leads to a position of the upwelling cells that is shown in Figure 3.17. However, Fratantoni et al. (2000) obtained very different results. Although they used the same wind field used in this study, they found that the Ekman divergence is equally strong north and south of the equator. This discrepancy is presumably due to their method of analyzing the flow field: They estimate the relative contributions by computing the meridional transport in their first model layer at 5S and 5N. However, the core of the NECC is located at 5N, and the water that crosses 5N towards the north does not necessarily come directly from the equatorial upwelling

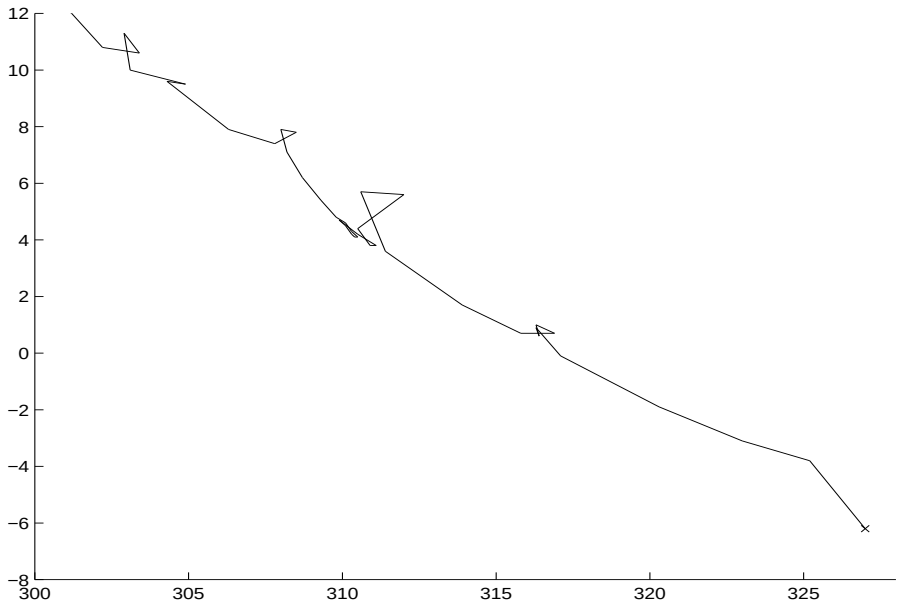


Figure 3.18: The path of a float that has been entrained into a NBC ring. It stays in the LTW throughout its journey. 22 out of 57 floats followed this path.

region, but most likely from the western boundary. The following table gives an overview over the different pathways for floats that originate in the UTW:

| north in a NBC ring | north via the Ekman layer | return south in the Ekman layer | still in the tropics after four years |
|---|---|---|---|
| 14 | 24 | 15 | 51 |

96 floats were launched in the LTW and here the distribution is very different. Only 9 floats took the previously described surface paths (3 to each path), 22 went north directly inside a NBC ring (Figure 3.18), 6 went north in the interior and 20 returned south in the LTW via the southern Tsuchyia jets (Figure 3.19). It is worth mentioning that no float entered the southern Tsuchyia jet from the western boundary. All of the floats came from the equator, a further indication that turbulent momentum fluxes are important for the generation of the Tsuchyia jets. The following table gives an overview over the different pathways for floats that originate in the LTW:

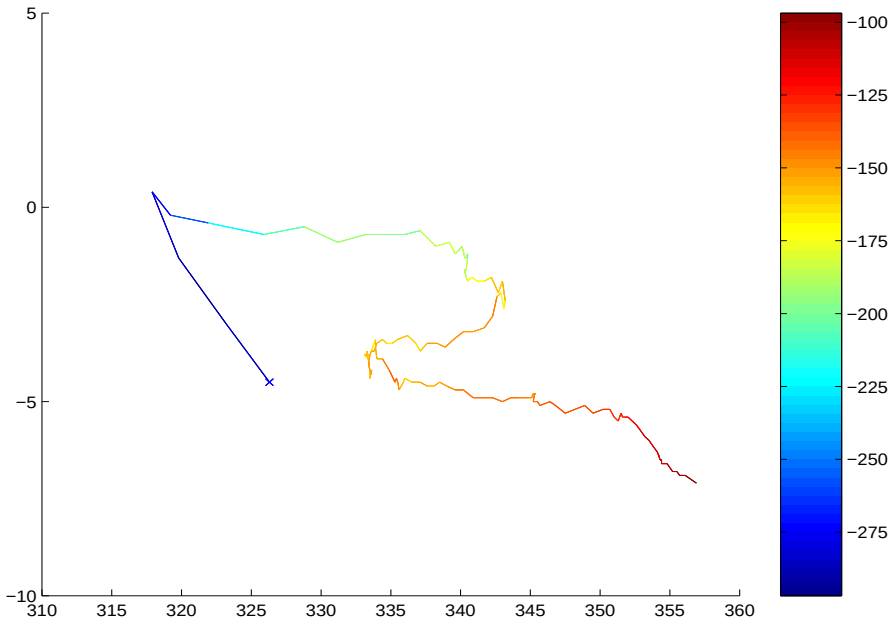


Figure 3.19: The typical path of a float that returns south in the southern Tsuchiya jet. After entering the EUC, the float becomes displaced by waves and then joins the southern Tsuchyia jet. No float joins the jet coming directly from the NBC.

| north in a NBC ring | north via the northern TJ | return south in southern TJ | escape in the Ekman layer | still in the tropics |
|---|---|---|---|---|
| 25 | 6 | 20 | 6 | 39 |

While this trajectory analysis of the floats gives a qualitative idea about the pathways, the floats are too few to make a quantitative statement. Furthermore all floats were all launched at the same time, leading to a bias towards the NBC ring pathway. Out of 25 floats that took this path, 22 arrived at the shedding latitude five to ten months after their launch. This means they arrived there between January and June, exactly the season were one would expect the largest NBC ring transport. Therefore only the time mean flow field will be used to estimate the transports. The mean transports are calculated in the following way:

- The layer depths are based on the mean position of the isotherms that are displayed in Figures 3.13, 3.14 and 3.15.
- The meridional velocities are based on the mean fields shown in Figures 3.20 and 3.21.

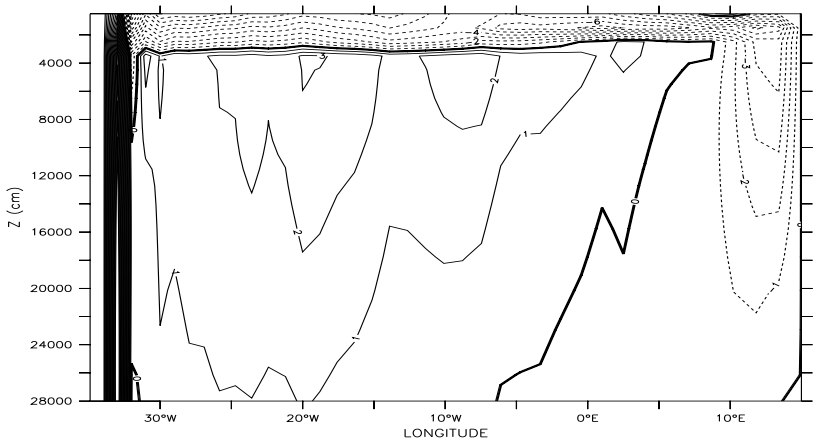


Figure 3.20: The meridional velocity at 15S, the solid lines indicate northward velocity. We can see the narrow western boundary current and the broad interior inflow below the Ekman layer as part of the southern subtropical gyre. In the east we see the outflow from the STJ.

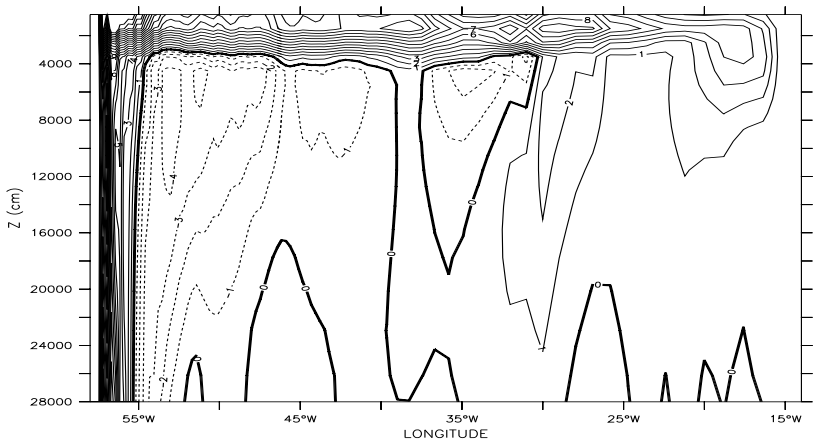


Figure 3.21: The meridional velocity at 10N. We can see the signature of the NBC rings west of 53W and the interior Sverdrup circulation east of it.

- The upwelling is computed as the transport divergence of the overlying layer.
- The passive tracer and the floats are only used for illustrative purposes, never for quantitative estimates.
- The surface layer (Fig. 3.13) is not identical with the Ekman layer but is determined by the mean position of the 23C isotherm.
- The NBC rings annually transport 1 Sv northward (see next chapter), 0.2 in the SW, 0.5 in the UTW and 0.3 in the LTW.

15S is chosen as southern boundary for the analysis because it coincides with the boundary of the EG. 10N is chosen as the northern boundary because this is north of the high eddy activity of the NECC but still south of the Grenada passage and the southernmost entrance to the Caribbean Sea. Because the structure of the flow is qualitatively similar in the LTW and UTW, these two water masses are combined into the thermocline water (TW).

### 3.3.1 The thermocline waters

Based on Figures 3.20 and 3.22 we can see that 17.5 Sv enter the domain at 15S, 8.2 (1.1) Sv in the NBC and 9.3 (1.8) Sv in the interior (the numbers in the brackets denote the standard deviation of the transport). At 6S the 9.3 Sv from the southern subtropical gyre join the NBC. 1.5 (0.4) Sv of this water returns south in the Ekman layer in the eastern part of the domain where the TW layer outcrops, and the sTJ takes 2.5 (1.0) Sv back across 15S (see Figures 3.19 and 3.20). Thus, there is a net inflow of 13.5 Sv of South Atlantic water into the tropical TW layer (see Figure 3.25 for a diagram). Furthermore, there is an upwelling of 0.9 Sv of AAIW into the TW layer.

We now focus on the section at 10N (Fig. 3.21). 0.8 Sv of the SA TW are trapped in NBC rings and leave the basin in the north (see next chapter). East of the ring path (53W), 3.2 (2.9) Sv of NA water enter the domain and 3.9 (1.8) Sv of water leave the domain between 30W and the African coast (Figure 3.21). This flow is the Sverdrup flow of the tropical gyre below the Ekman layer. Mass conservation implies that at least 0.7 Sv of these 3.9 Sv originate in the SA. Because the thermocline

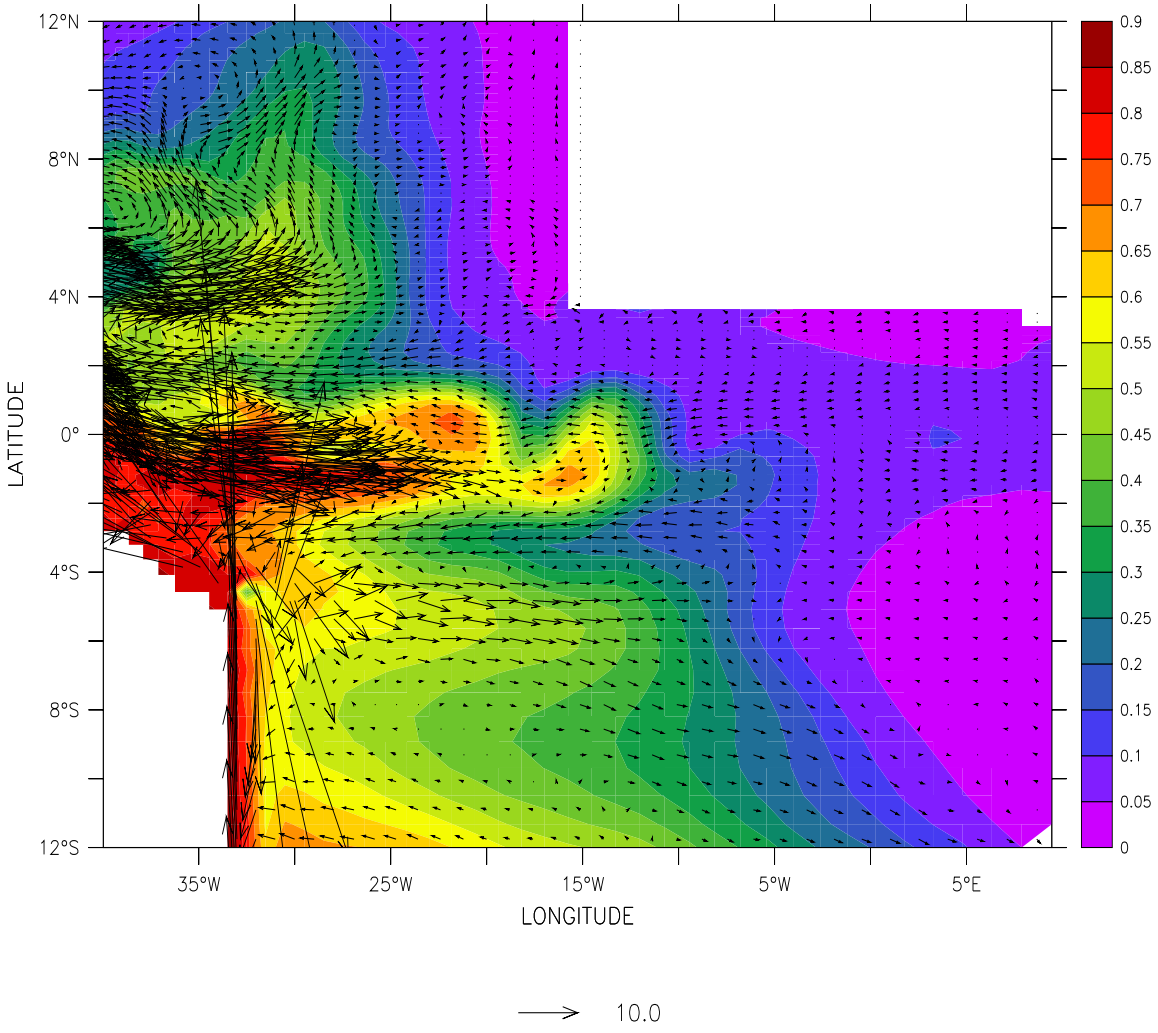


Figure 3.22: The concentration of a passive tracer and the time mean velocity on the 15C isotherm. We can see the two tracer tongues caused by the TJs at 5S and 5N as well as a extension of the northern tongue across 10N at 30W.

flow is southward south of 5N (Fig. 3.17) this water has to be supplied by NECC and the nTJ. Evidence for this can be seen in Figure 3.22, where we see a tracer tongue reaching east from 4N and then north at 30W. The total convergence in the TW layer is 12.9 Sv and this water upwells along the equator and the NBC/NECC

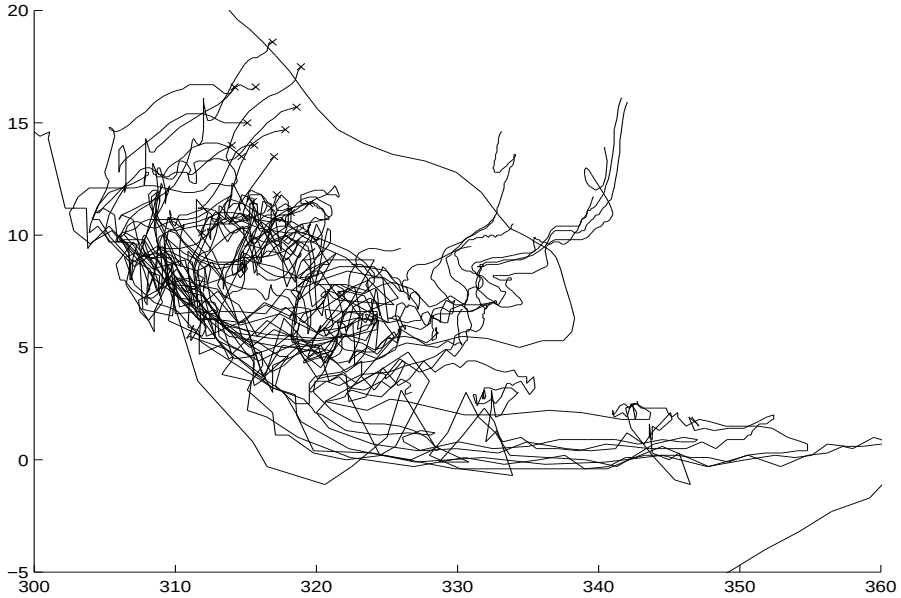


Figure 3.23: The path of several floats that were released in the TW between 10N and 20N and have entered the EG. 'x' denotes the launching position. Some of them return in the eastern basin whereas others are entrained in the EUC and will eventually supply the Ekman layer.

retroflection region into the SW. The source of this upwelled water will most likely be the South Atlantic. However, given the strong eddy activity in this region, one cannot exclude the possibility that part of the NA water does not return directly in the tropical gyre but instead becomes mixed across the NECC and NTJ and ends up at the equator. The trajectory analysis of Figure 3.23 and the tracer minimum between 40w and 30w at the equator (Figure 3.24) suggest an entrainment of NA water into the EUC. If one assumes that all of the NA water recirculates in the tropical gyre then all of the upwelled water must be of SA origin. The other extreme would be to assume that all the TW from the NA joins the EUC and upwells along the equator. In that case one would expect at least 9.7 Sv of the upwelled water to be of SA origin because not more than 3.2 Sv of NA water enter the tropical Atlantic in the TW. Similarly, we don't really know how the water enters the STJ, which has a strong seasonal cycle. The float trajectories (Fig. 3.19) indicate that it is fed by the EUC, but the time mean flow field suggests that direct supply from the NBC is possible as well. Chapter Seven will give a detailed account of the dynamics

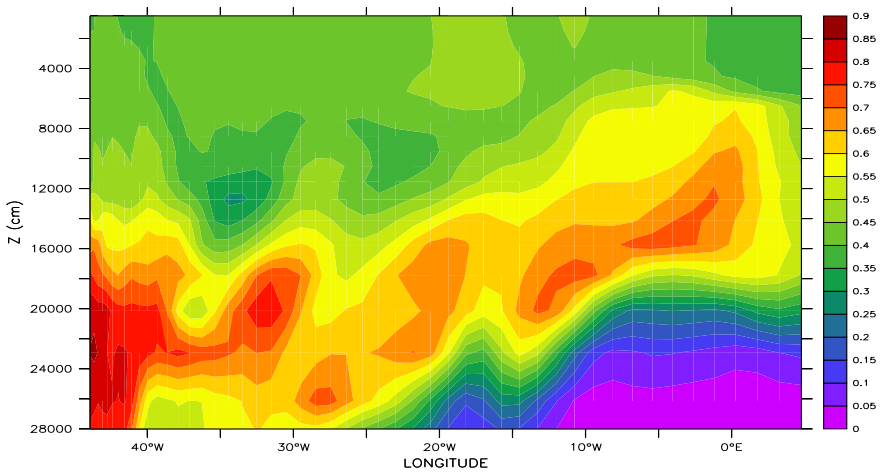


Figure 3.24: Tracer concentration along the equator. Note the minima between 40W and 20W which are caused by entrainment of NA water.

and sources of the TJs. Given the 4-D structure of the flow, all the diagrams should certainly be used with caution.

The interior path, in which SA water joins the NECC and nTJ and turns north in the interior is not described in Fratantoni et al. (2000), although their model results do allow for an interpretation that points towards an interior path. This is because they focus on the total mass flux instead of the pathways (D. Fratantoni, pers. comm.), thereby avoiding to differentiate between the waters from the NA and the SA. As seen in our model, it is difficult to give a quantitative account for the different water masses, but it is still worth pointing out that a potentially important interior path exists. To our knowledge this path has not been described before, although it is more important than the NBC ring pathway and can, depending on the details of the tropical circulation, rival the thermocline-surface path in importance. In this model, the interior thermocline path accounts for approximately between 0.7 Sv and 3.9 Sv of the MOC return flow. Schmitz and Richardson (1983) find that the Florida current contains 0.8 Sv of SA thermocline water which suggests that this interior path might not be very important. This path, however, is so convoluted that it cannot be expected that the SA thermocline water exactly conserves its properties

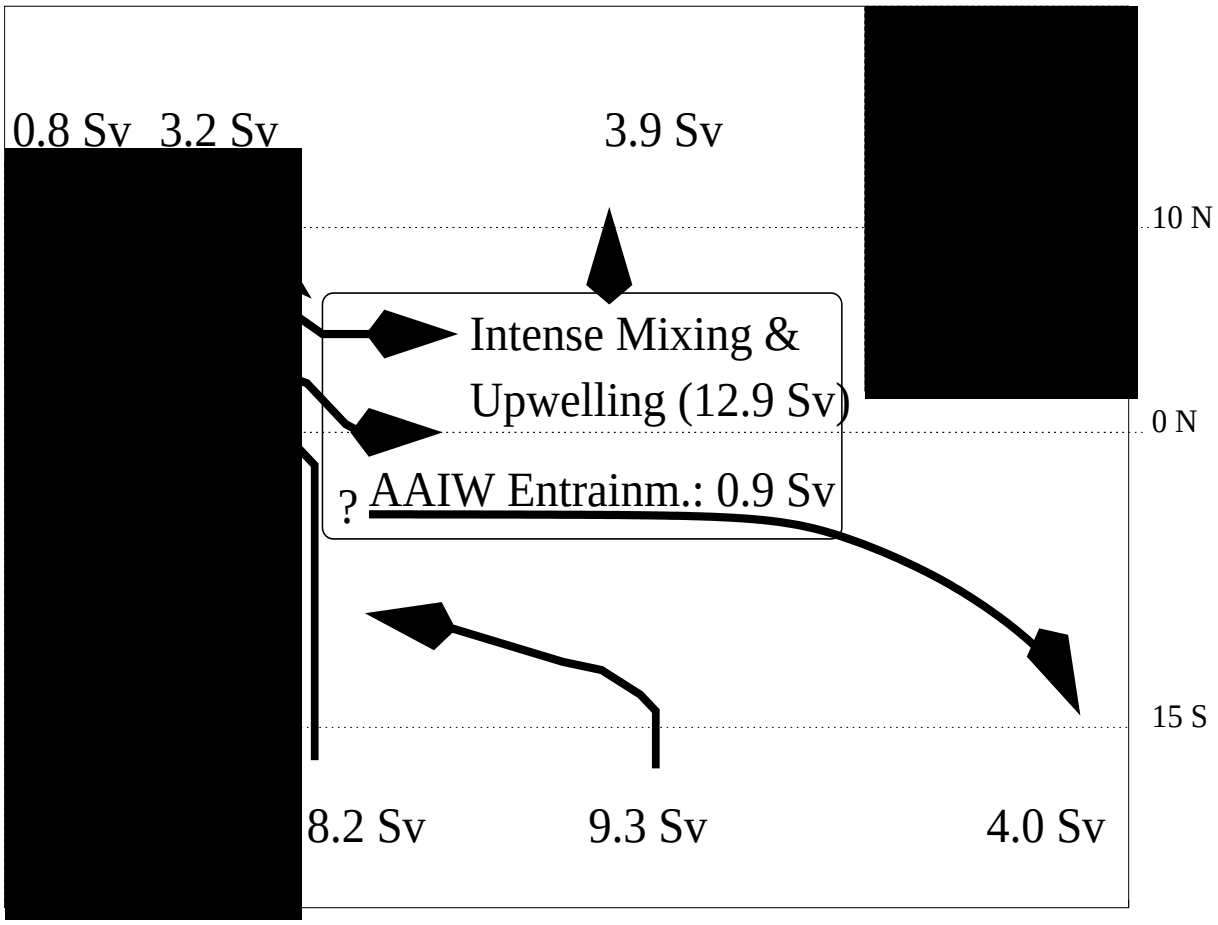


Figure 3.25: A cartoon of the circulation in the tropical Atlantic. The NBC feeds the EUC and NECC. Furthermore, there is inflow of NA thermocline water and upwelling of AAIW. The water leaves the domain in NBC rings (the circle in the northwest corner), in the interior as part of the tropical gyre and in the south across 15S via the STJ and the Ekman layer.

along the way. Weak observational evidence for this interior path can be found in Cochrane et al. (1979), who analyzed historic hydrographic data in the tropics. The published acceleration potential indicates a weak northward flow east of 30W across 10N that is, as in our model, fed by the NTJ. An overview of the time mean path of TW is presented in Figure 3.25.

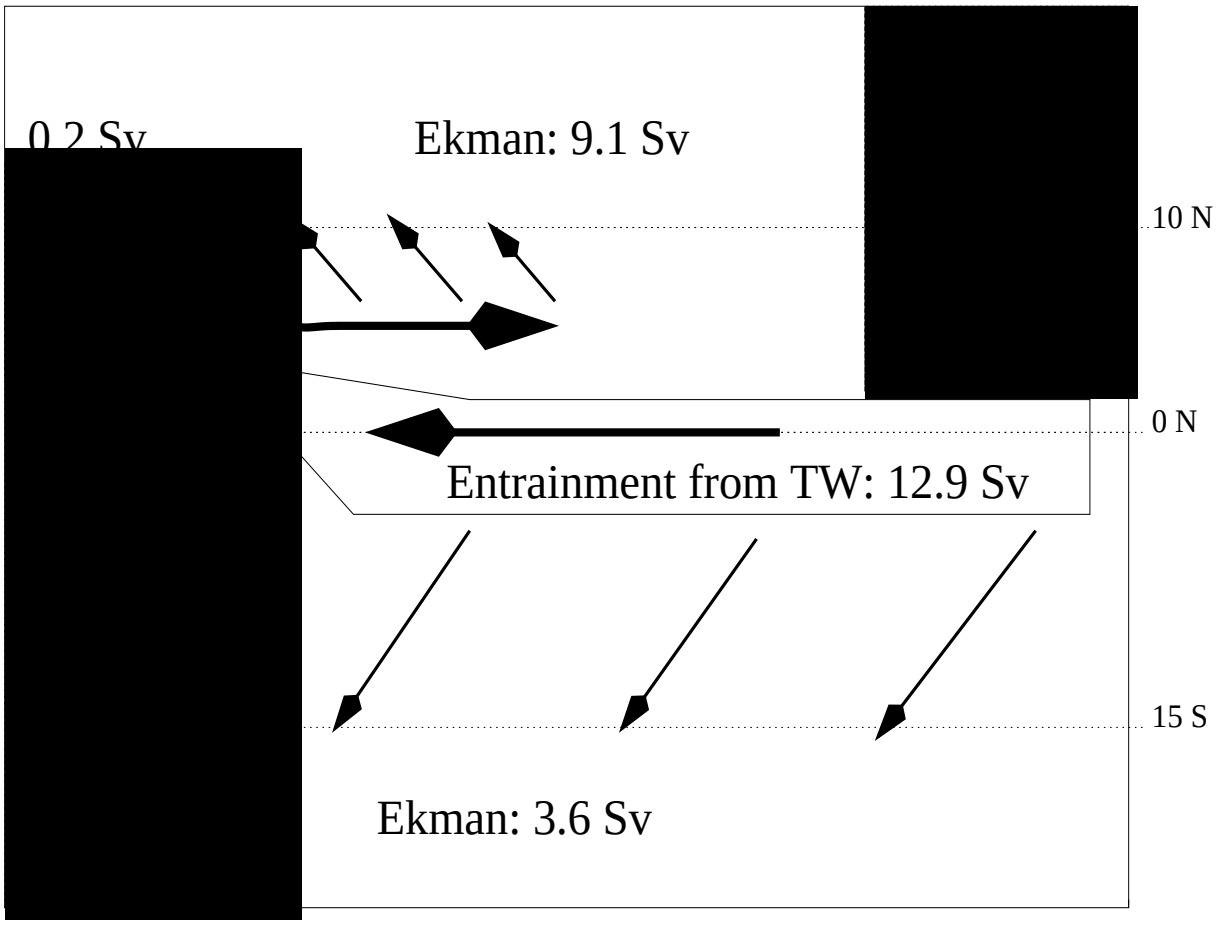


Figure 3.26: A cartoon of the pathways of South Atlantic water after it upwelled into the equatorial mixed layer. Note that there is no direct flow from the equator to the NECC: After upwelling the water must return to the western boundary and enter the NECC via the NBC.

### 3.3.2 The surface waters

For the Hellerman-Rosenstein wind field the Ekman divergence between 10N and 15S is 19.7 Sv; the model calculation for the surface layer (warmer than 23C) shows a total divergence of 12.9 Sv, 3.6 (2.0) Sv leaving the domain to the south and 9.3 (4.5) Sv to the north (Figure 3.26). The difference between these two values is due to the fact that the surface layer is not identical with the Ekman layer everywhere and that it contains Ekman transport as well as geostrophic transport. The ratio of NA/SA involved in the upwelling and the position of the upwelling maximum

makes it reasonable to assume that only a negligible amount of NA water reaches the southern subtropical gyre. This means that 3.6 Sv of upwelled SA water returns south in the Ekman layer. The Ekman transport in the north consists of NA and SA water, the ratio depending on our assumptions of the fate of the entrained NA thermocline water. If the maximum amount of NA water upwells, we would conclude that the northward transport through the surface layer consists of 5.9 Sv of SA water and 3.2 Sv of NA water. The minimum amount of NA upwelling would yield a relation of 8.8 Sv to 0.3 Sv. Likewise, the interior thermocline path for SA water to reach the NA contains between 1 Sv and 3.9 Sv of SA water. This is in stark contrast to the results of Fratantoni et al. (2000), who find that no SA water is transported north in the thermocline and 3.8 Sv is transported north in the surface layer along the western boundary, 3 Sv of which are trapped in NBC rings and 0.8 Sv flow in a northward western boundary current (which does not exist in our solution). However, their values are based on model results AND observations, rendering it difficult to make a quantitative comparison between our model results and theirs.

# Chapter 4

# The importance and generation of North Brazil Current rings

## 4.1 Introduction

Since their first description a decade ago (Johns et al. (1990) and Didden and Schott (1993)), NBC rings have received increasing attention. Their dynamics not only pose a GFD problem, but the rings are also thought to transport a significant part of the return flow of the meridional overturning circulation (MOC). The NBC rings are shed at the western boundary of the tropical Atlantic where the North Brazil Current (NBC) retroflects into the North Equatorial CounterCurrent (NECC). After separating from the retroflection region, NBC rings travel northwest along the Brazilian coast and carry water of South Atlantic origin northward, some of it into the northern subtropical gyre (Fratantoni et al. (1995)).

The NBC rings are difficult to study, theoretically as well as observationally. The flow field and location of their origin renders the problem highly nonlinear (see, however, da Silveira et al.'s (2000) quasi-geostrophic approach). Furthermore, the proximity of the western boundary and the nonzonal nature of the NBC makes it difficult to understand the instability by applying classical methods (see Pedlosky (1979) for a review of instability theory). Unfortunately, the problems are not only of theoretical nature. Merely estimating the large-scale flow field in the tropical Atlantic is very difficult due to the existing strong seasonal cycle (see Johns et al. (1998) or Schott et al. (1998)). All this makes OGCMs a natural tool to study the

NBC rings, although the uncertainties of OGCMs due to uncertain boundary conditions are well known. Because the focus of our study is on NBC rings, an OGCM is constructed that is as simple as possible but still reproduces all the features that theory and observations suggest are important. Then this model is used to weave together the different ideas which are thought to be important for the NBC rings' life cycle.

This work is part of an ongoing effort to single out specific processes and to understand them in relation to the complex circulation of the tropical Atlantic. The first part of this effort focused on the impact of the MOC on the tropical circulation (Jochum and Malanotte-Rizzoli (2001)). Here, the focus is on the dynamics and importance of NBC rings. This "bottom up" approach contrasts the work of Fratantoni et al. (2000): they used a very realistic OGCM to describe in detail the circulation in the tropical Atlantic, and pointed out potentially important processes. Their purpose was not, however, to explore the detailed dynamics of those processes. The NBC rings represent one such process in the tropical Atlantic and in this paper will address the following questions:

- How are the North Brazil Current rings generated?
- What explains their vertical structure?
- What is their significance for the MOC?

The following section will describe the model and the subsequent sections will each address one of the aforementioned questions. The last section provides a discussion and will put out work into context.

## 4.2 The Ring Shedding

### 4.2.1 Rings without wind

The previous chapter showed that the model is capable of generating realistic NBC rings and we can now explore their generation mechanisms in more detail. It is helpful for our understanding to analyze exp3 (without wind) first. In this experiment

the water enters the domain through the southern open boundary, moves north along the western boundary (only there can it change its potential vorticity) and leaves the basin again through the northern boundary. Near the equator the flow breaks up into eddies (about 6 per year) that propagate northwest along the coast (Figure

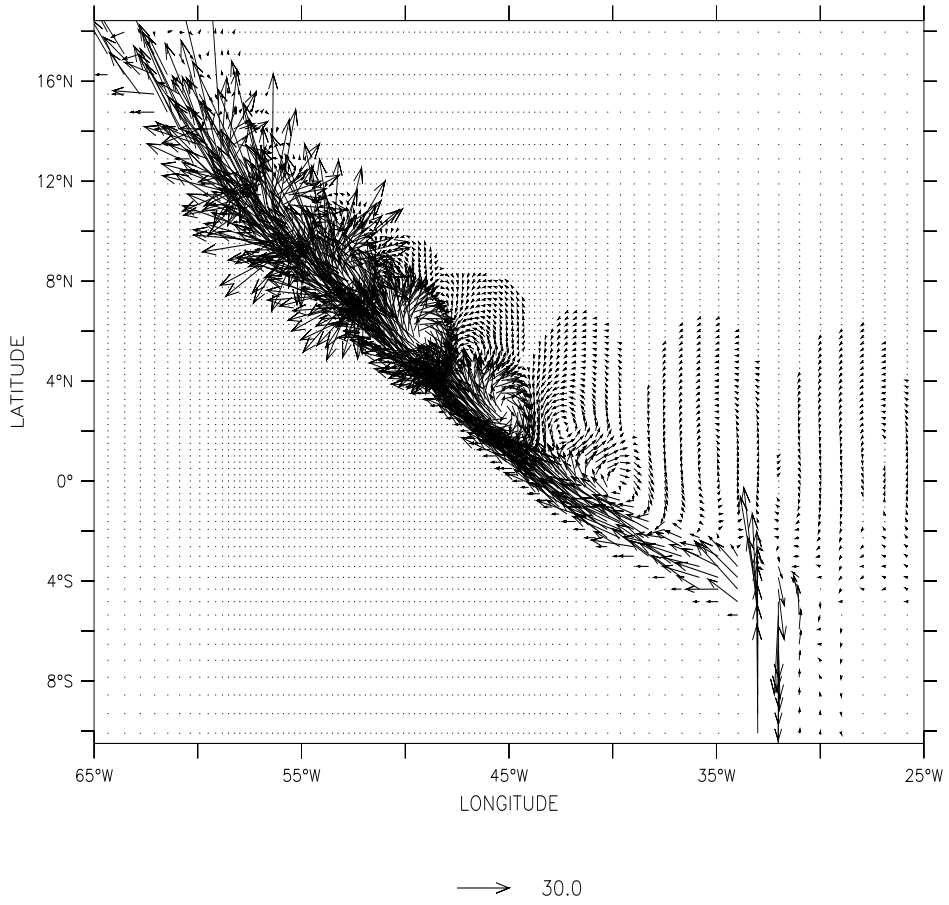


Figure 4.1: A snapshot of the flow field at 50m depth in exp3. The western boundary current approaches the equator as a laminar flow and breaks up into eddies on crossing the equator. These eddies become stronger as they continue north until they move beyond 12N where the decreasing resolution and increasing viscosity dissipate them. The flow continues then as a laminar western boundary current until it leaves the model domain at 30N.

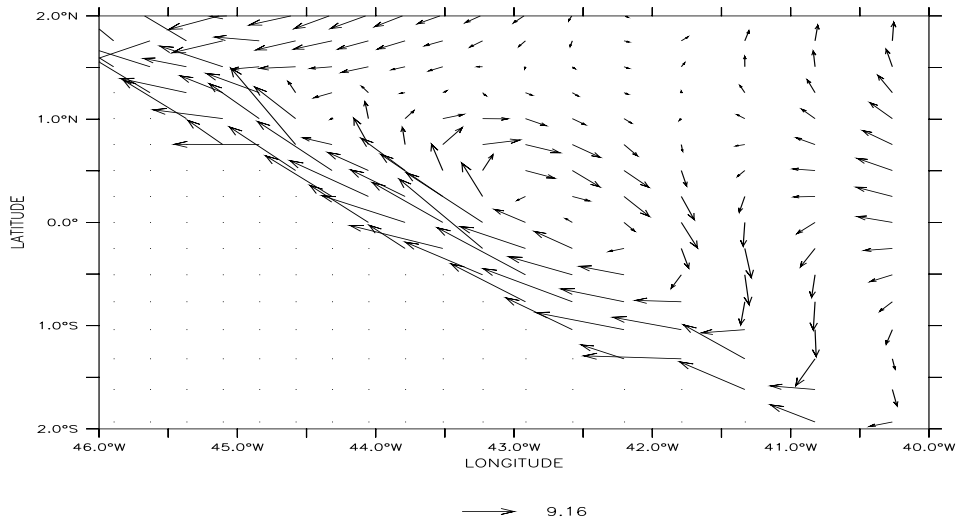


Figure 4.2: The flow field of an eddy that has been shed by the IWBC at 700m depth.

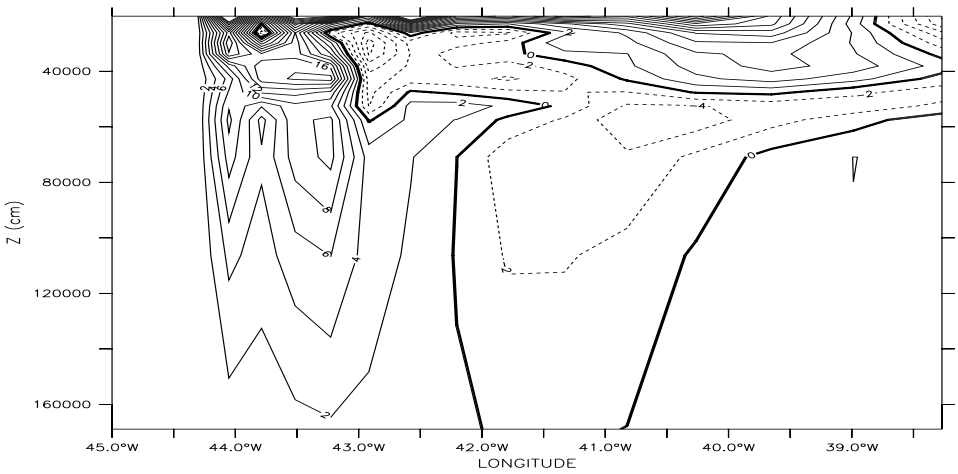


Figure 4.3: The profile of the meridional velocity in the intermediate eddy of Figure 4.2 at the equator (in cm/s). The center of the eddy is at 42.5W and it reaches from 400m down to 1500m depth.

4.1). This effect has been thoroughly analyzed in a paper by Edwards and Pedlosky (1998): on crossing the equator, the water must change the sign of its potential vorticity, but if the frictional boundary layer becomes too thin, the flow must break up into eddies to achieve this.

If wind is added as an additional forcing, the surface and thermocline waters may have other means of changing their potential vorticity: wind in the Ekman layer or diabatic mixing in the upwelling regions. However, the water below the thermocline will be largely unaffected by the wind (most of the upwelling happens in the upper 300m). Therefore, for subthermocline and intermediate flow (not distinguished in the present analysis), similar dynamics as for the flow without wind is to be expected. Figures 4.2 and 4.3 show that this is indeed what happens: We see an intermediate eddy (without any thermocline signal) after it was created upon crossing the equator. This intermediate eddy will continue north along the coast (see section 4). As in the case without wind, there are about six eddies created every year.

### 4.2.2 No rings with wind

Observations show that after crossing the equator most of the surface and thermocline water feeds the EUC and the NECC at around $2^oN$ and $7^oN$ respectively (Schott et al. (1998)). The numerical solution shows that a small part of it enters a recirculation gyre that is part of the NBC/NECC retroflection and is centered at approximately $4.5^oN$. This recirculation gyre is the seed for a NBC ring (as shown observationally by Johns et al. (1990)). It is important to note that the flow does not break up into eddies before $4^oN$. Thus the dynamics between the upper layer (0-300m) and the intermediate layer (300-1000m) must be different. First of all, the NBC entrains high potential vorticity water from the northern South Equatorial Current (SEC) that replaces the low potential vorticity water which the NBC lost to the EUC. Secondly, the upper layer flow is highly nonlinear. This can be verified by comparing their Reynolds numbers, defined as $UL/A_h$ where L is the current width. The intermediate layer has a Reynolds number of about 30 with speeds of around 10cm/s whereas the upper layer can reach Reynolds numbers of more than 500 and speeds of up to 2m/s. This suggests that we may treat the upper layer flow

as an inviscid system.

Killworth (1991) studied the inviscid adjustment problem for cross equatorial flow and found that a highly nonlinear flow can penetrate more than two Rossby radii of deformation into the Northern Hemisphere without any adjustment of its potential vorticity. But to compensate for the lower angular momentum of the higher latitudes, the water has to gain eastward momentum upon flowing north. This leads to the third major difference between the upper and the intermediate layer. The intermediate layer water has to flow north not only two Rossby radii but all the way to the northern boundary where it leaves the basin again because of the northern open boundary conditions. On the other hand, the upper layer water has an immediate sink nearby the equator - the wind-driven NECC. Eventually it has to change its potential vorticity too, but it can do so with the help of the wind in the Ekman layer of the tropical gyre. Figure 3.2 illustrates this path: the water leaves the NECC (the convergence of lines at $5^oN$) in the interior and flows north in the Ekman layer which contains most of the transport of the tropical gyre.
Killworth (1991) never actually mentions the NBC or the NECC, and his studies are too idealized to claim an equivalence between his results and our upper layer NBC. However, we still believe that his work explains the basic dynamics of the upper layer cross hemispheric flow.

### 4.2.3 The role of Rossby waves

We now discuss the mechanism of shedding of NBC rings. To ensure that the observed variability is not directly caused by fluctuations in the wind field the results from exp2 (steady winds) will be discussed here. The main differences between exp1 and exp2 with regard to the rings are that the rings in exp1 are more variable in strength and that the generation frequency in the two experiments is slightly different (every 50 days in exp1 and every 70 days in exp2).

Ma (1996) proposed the following generation mechanism: a long Rossby wave reflects at the western boundary and creates a short Rossby wave with its characteristically high anomalies in relative vorticity. Due to the $\beta$-effect and the interaction with the boundary those potential vorticity anomalies detach from the reflection

region and propagate northwest along the coast. While this is indeed what happens in our model, Ma (1996) does not discuss the process in detail as we do below.

A close look at the properties of the dominant waves in our model reveals a phase speed c between -9cm/s and -13cm/s (Figure 4.4), a meridional wavenumber l of approximately $2\pi/1200km$, a zonal wavenumber k between $2\pi/700km$ and $2\pi/900km$ (Figure 4.5), and a period of approximately 70 days (Figure 4.6). The background velocity U was calculated by averaging over an area 500km x 500km centered at 7N/44W and estimated to be at 10cm/s.

From these values the dispersion relation can be computed:

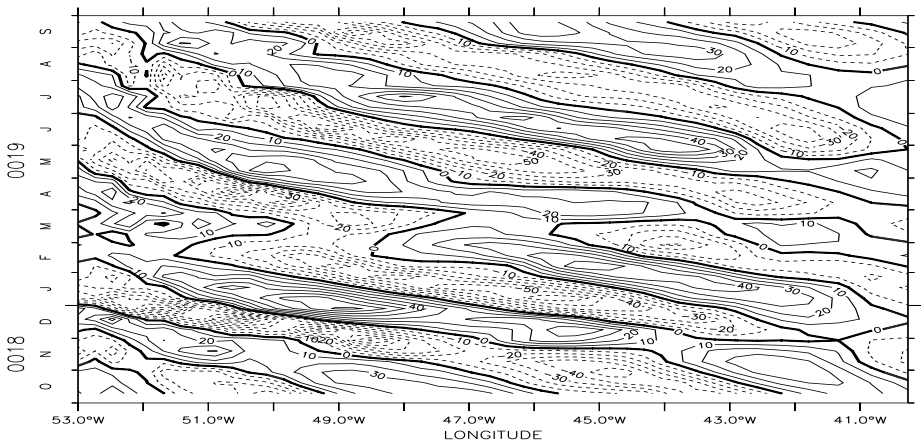


Figure 4.4: Hovmoeller diagram of the anomalies of the meridional velocity at 6.8N and 100m depth (in cm/s). The phase speed of those anomalies is approximately -10cm/s.

$$c = \frac{U(k^2 + l^2) - \beta}{k^2 + l^2 + \lambda^{-2}} \tag{4.1}$$

with $\beta = 2.4e - 11/ms$ and the deformation radius of the first mode $\lambda = 115km$ (Pedlosky (1979)). The result is shown in Figure 4.7. We see that our observations are consistent with the idea that the spectrum is dominated by long Rossby waves of the first baroclinic mode. A further indication for this can be found by looking at the vertical structure of the waves (Figure 4.8).

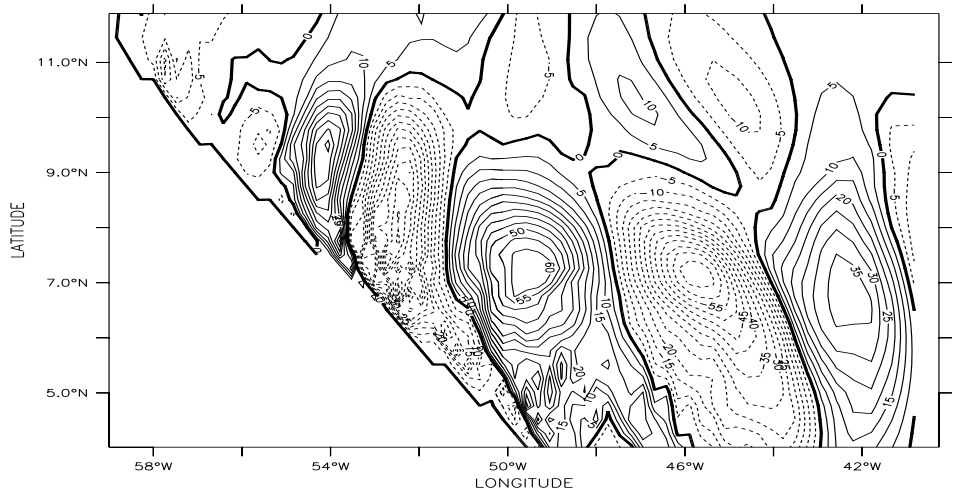


Figure 4.5: Anomalies of the meridional velocity at 100m depth (in cm/s). This is an indication of a Rossby wave approaching the coast and reducing its wavelength upon reflection to the North.

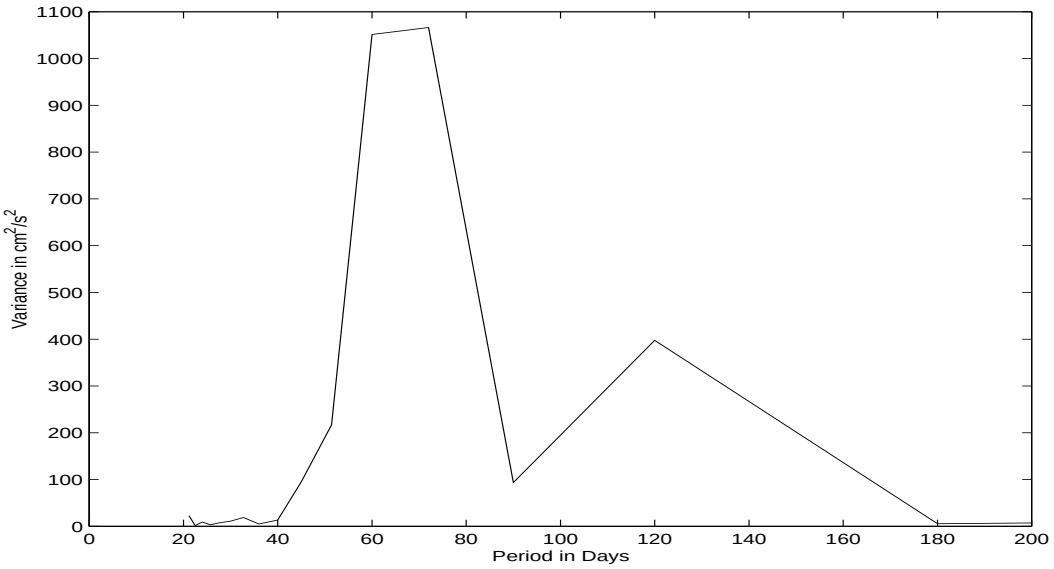


Figure 4.6: Energy spectrum of anomalies of meridional velocity at 6.8N/44W in 100m depth. The peak corresponds to a period of 70 days.

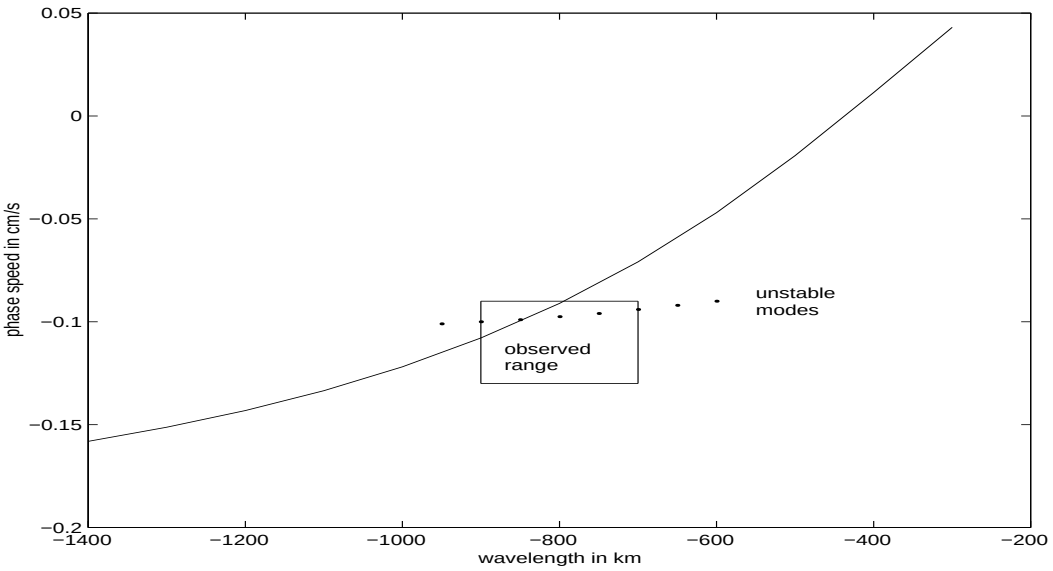


Figure 4.7: Dispersion relation for a first baroclinic mode Rossby wave with a background velocity of 10cm/s and a meridional wave length of 1200km. The box indicates the range of the observed waves and the dots the phase speed of the most unstable modes (see later in the text).

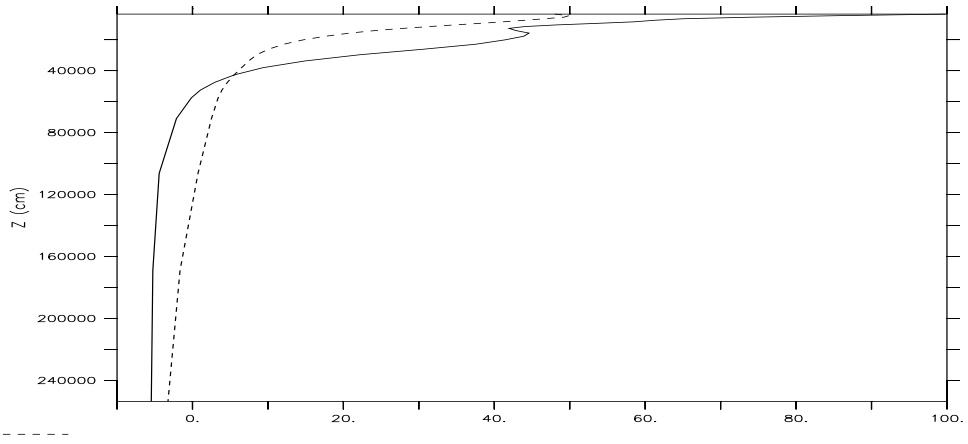


Figure 4.8: Vertical profile of meridional velocity anomalies at 6.8N (in cm/s). The stippled line is the profile at 42W, the solid line the profile at 50W (snapshots taken at the same time). The wave doubled its amplitude between 42W to 50W.

We discuss now how such a wave reflects at the Brazilian coast. Following LeBlond and Mysak (1978) Rossby wave energy is reflected according to Snell's law. This yields the wavenumbers of the reflected wave (graphically one can obtain the results by using a slowness circle with an inclined coastline). For a Rossby wave with $\lambda_x$ between 700km and 900km and $\lambda_y \approx 1200$km, the reflected zonal wavelength would be between 400km and 500km (Fig. 4.9). The resulting group velocity would be northwestward along the Brazilian coast. This compares well with the model result of 400km (Figure 4.5). Johns et al. (1990) find first mode baroclinic Rossby waves at 8.5N/52.1W (where the reflected wave would already be present) with a timescale of 40-60 days and wavelengths between 390km and 740km.

It is difficult to prove that what we see is indeed a first mode Rossby wave. The

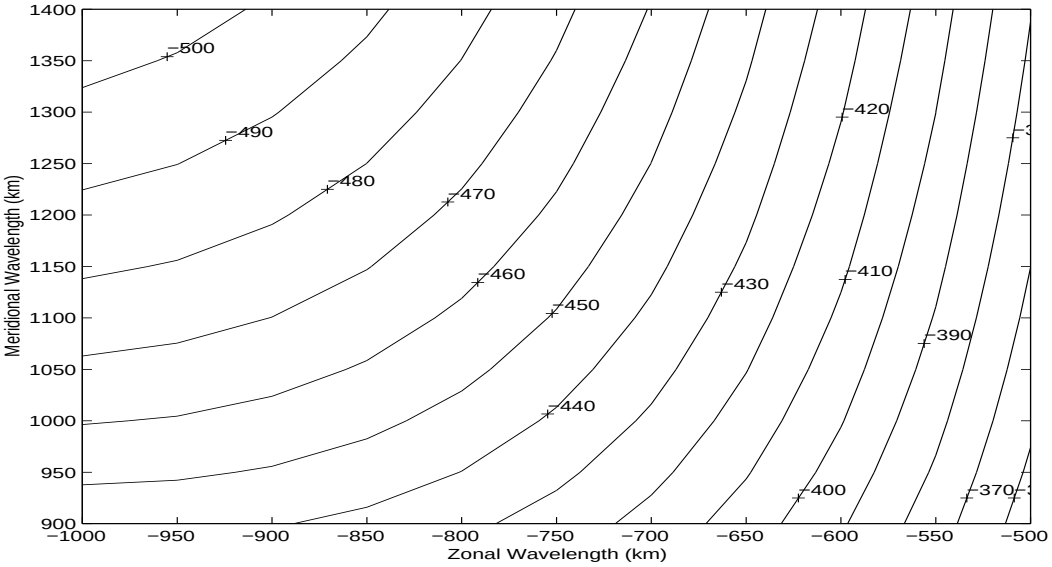


Figure 4.9: The zonal wavelength of a reflected Rossby wave (in km) as a function of the properties of the incident wave.

background flow and the stratification are by no means homogeneous, the waves are nonlinear and they are growing while they are propagating west (Figure 4.8). The reflection problem is clearly not straightforward either, because a part of the Brazilian coast is dominated by the strong NBC. However, the close resemblance of our results with theoretical predictions and observations gives us confidence in our interpretation. Given that the structure of these first mode Rossby waves is not the main focus of this work, the interested reader is referred to Johns et al. (1990) and

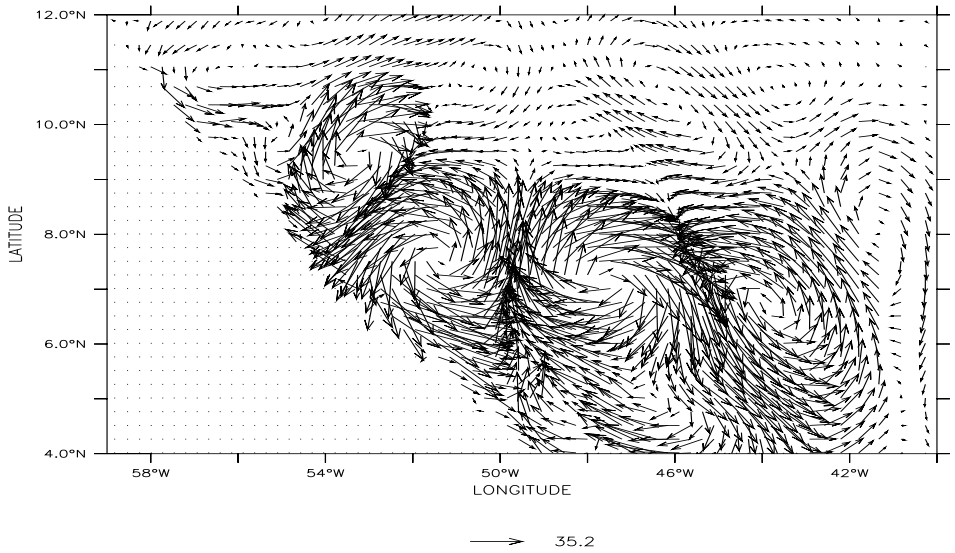


Figure 4.10: The vectors of velocity anomalies at 100m for the same time as in Figure 4.5.

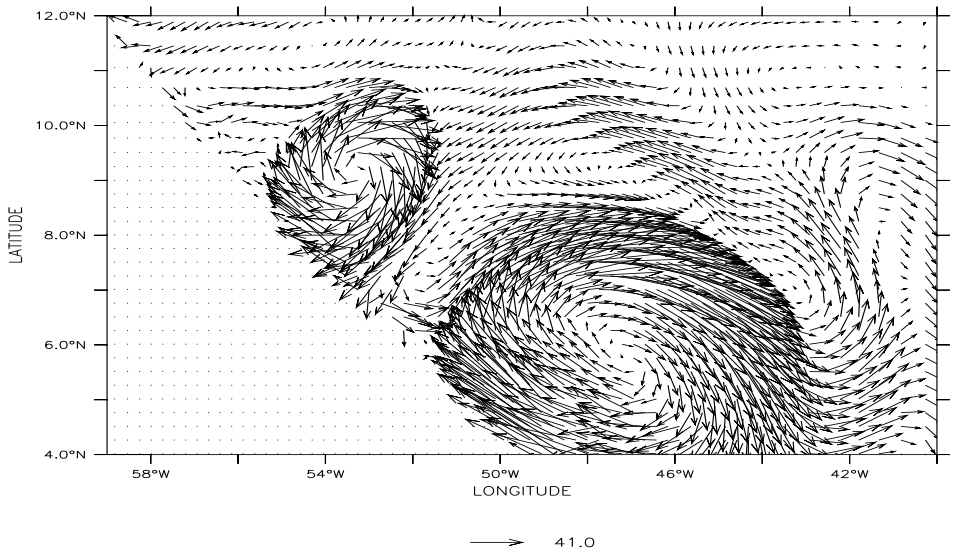


Figure 4.11: Like previous figure but for absolute velocity.

McClean and Klinck (1995) for an in depth discussion of their properties.

We now discuss how the Rossby waves on the NECC relate to NBC rings. There are about five NBC rings generated every year which is the expression of the 70d period Rossby waves. The analysis of the model results show that indeed every anticyclone sheds a ring. The details of this process are displayed in Figures 4.10 and 4.11. Figure 4.10 shows the velocity anomalies of a Rossby wave (the same wave as in Figure 4.5). We see as in Figure 4.5 that the wave becomes deflected northwestward and propagates along the coast, cyclones and anticyclones being equally strong. The absolute velocity gives us a very different picture (Figure 4.11): after the reflection the anticyclones are much stronger than the cyclones. This suggests that the anticyclonic NBC/NECC retroflection acts as a filter for the incoming Rossby waves: cyclones become weaker or eliminated, whereas anticyclones become amplified and transformed into nonlinear NBC rings.

### 4.2.4 The unstable NECC

Finally we have to discuss the generation mechanism of the Rossby waves. The wind is steady, therefore their cause must be the internal dynamics of the ocean. At these latitudes it is difficult to achieve baroclinic instabilities in eastward flowing currents (Pedlosky (1979), ch 7.9), but it turns out that the NECC fulfills the necessary conditions for barotropic instability ($u_{yy} > \beta$) throughout most of the year (Figures 4.12 and 4.13). Moreover, the amplitude of the wave doubles while the wave propagates from 42W to 50W (Figure 4.8). Our results are different from the findings of McClean and Klinck (1995), who found that the NECC in the CME model is not barotropically unstable. Of course, the fact that $u_{yy}$ exceeds $\beta$ does not establish the fact that the NECC is barotropically unstable. Therefore we investigate where the Rossby waves draw their energy from. Following Masima et al. (1999) we compute the energy flux from eddy available potential energy to eddy kinetic energy (baroclinic conversion, $-g\rho' w'$) and from the mean kinetic energy to eddy kinetic energy (barotropic conversion, $-\overline{u'v'}U_y$). Figure 4.14 and 4.15 show the results. Locally, the baroclinic conversion is an order of magnitude smaller than the barotropic conversion. This strongly suggests that barotropic instability is a generation mechanism for

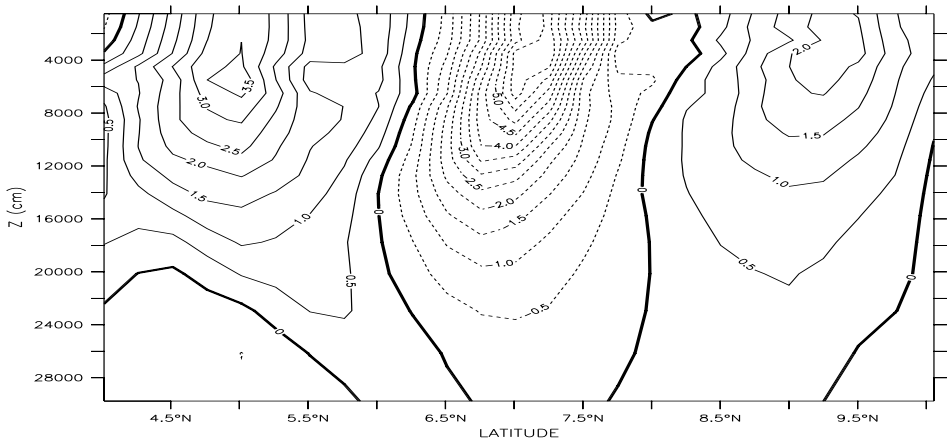


Figure 4.12: The time mean value of $u_{yy}$ in exp2 in a cross section at $44^oW$ (in $(ms)^{-1}$, scaled by 1e11). The NECC is potentially unstable where the value exceeds 2.4 ($= \beta$).

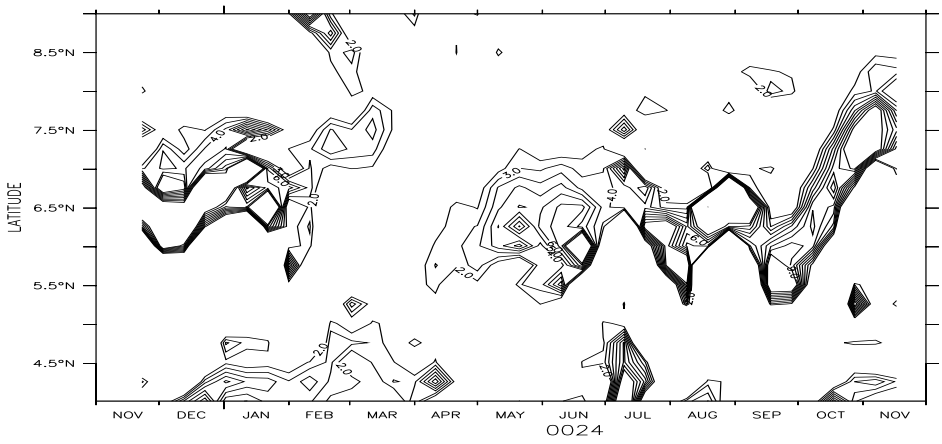


Figure 4.13: Value of $u_{yy}$ in 80m depth for exp1 (scaled again with a factor of 1e11). Shown is the value only in areas where $u_{yy}$ exceeds 2. We see that even in the case of seasonally varying wind the NECC is potentially unstable throughout the year.

the waves that trigger the ring shedding. However, if the energy fluxes are averaged over the unstable area of the NECC (5N-10N, 50W-42W, 0-100m), the barotropic conversion averages to 2.0 $\cdot 10^{-9} m^2/s^3$ and the baroclinc conversion averages to 0.7 $\cdot 10^{-9} m^2/s^3$. This shows that baroclinc processes cannot be neglected in the growth of the instabilities.

To link the Rossby waves that are seen in the model solution with the NECC,

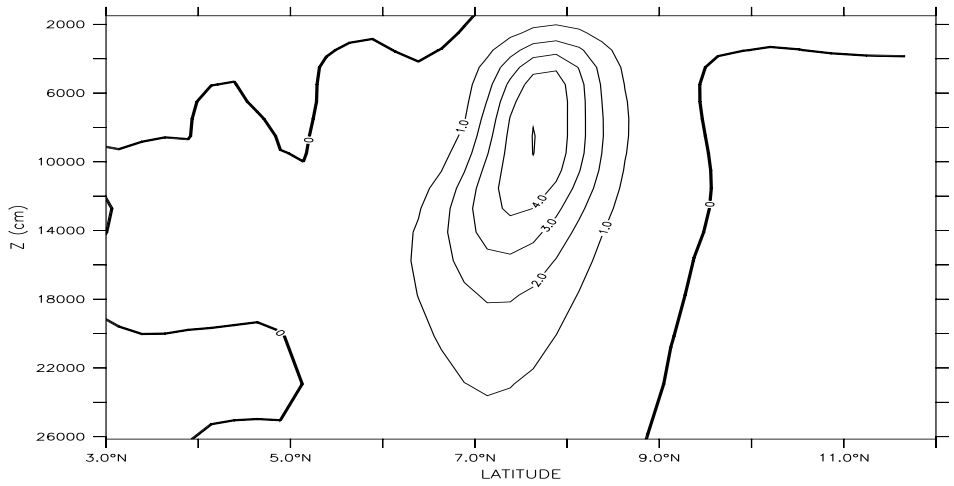


Figure 4.14: Yearly mean baroclinic conversion averaged between 50W and 42W (in $10^{-9} m^2/s^3$). Positive values indicate an energy flux from eddy available potential energy to eddy kinetic energy.

we performed a linear quasi-geostrophic instability analysis, anticipating that the strongest growing modes of the NECC are similar to the waves in the model. In our experiments the NECC has a Rossby number of 0.2 and the ratio between the average thermocline depth and its meridional deviation is estimated at 0.4. This clearly stretches the validity of QG but the strong similarity between its predictions and the OGCM results gives us confidence in the results.

The linear form of the QG equations is written in terms of the streamfunction $\psi$ as:

$$\nabla^2 \Psi_t + \beta \Psi_x - f_o w_z = 0 \tag{4.2}$$

$$\Psi_{zt} = (N^2/f_o) w \tag{4.3}$$

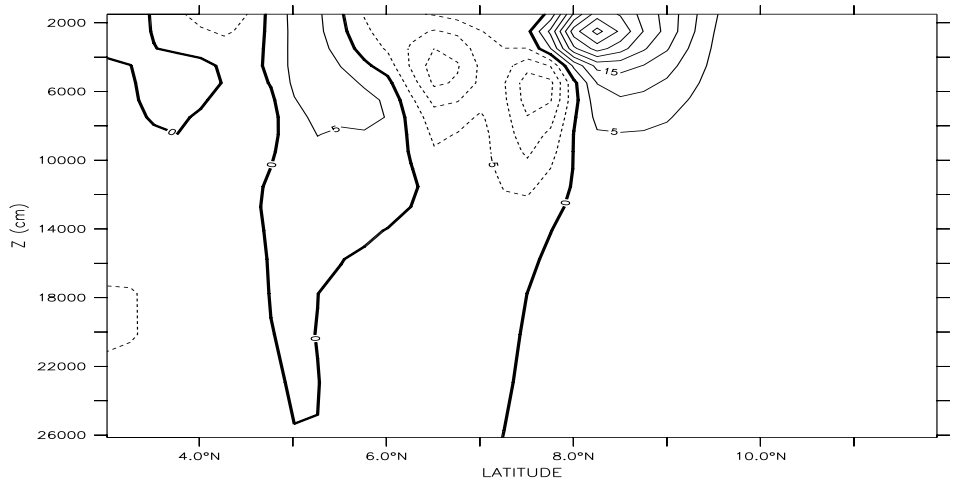


Figure 4.15: Yearly mean barotropic conversion averaged between 50W and 42W (in $10^{-9}m^2/s^3$). Positive values indicate an energy flux from the mean kinetic energy to the eddy kinetic energy.

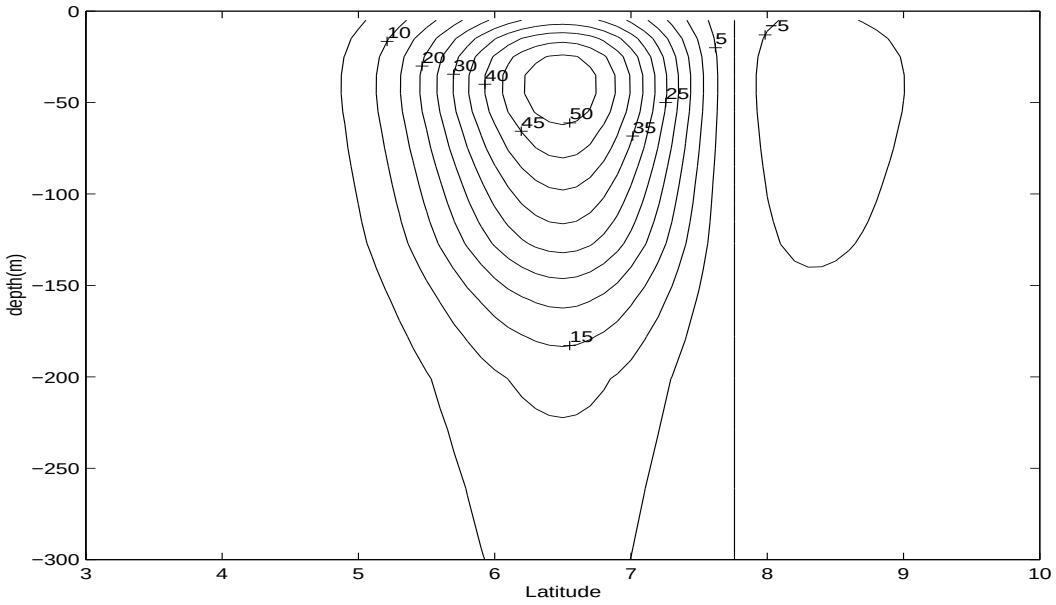


Figure 4.16: The idealized NECC profile used for the instability analysis. Shown is zonal velocity in cm/s.

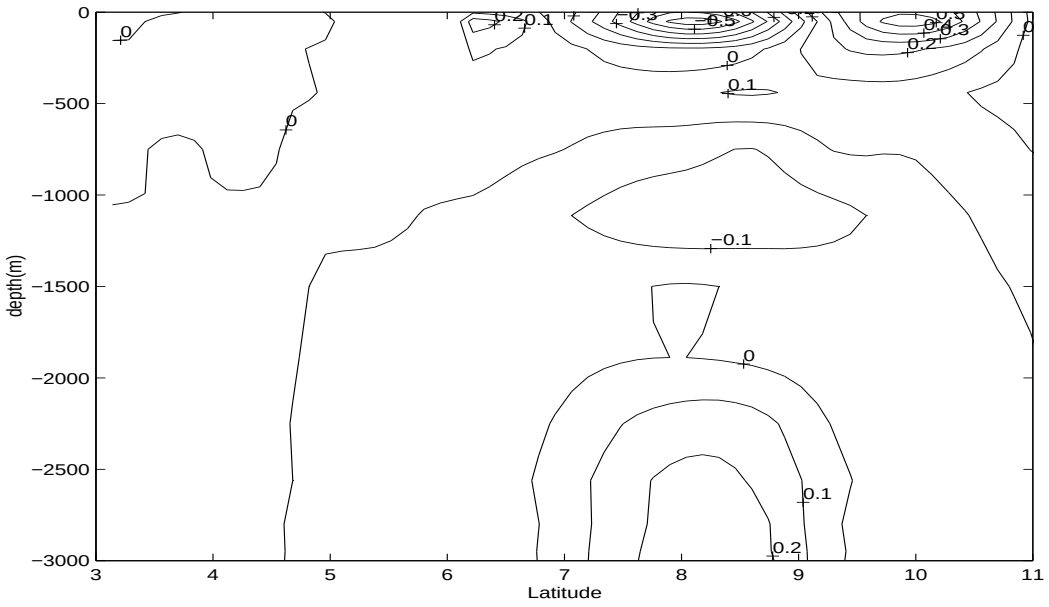


Figure 4.17: The spatial pattern of the strongest growing mode. Note its vertical structure which resembles a first baroclinic mode and the second maximum at 10N (compare with Figure 4.15).

The mean density profile is taken from the model results and the NECC profile (Figure 4.16) is created in accordance with snapshots of the model output. Both profiles should represent the unperturbed state which, of course, is unknown. However, to make progress we chose a profile that resembles a typical NECC profile from our model output in terms of maximum speed, width and depth. Fortunately, the results of the following analysis are not overly sensitive to the details of the profiles. These reference density and velocity profiles define a mean state streamfunction $\Psi(y,z)$ that together with a perturbation streamfunction $\Phi(x,y,z,t)$ constitute the total streamfunction. Following the analysis of Beckmann (1988) and Spall (1992), the perturbations are assumed to have a wave form of:

$$\Phi = M(y)F(z)exp[i(kx - \omega t)]. \tag{4.4}$$

Substitution of this form into Eqs. (2) and (3) results in an eigenvalue problem for the complex frequency $\omega = \omega_r + i\omega_i$. The system of equations is solved using a second-order finite differences scheme in the horizontal and Chebyshev polynomials in the vertical. Details of the solution procedure can be found in Beckmann (1988).

The horizontal grid spacing is 15.6km and 12 polynomials are used in the vertical. Different numerics could change the results; however, we find that a higher horizontal or vertical resolution does not change the results. Figure 4.7 shows the phase speed for the fastest growing westward propagating modes. The predicted values clearly cross the dispersion curve within the observed range. The spatial pattern of the 850km mode is shown in Figure 4.17. Its vertical structure compares well with the vertical structure of the observed waves (Figure 4.8) and its meridional structure predicts the second maximum at 10N (see Figure 4.5). The predicted growth rate for an 800km wave is 2.85e-7/s ($\approx (40 days)^{-1}$), and the rates observed in the model are between 2.6e-7/s and 6.5e-7/s. As in the previous subsection it is clear that the simulated flow field is much more complex than the one analyzed here. Nevertheless we believe that the strong similarity between our theoretical prediction and the observed features justifies our approach.

W. Johns (pers. comm.) pointed out that the observational evidence for the structure of these Rossby waves is largely missing. The sharpness of the wave crests in Mueller-Karger et al. (1988) may suggest stationary waves on the NECC rather than propagating waves. However, a recent publication by Leeuwenburgh and Stammer (2001) clearly shows westward propagating SSH anomalies on the NECC (see their Figure 10). This shows, that there is definitely a need for more observations to study the features of the NECC. Space based measurements of SSH, SST (Leeuwenburgh and Stammer (2001)) and ocean color (Fratantoni and Glickson (2001)) prove to be powerful tools to analyze mesoscale processes in the tropics and they should be used to verify the theoretical results discussed above.

From this section we conclude that the NECC is barotropically unstable and radiates Rossby waves of the first baroclinic mode with a period of approximately 70 days (50 days in exp1). These waves reflect at the Brazilian coast and create about five nonlinear anticyclones per year (seven in exp1) which we observe as NBC rings.

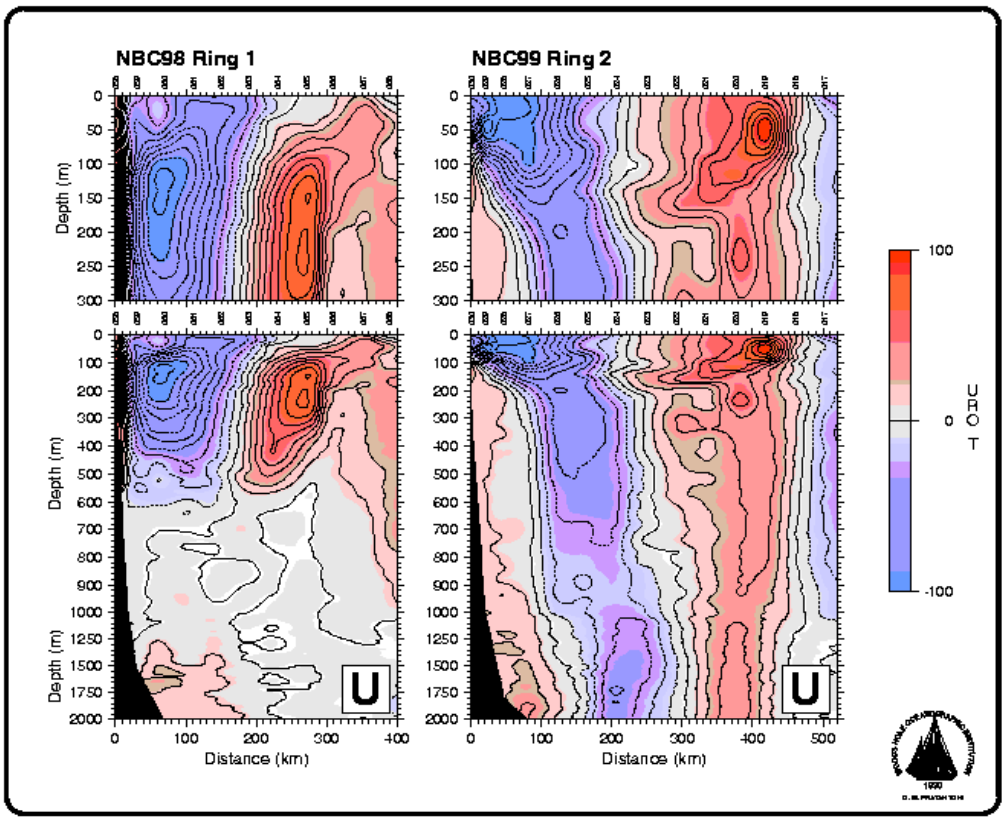


Figure 4.18: The velocity structure of two very different NBC rings (Fratantoni et al. (1999)). The color indicates the swirl velocity in cm/s. Note that NBC ring 2 reaches down below 2000m whereas NBC ring 1 is very shallow and lacks a surface expression.

## 4.3 The vertical structure, seasonality, and transport of NBC rings

A recently concluded observational campaign, the NBC Rings Experiment, showed that the NBC rings have a wide variety of shapes with two extreme cases: Deep, surface intensified NBC rings that can reach down to 2000m and thermocline intensified NBC rings that have no signal at the surface. The retroflection does not reach below the thermocline and has its maximum velocity near the surface. This poses two questions: why are some of the NBC rings so deep and why do some of them

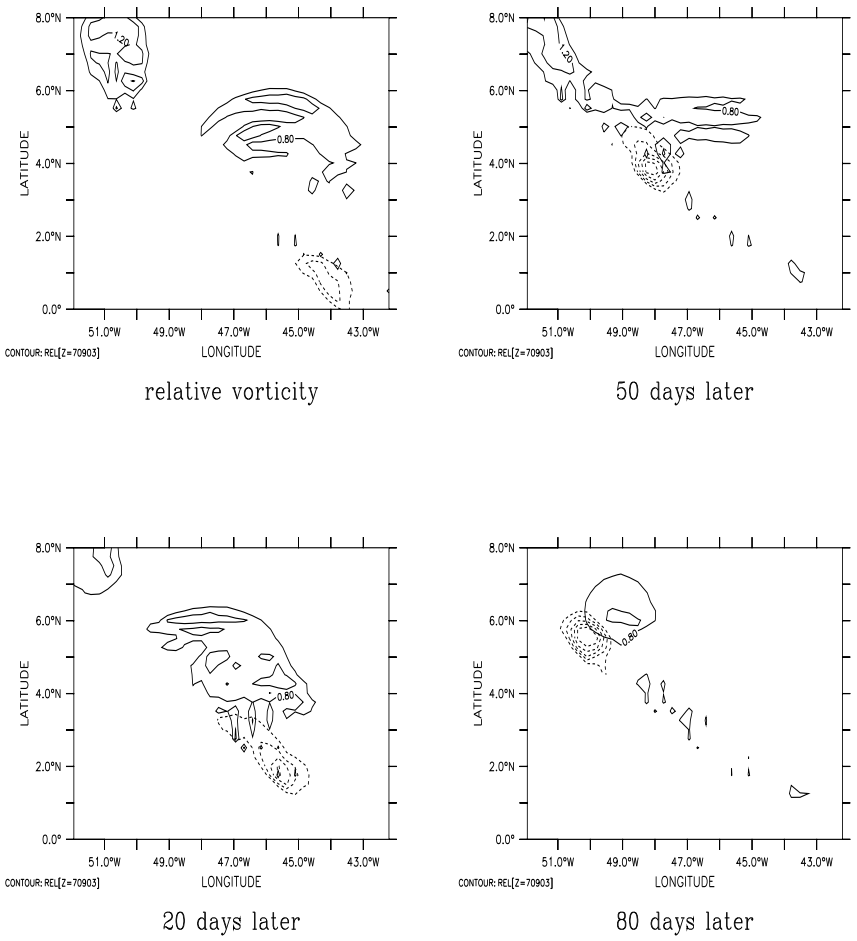


Figure 4.19: Four successive snapshots of negative relative vorticity ($\zeta$) to illustrate the merger of an intermediate eddy with the shallow retroflection ring. The solid lines show $\zeta$ in 100m depth in contours of -0.8e-5/s and -1.2e-5/s. The broken lines show $\zeta$ in 700m depth with each contour indicating -.2e-5/s.

lack a surface signal?

The deep signal can be readily explained by the merger of a deep intermediate eddy (their generation has been discussed in the previous section) with the retroflection eddy. Figure 4.19 shows negative relative vorticity in two layers, the solid line contours $\zeta$ at 100m depth and the broken line contours $\zeta$ at 700m depth. We chose to display the relative vorticity instead of the dynamical more relevant potential

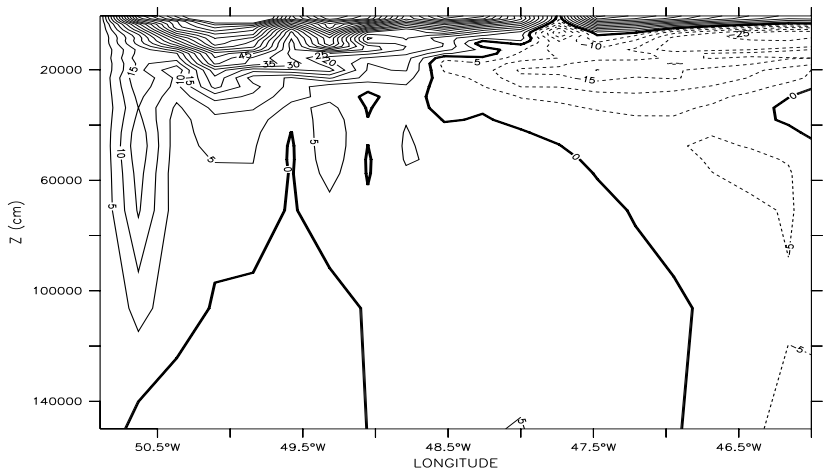


Figure 4.20: Contours of meridional velocity across the shallow retroflection ring at $5^oN$ (contour lines every 5cm/s). This snapshot was taken 40 days after the first $\zeta$ plot of Figure 4.19.

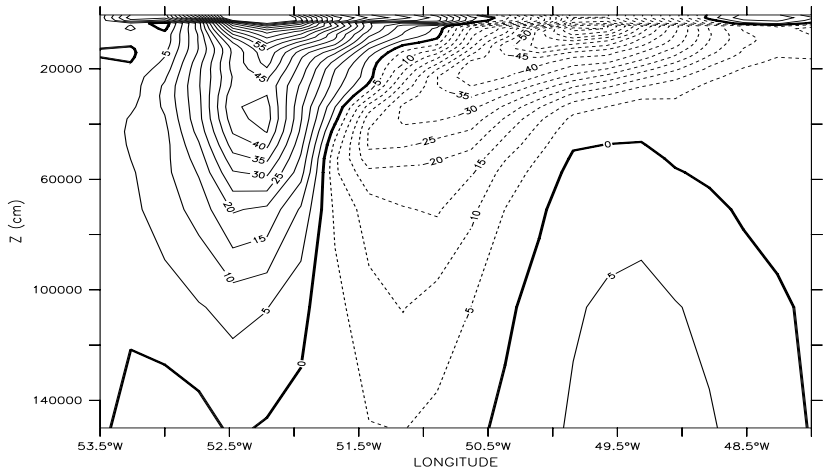


Figure 4.21: Contours of meridional velocity across the NBC ring of Figure 4.19 (7N, after a 100 days) after the merger (contour lines every 5cm/s).

vorticity for illustrative purposes. Beyond 5N the planetary vorticity dominates the relative vorticity and it becomes difficult to identify the the eddies. The negative relative vorticity indicates anticyclones: the NBC/NECC retroflection at 100m and the intermediate eddy at 700m. We can see in this figure how the intermediate eddy (see Figures 4.2 and 4.3) travels north along the coast and becomes stronger, compensating for the increasing planetary vorticity. Eventually it merges with the retroflection eddy and the two eddies continue north as one entity. The detailed interaction between the intermediate and the retroflection eddy is not addressed here, it would require a more idealized and or even an analytical study that is beyond the scope of this thesis. Figure 4.20 shows the shallow retroflection eddy before the merger, there is only a very weak signal below the thermocline. This changes after the merger when the newly created NBC ring shows a strong signal beyond 1000m (Figure 4.21). Whereas there are about six intermediate eddies generated per year, only 1 or 2 of them make it beyond 5N. This is different from the exp3 where the eddies are coherent from the surface to the intermediate layer. Here, the shear between the surface layer and the intermediate layer as well as the interaction with Rossby waves that arrive from the interior can destroy the intermediate eddies.

The seasonal variation in the structure and distribution of the NBC rings can be attributed to their differing strength and their differing propagation speed. It was shown in Chapter 3 that the NECC has a substantial seasonal variation in its strength. Figure 4.22 shows that the strength of the instability waves is correlated to the NECC's transport. These unstable Rossby waves form the NBC rings and the Figure 4.22 shows how this maximum of velocity variance arrives several months later at 8N where the NBC rings are formed. Thus, the maximum NECC transport in late fall leads to the strongest NBC rings in the early winter.

To explain the lack of a surface signal in the observations of Fratantoni et al. (1999), we have to look to the north of the retroflection region. In the previous section it was found that NBC rings are generated in regular intervals, even in exp1. Figure 4.23 shows that there is a seasonality in the appearance of rings at $10^o N$, they appear preferentially in the spring. In the summer on the other hand, NBC rings are formed but they stall after their shedding and dissipate without moving further north (Figure 4.24). It seems that the background velocity at the western boundary plays an important role. Therefore, a lowpass filtered timeseries of velocity at the

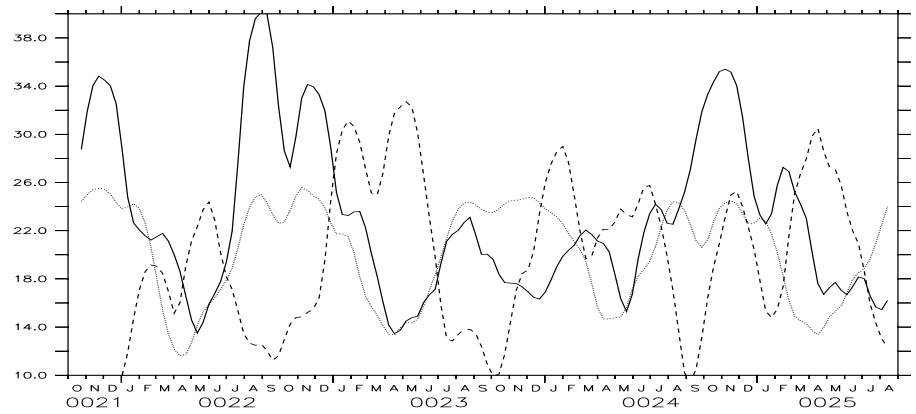


Figure 4.22: The dotted line shows the scaled transport index of the NECC at 48W. The solid line shows the rms of the meridional velocity at 7N/48W (cm/s) in 100m depth, the maximum of variability coincides with the maximum of NECC transport. Several months later this rms maximum arrives at 8N/52W (dashed line, in cm/s) where it is expressed in the NBC rings. All data is filtered with a two month low-pass filter.

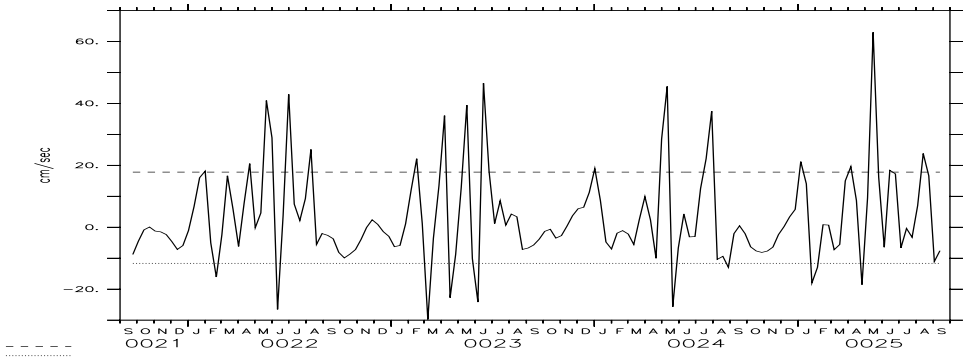


Figure 4.23: Time series of meridional velocity at 10N/56W in 100m depth (for exp1). The straight lines indicate the standard deviation around the mean. NBC rings can be identified as peaks above or below the standard deviation. We can see that NBC rings preferentially pass by 10N in the late spring at an average rate of approximately 4 rings per year.

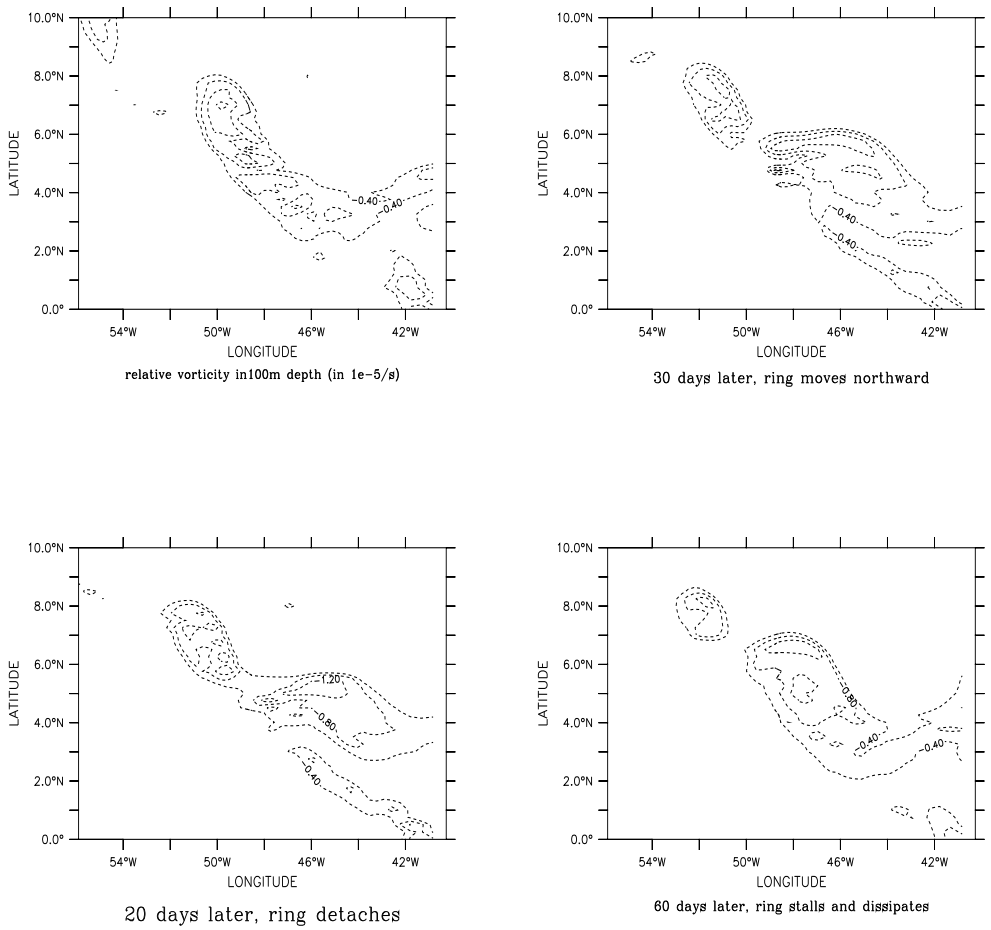


Figure 4.24: The life and death of a NBC ring born in August. Shown are the negative values of relative vorticity in 100m depth.

western boundary is displayed in Figure 4.25. We see seasonal variation around a mean of approximately zero and a southward flow from early summer to winter. Thus, the NBC rings stall in the summer because they face an adverse LWBC. This southward current never reaches deeper than 200m, but it is still strong enough to block the NBC rings. However, even if the rings are not entirely blocked, they will still lose a part of their surface signal after running against a southward LWBC (Figure 4.26). The reversing LWBC is a direct response to the interior wind field

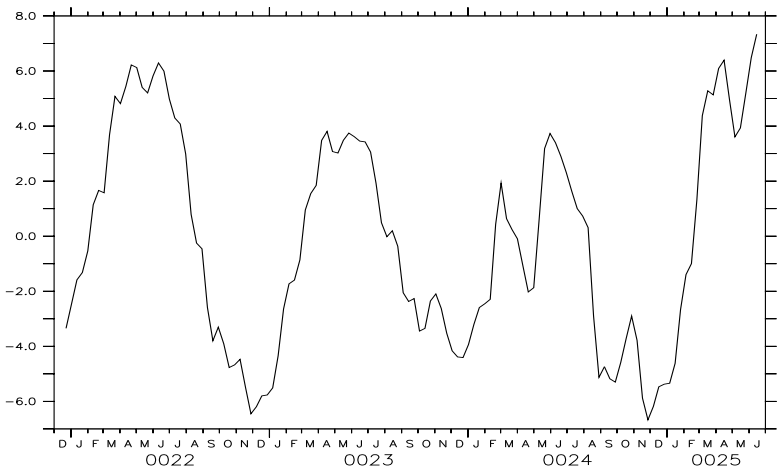


Figure 4.25: Lowpass filtered alongshore velocity along the western boundary at $10^o N$, 80m depth in cm/s.

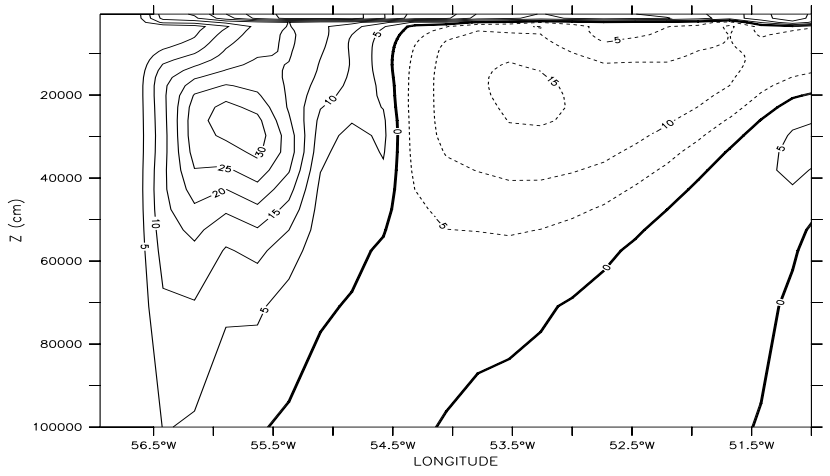


Figure 4.26: Meridional velocity across a ring whose surface signal has been eroded by a southward LWBC. The velocity maximum is between 200m and 300m (in cm/s).

as shown by Anderson and Corry (1985). Of course, there is a superimposed MOC, but it will only add a northward component to the wind-driven southward flow. It never completely eliminates it throughout the year. To verify this, the western boundary current strengths were analyzed in two different experiments. In exp3 (no wind) the maximum mean flow across $10^oN$ has a northward component of 35cm/s. In a wind-driven experiment with closed boundaries it is found that at $10^oN$ the wind-induced LWBC has a mean southward component of 40cm/s. As the MOC supplies a constant flow of water and the wind-driven flow varies in magnitude, one would expect exactly the LWBC behavior that is displayed in Figure 4.25.

We now discuss the importance of NBC rings for the large scale circulation, or to be more precise, the proportion of the MOC return flow that is carried by the NBC rings. We could see in the previous section that the LWBC plays an important role in the NBC ring propagation and that because of it, some NBC rings are not able to leave the retroflection region. Therefore it was decided to base our analysis on data along 10N. Rings that can't propagate up to that latitude are under the influence of a southward LWBC and their properties will be swept into the NECC from where the water either recirculates into the equatorial gyre or continues north in the interior of the tropical gyre. We used different methods to estimate the volume of South Atlantic water (=core volume) in a NBC ring:
a) we defined core volume as the water for which $\frac{pv-\overline{pv}}{\overline{pv}} < 0$. "pv" is the potential vorticity and $\overline{pv}$ its mean over four years.
b) we defined core volume as the water for which $\frac{c-\bar{c}}{\bar{c}} > 0$. "c" is the concentration of a passive tracer that has been injected at the southern boundary and makes it easy to identify water of Southern Hemisphere origin.
An average of four rings per year pass by 10N. Their average core volume is according to method a) $6 \cdot 10^{12} m^3$, and according to method b) $14 \cdot 10^{12} m^3$, which leads to a yearly mean transport of 0.8 Sv and 1.8 Sv respectively. Method a) gives systematically lower estimates than method b) and we decided to look more closely at the evolution of the NBC rings. It turns out that the pv minima really mark the core of the rings (as expected) but a lot of South Atlantic water is swept around the core outside the swirl speed maximum. Eventually this water will be lost to the ring but for the relatively small distances that these rings travel this loss might be negligible. We will proceed by assuming that 1.8 Sv is an upper and 0.8 Sv a lower limit for

the amount of South Atlantic water that the NBC rings transport north. This is significantly smaller than the lower bound of 3 Sv mentioned by Fratantoni et al. (1995). Two things might account for this difference. First, for reasons mentioned above the transport was measured at 10N instead of 8.5N. Secondly, Fratantoni et al.'s (1995) values are based on observations that contain very deep NBC rings with penetration depths well beyond 1000m which the present model is not able to reproduce because of its coarse vertical resolution below 1000m depth. However, we don't think that the actual penetration depth of the NBC rings is relevant as long as they penetrate below the thermocline. The working assumption in this study is that the strength of the MOC (and therefore the intermediate layer transport) is determined by processes outside the model domain. This is reflected in the open boundary conditions of the model setup and it follows that the intermediate layer transport is independent of the depth of the rings. Of course, the rings could act as strong mixing agents and replace NA intermediate water with SA intermediate water. However, the ring activity is restricted to the western boundary and there are no zonal currents in the intermediate layer so that the rings would essentially mix new SA water with older SA water. Therefore it is unlikely that the NBC rings significantly change the flow of SA water in the intermediate layer. This is very different above the thermocline, where the NBC rings carry water north across the boundary between the equatorial and tropical gyre. Without the NBC rings the SA water could not cross this boundary, but would enter the NECC and flow east.

The average core depth of a NBC ring at 10N is between 360m (method a) and 500m (method b). Together with the values above we estimate that 1 Sv is an upper bound for the NBC ring transport above the thermocline. How does this compare to the other pathways across $10^oN$? The analysis of the flow field yields that 6.2 Sv flow north in the IWBC, 10 Sv in the Ekman layer and a total of 1.8 Sv in the thermocline (see Figure 3.3). The thermocline flow that is not captured in the NBC rings flows north in the interior as part of the tropical gyre. It seems that the NBC ring contribution to the warm water return flow of the MOC is rather small compared to the contributions of the Ekman and the intermediate layers. However, the only way that South Atlantic thermocline water can enter the North Atlantic without being mixed is by being trapped in a NBC ring. The results presented here compare well the observations of Schmitz and Richardson (1991) who found 0.8 Sv

of South Altantic thermocline water in their water mass census of the Florida straits.

# Chapter 5

# The flow of AAIW along the equator

## 5.1 Introduction

The idealized experiment that was discussed in the second chapter showed that intermediate waters (IW) flow north along the western boundary below the wind-driven thermocline. Observations indicate that some of this IW enters the interior of the equatorial Atlantic. The details of this IW flow are the focus of this chapter and we analyze its dynamics with the more realistic model that is described in chapter 3. It is important to realize that the model treats the wind-driven circulation as a perturbation on the background stratification. This means that the initial stratification and the conditions at the open boundaries are prescribed in accordance with observations and are not part of the model dynamics. Therefore the strength of the IW flow is determined by conditions outside the model domain. What drives the flow below the thermocline is still a field of intense research and is beyond the scope of our discussion (see however Stommel (1961), Munk (1966), Toggweiler and Samuels (1995) and Greatbach and Lu (2000) for interesting, but different views on this topic). Still, apart from completeness, there is one reason to include a discussion of the IW: the path of the AAIW along the equator is still unknown because the highly energetic tropical wave field makes it very difficult to analyze the scarce data.

This chapter is structured in the following way: first the observational evidence for the spreading of the AAIW is reviewed, then it is shown that the model results

are consistent with these observations. Once we have gained trust in the model, the AAIW flow along the equator is analyzed.

## 5.2 Observations

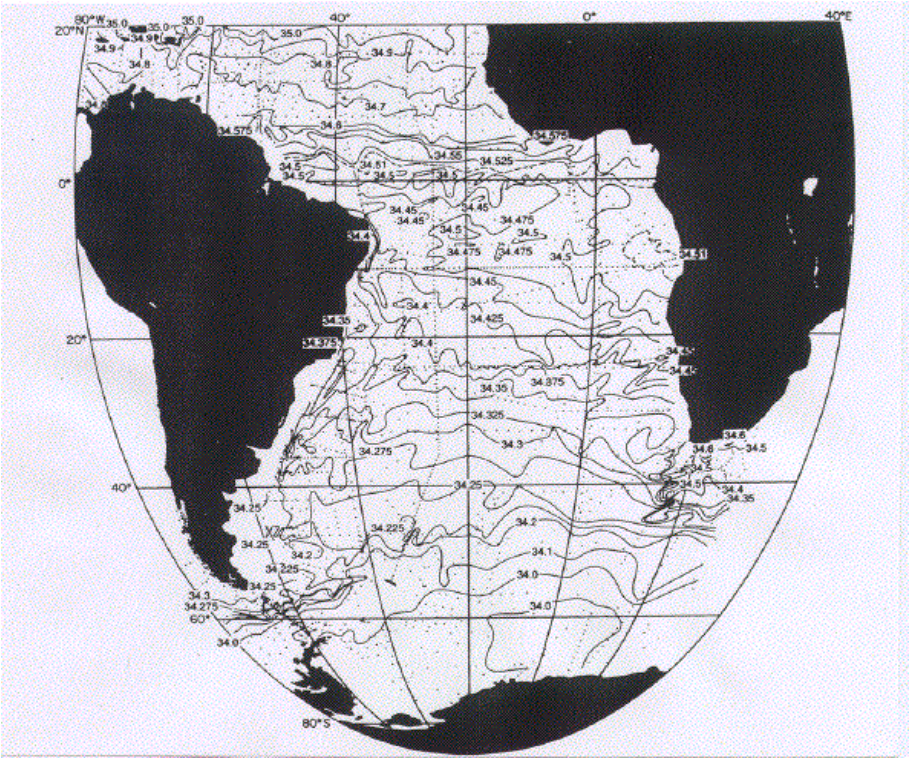


Figure 5.1: The salinity distribution on the $\sigma = 27.3$ isopycnal (core depth of the AAIW) as observed by Suga and Talley (1995). Note the tongue of low salinity that spreads eastward from the western boundary slightly south of the equator.

The origins and pathways from which the AAIW enters the south Atlantic are still unclear (Suga and Talley (1995)), but around 10S it appears to flow north in an Intermediate Western Boundary Current (IWBC). The water is characterized by a salinity minimum and a local oxygen maximum which have their depths in the tropics at approximately 700m. Suga and Talley (1995) show that the AAIW is confined to the western boundary except for a long tongue that reaches east at 4S (Figure 5.1). Two recent zonal hydrographic sections by Arhan et al. (1998) corroborate this

picture: the AAIW enters the equatorial region at 4.5S in an IWBC and no AAIW crosses the 7.5N section in the interior. The actual transport of AAIW is less clear. Based on six hydrographic sections, some of which include LADCP measurements, Schott et al. (1998) find that the IWBC has a strength of 10 $\pm$ 3Sv between 5S and 10S. Roemmich's (1983) inverse calculation that is based on two hydrographic sections at 8S and 8N yield a transport of 9 $\pm$ 3Sv. After a water mass analysis of the Florida current, Schmitz and Richardson (1991) conclude that 5Sv of AAIW enter the northern subtropical gyre. Float (Boebel et al. (1999b)) and mooring data (Johns et al. (1990), Johns et al. (1998) and Schott et al. (1993)) are consistent with those estimates, although it is difficult to calculate transports with their data.

Interesting features are the low salinity and high oxygen tongues south of the equator (a smaller one can be seen at 3N) and the strong cross equatorial salinity and oxygen gradients. One could think of three different mechanisms that are important in creating such features: advection, tropically enhanced mixing or Stokes drift. Schott et al. (1998) claim the existence of strong zonal intermediate currents that reach far into the eastern basin. Their claim is based on 4 meridional sections at 35W, close to the American continent. Suga and Talley (1995) find that the equatorial tracer distribution allows for three different conjectures about the flow along the equator: westward flow, eastward flow which is weaker than that to the north and the south, or eastward flow with possible large vertical mixing. Float observations by Schmitz and Richardson (1993) show eastward flow whereas floats by Boebel et al. (1999a) and Ollitrault (pers. comm.) show that the direction of the zonal currents reverses over the course of a year. To explain these seemingly contradicting observations is the focus of this chapter.

## 5.3 The AAIW in the model

Traditionally the AAIW is determined by the salinity minimum and the oxygen maximum. While the vertical extent of this water mass is not strictly defined, most authors agree that its maximum vertical extent reaches from 1200m up to 300m, depending on the location. This model does not include salinity or oxygen so a water mass is defined called IW that denotes all the water between the 5.5C and the 13.5C isotherms (approximately between 300m and 1000m at the equator) that originates

at the southern open boundary. Several factors led to this choice. First, the resolution below 1000m becomes very coarse (2 layers for 1700m). Secondly, the only two authors that made a quantitative estimate of the AAIW flux through the tropics chose as vertical limits 330m-870m (Roemmich (1983)) and 300m-1000m (Schott et al. (1997)). Our choice makes it more meaningful to compare our results with theirs.

The comparison with the available current meter data is rather encouraging.

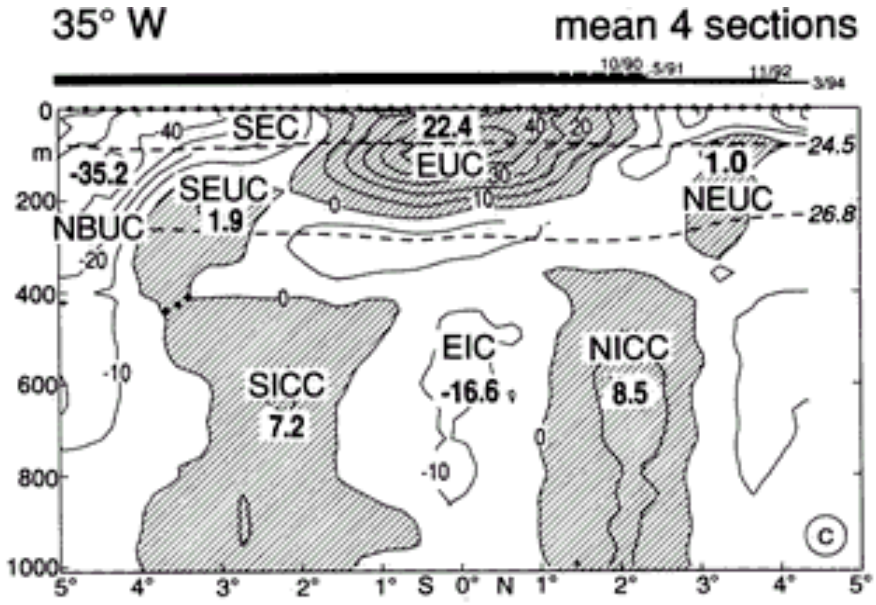


Figure 5.2: The zonal velocity at 35W.

On crossing the equator, the model's IWBC has a mean and variance similar to Schott et al.'s (1993) observations: the modeled IWBC has an alongshore velocity of 8 ± 6cm/s at 850m depth. Schott et al. (1993) measure 5 ± 19 cm/s at the same location. The model's lower variability might be due to the absence of topography, to a wind field with an unrealistically low variability or to insufficient resolution at the western boundary. A comparison of the model results with the currents meter data of Johns et al. (1998) is shown in Figure 3.4 and it, too, shows that the model is able to reproduce the IW flow along the western boundary reasonably well.

Direct LADCP measurements along 35W are available from Schott et al. (1998, Fig. 5.2) and 2S, 2N and the equator we can see the bands of zonal velocity that Schott et al. (1998) describe as intermediate currents. An average of the model's zonal velocity calculated from the same four times that the observations were taken

yields a very similar picture (Fig. 5.3): westward flow at the equator and eastward flow poleward of it. The eastward flow in the model seems to be weaker and a bit further poleward than the eastward flow in the observations. This will be discussed in more detail in the next section.

We attempted to reproduce the tracer tongues from Suga and Talley (1995) by injecting a passive tracer in the IWBC. As it turned out, the numerical meridional (and to a lesser degree the zonal) diffusion is a dominating term in the tracer balance, so that the strong tracer gradient at the equator could not be reproduced. This was a surprising result because a high resolution and a small numerical diffusion were used in the equatorial waveguide. Another problem for tracer is that the low variability at the western boundary makes it difficult for them to get entrained into the interior. According to Claus Boening (pers. comm.) the inability of the equatorial deep interior to entrain tracer from the western boundary is one of the main problems that the Kiel modeling group has faced in trying to reproduce the

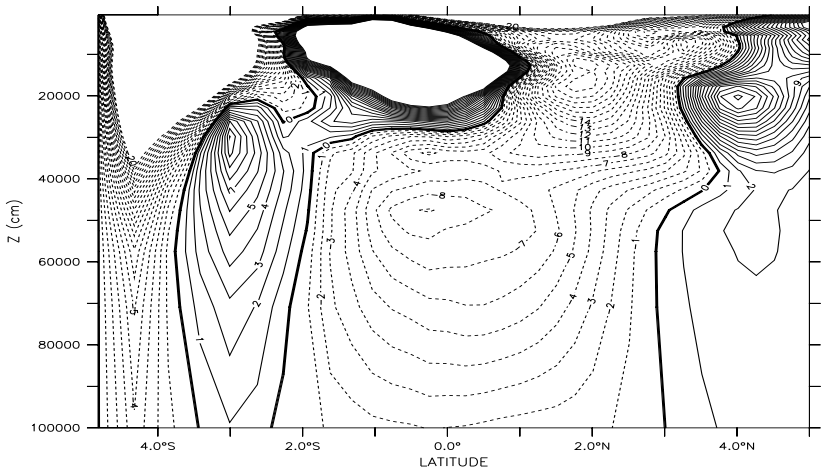


Figure 5.3: The zonal velocity at 35W, averaged out of 4 sections taken in the same months (March, June and twice in October) as Schott et al.'s (1998) sections. The alternating velocity bands at 600m depth are interpreted by Schott et al. (1998) as (starting at 3S) southern equatorial counter current, equatorial intermediate current (to the west), and northern intermediate counter current. Shown is only the range from -20cm/s to 10cm/s to emphasize the intermediate layer.

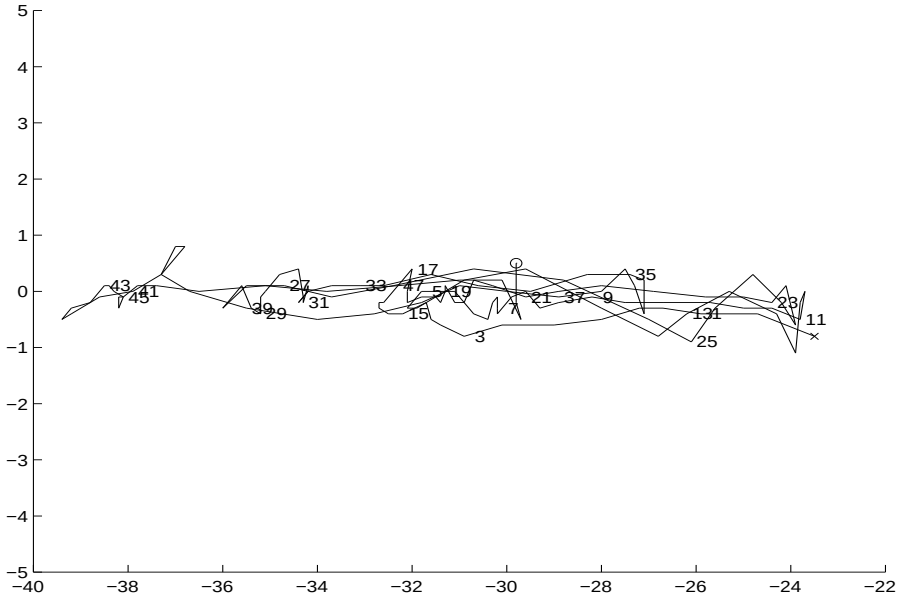


Figure 5.4: The trajectory of a single virtual particle in our model. It is launched at 23W in 450m depth (x) and can reach zonal velocities of more than 5cm/s over a period of several months. The numbers in the pictures denote the time after launching the float (in months), the circle shows its final position after 4 years.

Atlantic tracer distribution. Because the tracer distribution cannot be investigated with the present model we will focus in this chapter on the reconciliation of the float data with the velocity observations.

The few available float data have essentially 2 features: eastward flow along the equator (Schmitz and Richardson (1993)) or zonal flow that reverses direction during the year (Boebel et al. (1999a,1999b) and Ollitrault (pers. comm.)) The simulated floats in the model show a similar behavior as can be seen in Figure 5.4. It shows the typical path of a float in the interior of the equatorial Atlantic at intermediate depths: It covers a large zonal distance before turning around and returning towards its initial longitude. We found the comparison with the observations very encouraging and will conclude this section with a volume balance of the intermediate layer.

Although the comparison between model and data is encouraging, an accurate volume budget must be made to ensure that no large sources of up- or downwelling lead to wrong conclusions. Causes for upwelling are commonly Ekman divergence (which is not expected to reach down to the AAIW level), vortex stretching (enforced by PV-

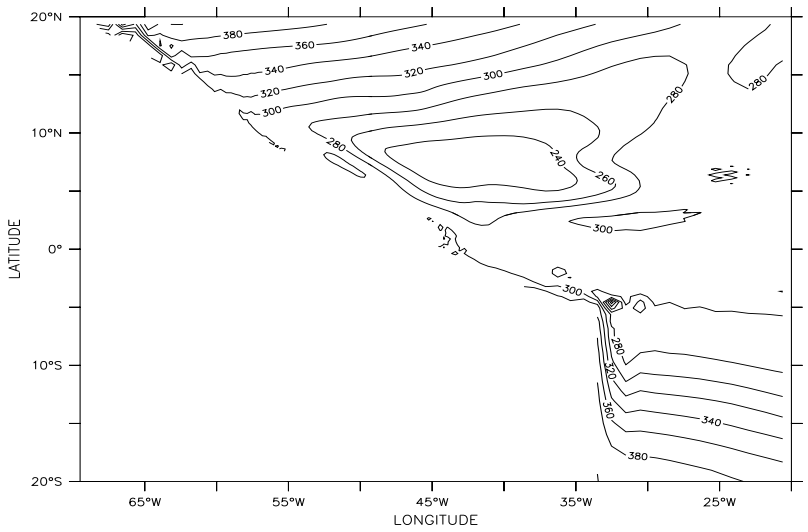


Figure 5.5: The mean depth of the 13.5C surface (in meters).

conservation ), the $\beta$-effect (to maintain a constant transport, a poleward western boundary current has to increase its crossfrontal temperature gradient by upwelling (Huang and Yang (1996))) and diapycnal diffusion. To avoid the problem that the first three phenomena appear as spurious sources in the volume budget, the layer between 5.5C and 13.5C will be analyzed instead of the layer between 300m and 1000m. At the equator this water is found between 300m and 1000m but at 5N the tropical gyre causes considerable vortex stretching (Figure 5.5).

Diapycnal flow can have two causes: turbulent heatflux, which would be expected to be important in the NBC/NECC retroflection region, and numerical diffusion which can lead to the Veronis effect (Veronis (1975)). The Veronis effect has its roots in the numerical diffusion employed in z-coordinate GCMs. This diffusion causes a weakening of the crossfrontal density gradient. To maintain this gradient (and the resulting transport), the flow induces an upwelling and downwelling adjacent to the front. Unfortunately the diffusion is needed for numerical, not physical reasons, and it is almost certainly too high in low resolution models. Thus, it is necessary to verify that this effect is negligible in the present model. In the temperature balance

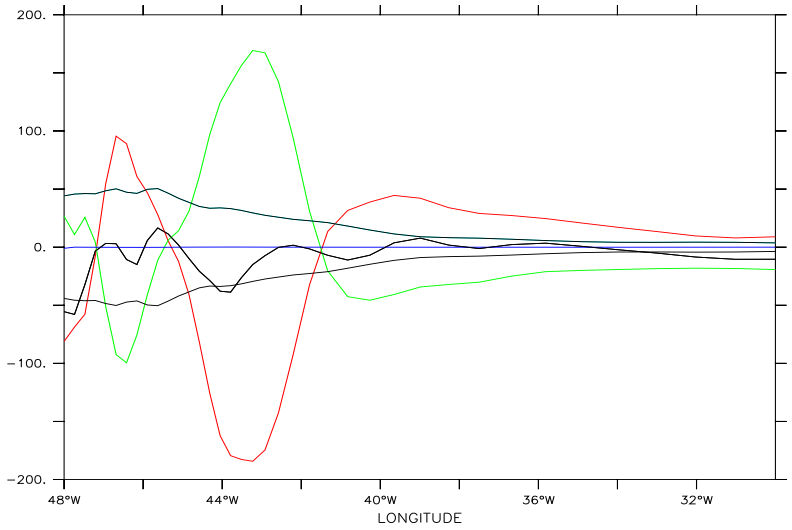


Figure 5.6: The yearly mean of the components of the temperature balance equation (4). Representative for the rest of the domain the values along 3.5N in 300m depth (in $10^{-9}$ K/s) are shown. The red line shows the total eddy temperature flux, the green line the total advective flux, and the blue line the diffusive flux. The sum of those fluxes is indicated by the thick black line. The thin black lines indicate the uncertainty of the mean turbulent fluxes ($= \frac{1}{N^2}\sqrt{\sum(F - F_0)^2}$).

equation:

$$\frac{D\mathbf{u}}{dt} = A_H \nabla^2 T + A_z T_{zz} + \overline{\nabla(\mathbf{u}'\mathbf{T}')} \tag{5.1}$$

the advective terms are on the lhs and the numerical diffusion and the turbulent temperature flux on the rhs. An analysis of the model results in the tropics (Figure 5.6) shows that numerical diffusion is negligible everywhere if compared with temperature advection and turbulent temperature flux. An analysis of the transport divergences in the different layers shows that between 15S and 10N 0.9Sv of IW are converted to lower thermocline water (LTW). Unfortunately, the structure of the upwelling distribution is so noisy that it is meaningless to attribute this upwelling to a certain area. Certainly there is a lot of up- and downwelling in the NBC/NECC retroflection area, but it is impossible to estimate a reliable net contribution for any dynamical distinct region. However, the diapycnal fluxes are comparable to the

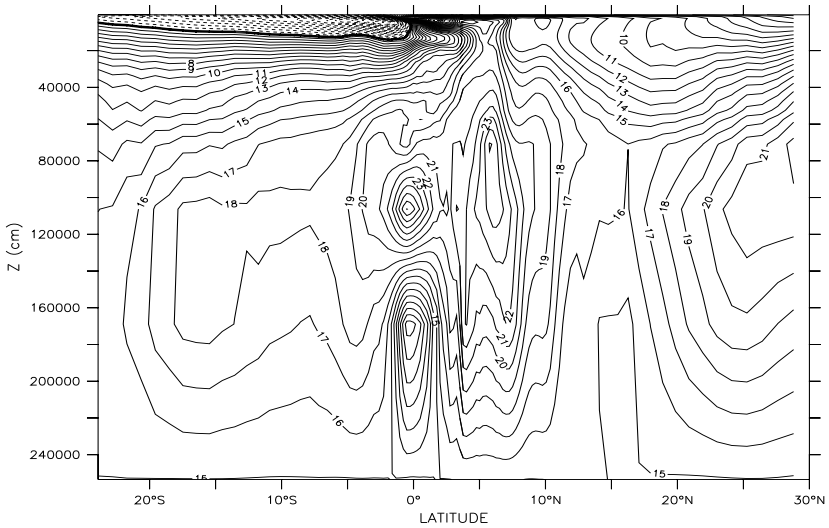


Figure 5.7: The zonally integrated streamfunction (in Sv). Note the two cells at the equator, centered at 1100m and 1800m.

1.4Sv between 9S and 9N that Fratantoni (1996) found in his study of a layered model.

It is nevertheless surprising to find 2.0 Sv of deep water converting into IW. The way the model is set up, almost no flow or turbulence would be expected in the abyss. The conversion rates were similar in Exp1, Exp2 and Exp3, which again is surprising since the boundary conditions and the dynamics are rather different in these three experiments. Snapshots of the MOC (Figure 5.7) suggest that the source of this deep mixing is related to two spurious deep cells at the equator. These cells were the focus of a study by Weaver and Sarachik (1990), and they result from an underresolved deep ocean. They demonstrate that these cells are caused by numerical instability of the temperature equation and vanish if the vertical resolution is increased. Their study furthermore suggests that, although problematic for the deep circulation, this numerical instability will not affect the circulation in the upper, better resolved layers.

After comparing our results to the the work of Fratantoni (1995) we conclude that

the conversion of IW into LTW is reasonable while the conversion of deep water into IW is spurious. The volume balance shows that in the model 4.8 ($\pm$0.4) Sv of IW enter the equatorial domain in an IWBC. Due to spurious mixing the IWBC gains 2.0 Sv by conversion of deep water into IW, and because of turbulent heatfluxes it loses 0.9 Sv to the overlaying LTW. The interior flow has no significant mean and is dominated by the tropical wave field. At 10N a turbulent IWBC leaves the equatorial domain with a strength of 5.9 ($\pm$3.3) Sv. Although these values are within the range of the observations, this volume budget is only of limited value because of the spurious deep mixing.

## 5.4 Synthesis of theory and observations

After reviewing the observations, one question arises immediately: How can we explain the seemingly contradictory observations? The velocity measurements suggest strong westward flow at the equator, the floats suggest eastward or reversing flow and the tracer do not allow for a definite answer either.

Before trying to understand the observations, the topic of equatorial waves is addressed. Because of the strong changes in the Ekman divergence along the equator and the high wave speed in the tropics it is expected that every observation in the region will be highly contaminated with waves. One of the advantages of using a GCM is that the structure of these waves can be analyzed to estimate how they may affect the signal of interest. In the equatorial Atlantic the strong stratification leads to the dominance of the second baroclinic mode (Philander (1990)). This is different from the Pacific which has a much deeper thermocline and therefore projects most of its seasonal variability on the first baroclinic mode (compare Busalacchi and O'Brien (1980) with Busalacchi and Picault (1983)). The reason for this difference is not clear; however, a comparative study of the Pacific and the Atlantic is beyond the scope of our work. Figures 5.8 and 5.9 display the model's two dominant modes of variability at 35W. The first EOF is much stronger than the second EOF and its zero crossings at 2200m and 650m illustrate the dominance of the second baroclinc mode and compare well with the theoretical predictions of 2200m and 500m (computed by Philander (1990) for the stratification of the model). The sidelobes at 5S and 5N are

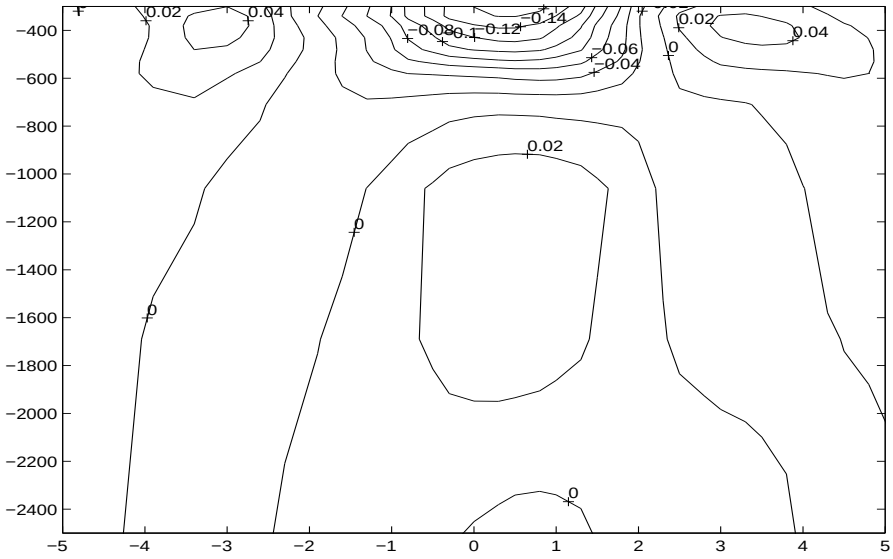


Figure 5.8: The first EOF of the zonal velocity at 35W. Only the flow below the thermocline (300m) was considered because the upper layer flow is governed by different dynamics. This mode explains 56% of the variability.

a part of the Rossby wave and can best be understood with the help of Figure 5.10 (Philander (1990)): the seasonal wind field variation causes an Ekman convergence

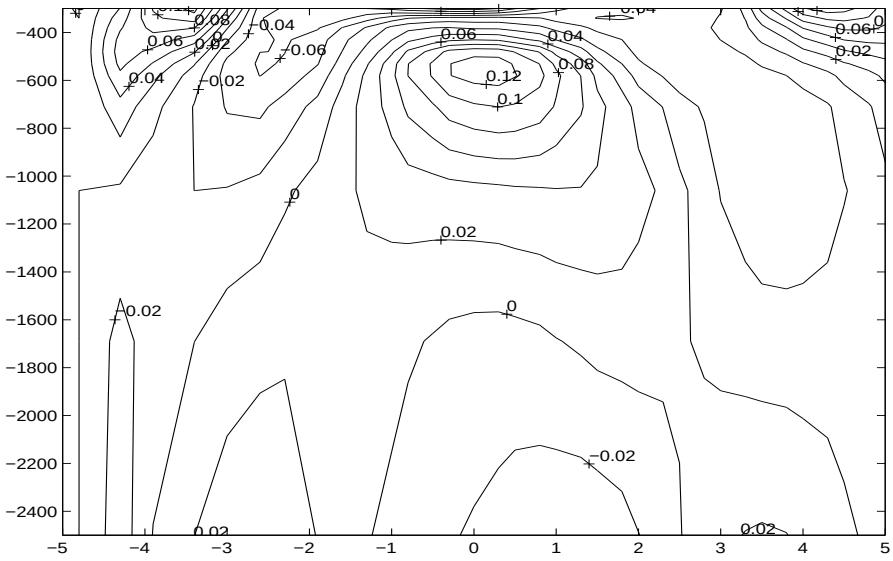


Figure 5.9: The second EOF of the zonal velocity at 35W. This mode explains 15% of the variability.

which will be expressed in a SSH anomaly (in his barotropic model). This height anomaly projects on a set of Kelvin and Rossby waves. The Rossby waves are an essential part of this set because the Kelvin wave does not have a signal outside the equatorial deformation radius. Thus, the sidelobes seen in the EOF are the result of the same two pressure anomalies that cause the strong velocity peak at the equator. The theoretical structure of the zonal velocity of the first two symmetrical meridional Rossby modes are shown in Figure 5.11. A comparison with the EOFs at intermediate depth suggest that the first EOF reflects the first symmetric mode and the second EOF reflects the second symmetric meridional Rossby wave mode. The relative strengths of the modes depends on the spatial structure of the wind field variability that projects on these modes. The corresponding Kelvin wave could not be detected in the model solution because its phase speed is more than 1m/s and the model results are only stored every 10 days. The Rossby waves are excited by the annual and semiannual wind field variations (see Figure 5.12) and have the following dispersion relation (Philander (1990)):

$$\sigma = -\beta\lambda^2 k/3, \tag{5.2}$$

where $\lambda = 250km$ is the Rossby radius of the 2nd baroclinic mode. From this, a Rossby wave with yearly forcing is expected to have a wavelength of 15000km and a phase speed of 0.47 m/s. Figure 5.13 shows that the waves seen in the model have a wavelength of more than twice the basin width (=6000km) and phase speed of approximately 0.4 m/s. Thus, below the thermocline the equatorial flow field is dominated by seasonal Rossby waves of the second baroclinic mode. Figure 5.13 can also explain why it is so difficult to move tracer from the western boundary to the interior. It is only in July that the waves are strong enough to interrupt the northwestward flowing IWBC (at 44W) and turn the flow towards the interior.

Unfortunately, water properties and floats are not advected by the time mean flow but instead by the turbulent flow. This makes the interpretation of observations much more complicated, especially in the presence of strong planetary waves. As an example, figure 5.14 shows the path of a virtual float in 500m depth. Although there is almost no mean eastward flow (Figure 5.15), the float ends up 1000km east of the western boundary (13 out of 95 floats took a detour through the interior).

After this introduction, we can now turn to the interpretation of the observations

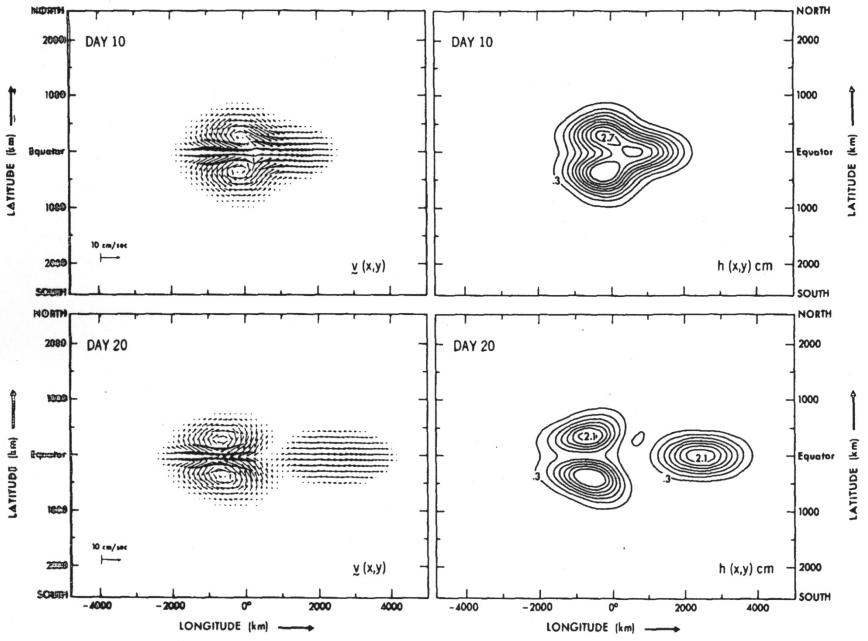


Figure 5.10: Current velocity and sea surface high anomaly caused by an initial Gaussian sea surface height disturbance at the equator (Philander (1990)).

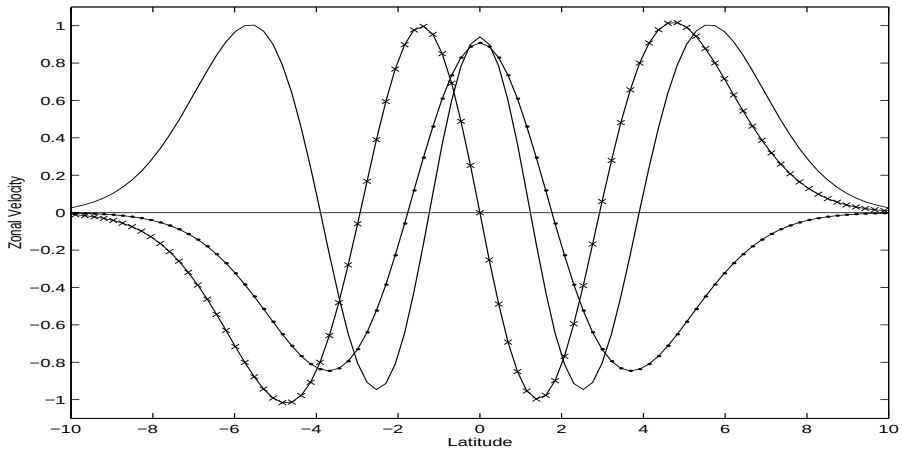


Figure 5.11: The meridional structure of the first (dotted line) and second (solid line) symmetrical mode of the zonal velocities of equatorial Rossby waves. The structure of the first antisymmetrical mode is indicated with crosses (-x).

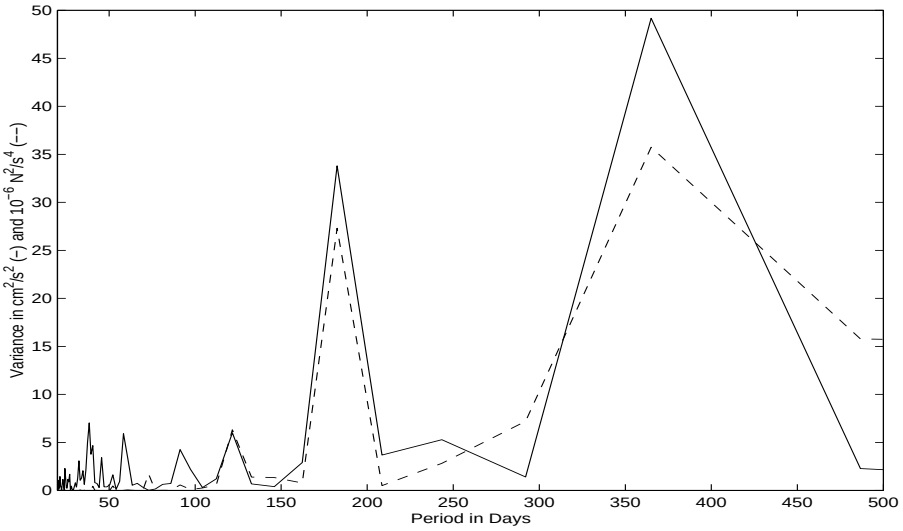


Figure 5.12: Variance conserving spectrum of the zonal velocity at 25W/0N in 500m depth (solid line, peak at $50 cm^2/s^2$), and the spectrum of the zonal wind stress at the same position (in $10^{-6} N^2/s^4$, dashed line).

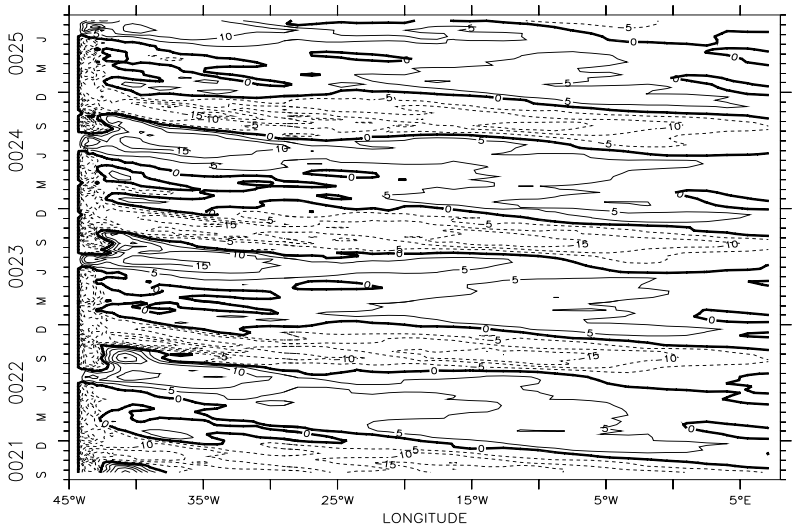


Figure 5.13: Hovmoeller diagram for the zonal velocity along the equator in 500m depth (cm/s).

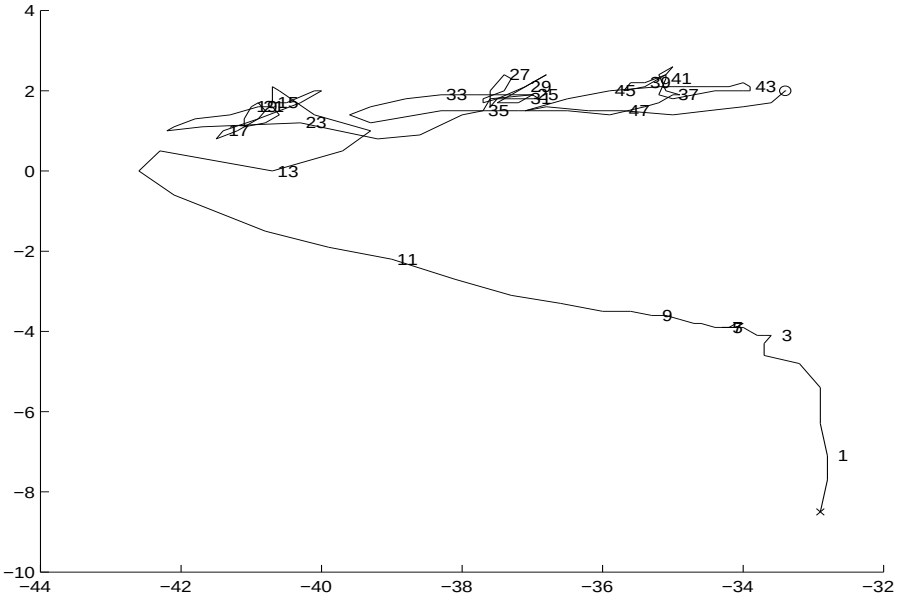


Figure 5.14: The pathway of a virtual float in 500m depth. The launch position in the IWBC is marked with an 'x' and its final position after 4 years is marked with a 'o'. The numbers are the months after launch.

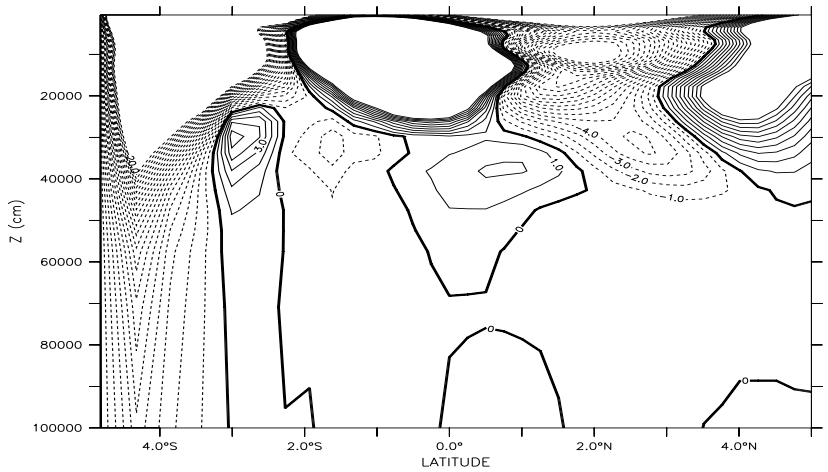


Figure 5.15: The 4 year mean of the zonal velocity across the equator at 30W. Only the velocity range between -10cm/s and 10cm/s is shown.

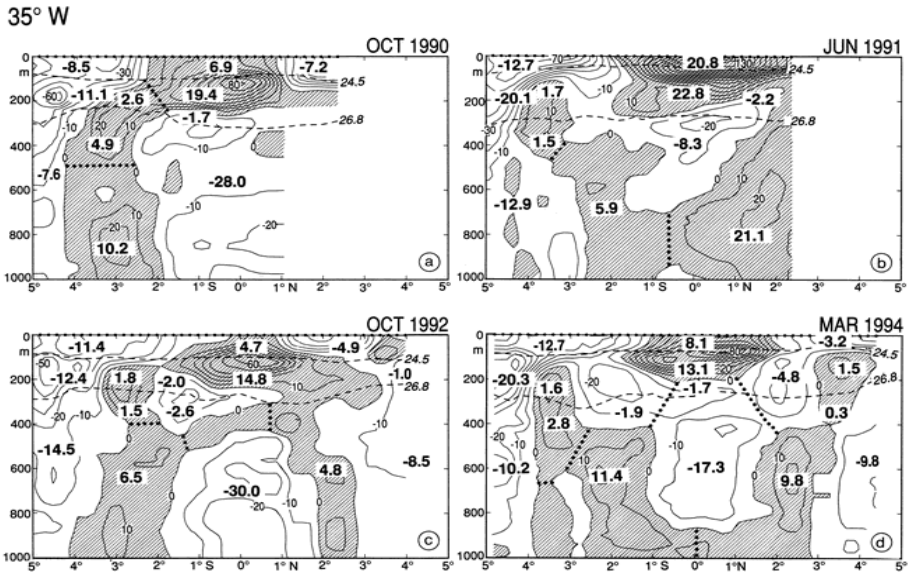


Figure 5.16: The zonal velocity across 35W as observed by Schott et al. (1998) during 4 LADCP sections across the equator. The shaded areas indicate eastward velocities with contour lines every 10cm/s. The bold numbers indicate the transport between the zero isotachs and the arbitrarily chosen dotted lines.

mentioned in the second section. Initial motivation for this research is Schott et al.'s (1998) observation of bands of strong zonal velocities at intermediate depths (Fig. 5.16, their mean is displayed in Fig. 5.2). They interpreted these observations as strong zonal currents, although their existence defied any explanation and contradicts the float observations by Richardson and Schmitz (1993). Strangely, this has not received any attention in the literature. In fact, model studies interpret the lack of strong intermediate currents as a deficiency of the model (Fratantoni (1996) or Blanke et al. (1999)). Figures 5.2 and 5.3 show that the present model is able to reproduce the observed spatial structure of the observations (the amplitude, however, is too small). The model also shows that there is no zonal flow in the yearly mean. This suggests that the Schott et al. (1998) interpretation of the observations can be explained by aliasing of the tropical wave field. Figure 5.17 shows again a Hovmoeller diagram of the zonal velocity in intermediate depths, this time the time and locations of the available measurements are indicated by crosses and circles. It illustrates that all six observations (4 ADCP sections and 2 float trajectories) can be explained by seasonal Rossby waves. The model predicts eastward flow for

the two floats in January, strong westward flow in October, weak westward flow in March and weak eastward flow in June. Given the uncertainties in the wind field, the comparison with Figure 5.16 is striking.

There are, however, differences between the observations and the model results. Figure 5.18 shows snapshots of zonal velocity from the model output, and they can be compared directly with the observations of Figure 5.16. Ideally, one would project a long time series of zonal velocity on the different possible equatorial modes and compare their amplitude in the model with the ones in the observations. Unfortunately, this is not possible because of the few observations. Furthermore, the zonal velocities of the different equatorial modes are not linearly independent. Therefore, one can only qualitatively compare the observations with the model snapshots. The October snapshots and the October observations compare well with the predicted structure of the first symmetrical mode (Fig. 5.11). The March observations are reminiscent of the second symmetrical mode, whereas the model's velocity field looks more like the first antisymmetrical mode (Fig. 5.11). The observations and the model results for June are difficult to interpret as a single mode, they are likely to be the

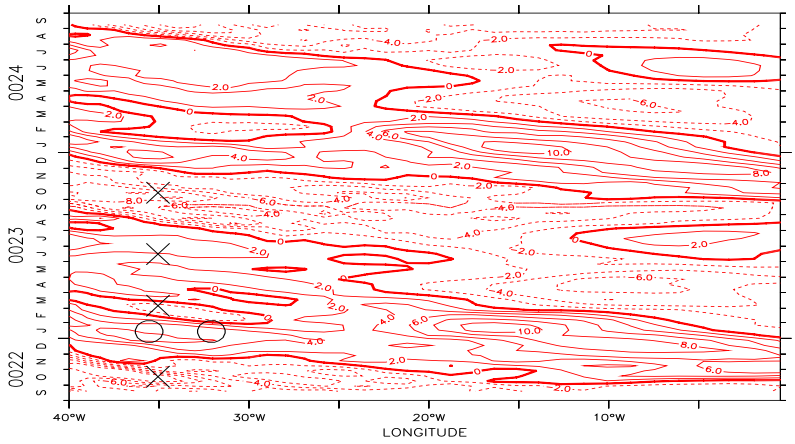


Figure 5.17: Hovmoeller diagram of the zonal velocity in 700m depth. The crosses indicate the time and position of the Schott et al. (1998) measurements and the circles show the launching time and position of the two Richardson and Schmitz (1993) SOFAR floats that were not released near the western boundary.

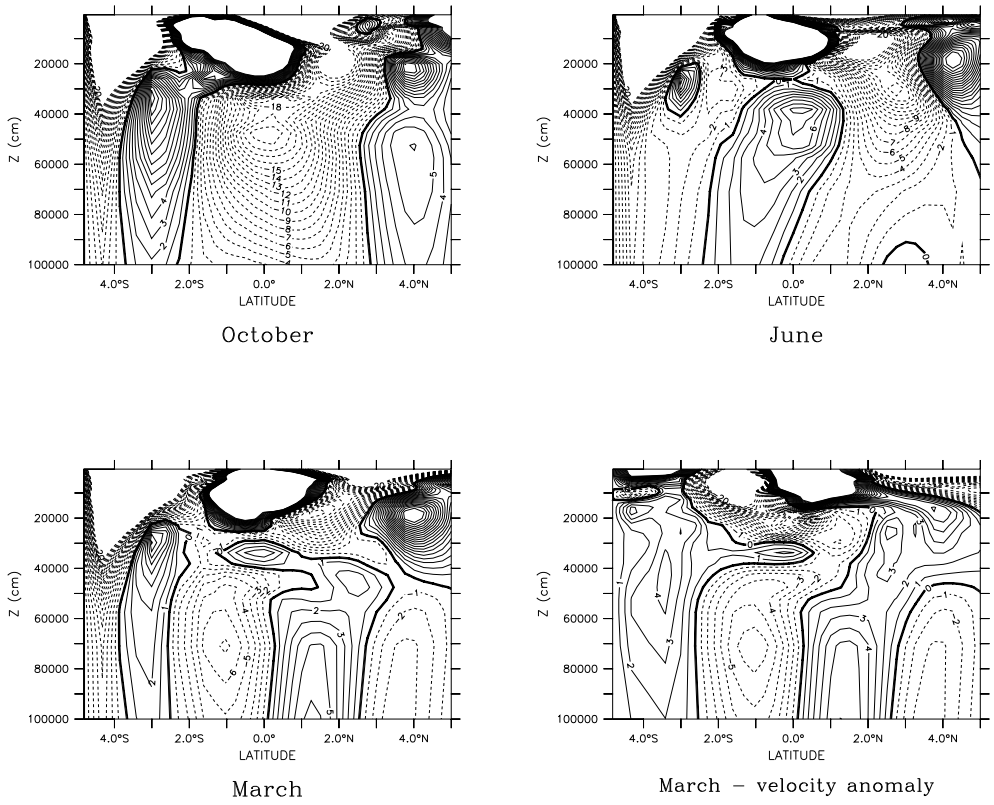


Figure 5.18: The zonal velocity across 35W as computed in the model. Only the range from -20cm/s to 20cm/s is shown. Comparison with Figure 5.16 and Figure 5.11 shows that October is dominated by a Rossby wave of the first symmetrical mode, in the model as well in the observations. The June snapshot is difficult to interpret and the March velocity anomalies suggest that March is dominated by the first antisymmetrical mode (see Fig. 5.11).

superposition of different modes.

While the model is not able to reproduce every single velocity section, it correctly predicts the phase and the strength of the first symmetric mode which in the model accounts for 56% of the variability. It furthermore predicts correctly the eastward flow in late January. The higher latitudinal modes are apparently not reproduced correctly which might be due to a an unrealistic stratification or an unrealistic wind field in the model. It is conceivable that the real wind, which excites the waves in

the ocean, has a different structure than the Hellerman-Rosenstein wind field in the model, and therefore projects differently on the higher modes than the model winds.

The previous analysis does not rule out the existence of intermediate currents along the equator, but the wave interpretation of the observations, like the current interpretation, explains four of the six available observations. We suggest here an alternative explanation for the observations that is as least as plausible as the previous one, but is much more appealing since the physics behind the waves is understood whereas it is not clear what should drive strong intermediate currents along the equator. Of course, eventually only a current meter mooring at the equator will be able to determine whether there are intermediate currents with a significant long time mean or not.

While this analysis does cast doubt on the existence of strong zonal currents, there is the possibility that the waves generate a weak mean flow along the equator. The remainder of this chapter will study this mean flow. For this purpose 100 floats were released in the equatorial waveguide in 450m depth (Fig. 5.19) and the flow

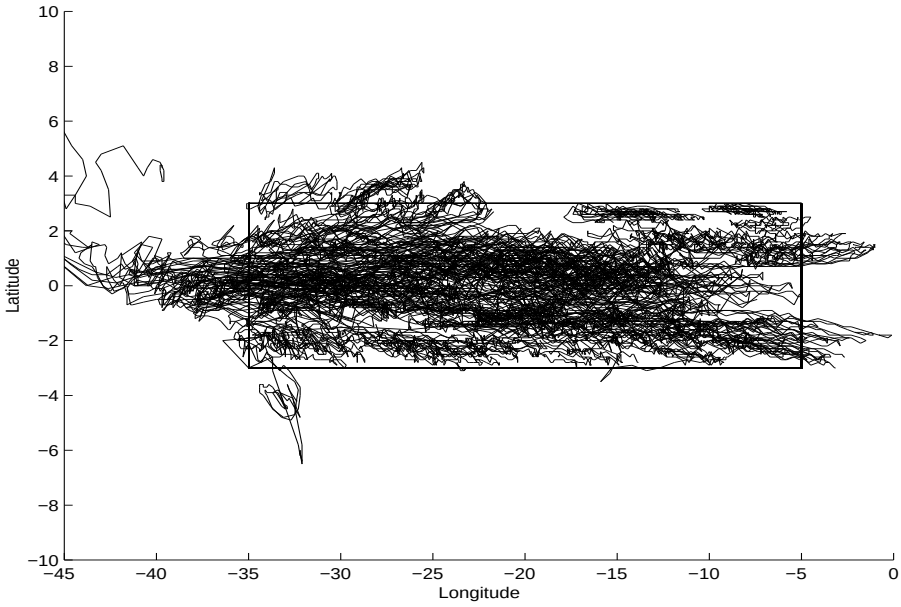


Figure 5.19: The trajectories of floats that were released in the box at 450m depth. After 4 years we can see the easterly tongues polewards of the equator and the westerly tongue on the equator.

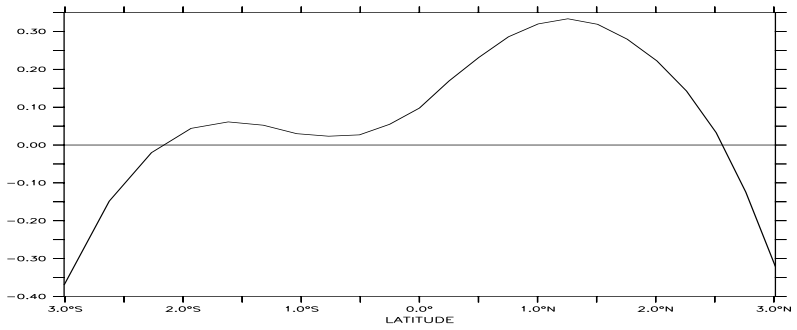


Figure 5.20: The zonally averaged Eulerian mean zonal velocity at 450m depth (in cm/s). The uncertainty of the mean is less than 0.1 cm/s everywhere.

properties of the AAIW layer were computed by analyzing the velocity statistics of the floats. This was motivated by a study of Li et al. (1996), who found that in the equatorial waveguide below the thermocline the Eulerian mean flow is very different from the Lagrangian mean flow. Instead, the Stokes drift that is induced by the seasonal Rossby waves dominates the flow and is of a sign opposite to that of the mean. This occurs in our solution too. The trajectories of the released floats are shown in Figure 5.19. A net eastward displacement polewards of the equator and a net westward displacement on the equator can be seen. To be more quantitative, the area between 36W and 0W, and between 3S and 3N was partitioned into 1x1 degree boxes and the Lagrangian mean velocity was computed in each of these boxes. Fig-

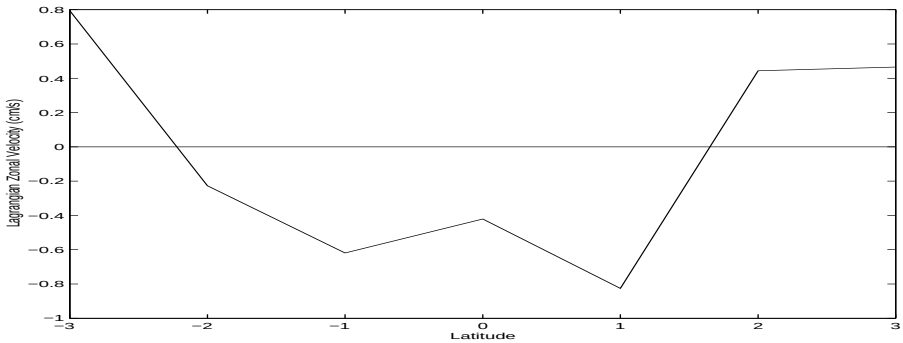


Figure 5.21: The zonally averaged Lagrangian mean zonal velocity at 450m depth (in cm/s). The uncertainty of the mean is less than 0.06 cm/s everywhere.

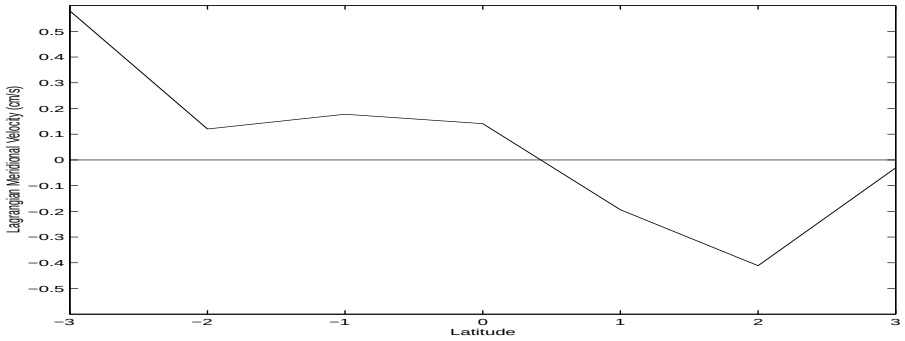


Figure 5.22: The zonally averaged Lagrangian mean meridional velocity at 450m depth (in cm/s). The uncertainty is less than 0.015 cm/s everywhere except for the flow at 3S where it is 0.05 cm/s.

ure 5.20 shows the zonally averaged Eulerian mean flow and Figure 5.21 the zonally averaged Lagrangian mean flow. Clearly, the Eulerian mean flow is a bad predictor for particle behavior. We estimate the magnitude of this Lagrangian circulation to be less than 0.5 Sv.

Figure 5.22 shows the Lagrangian meridional velocity that indicates an equatorward flow on both sides of the equator. Davis (1998) demonstrated that particles

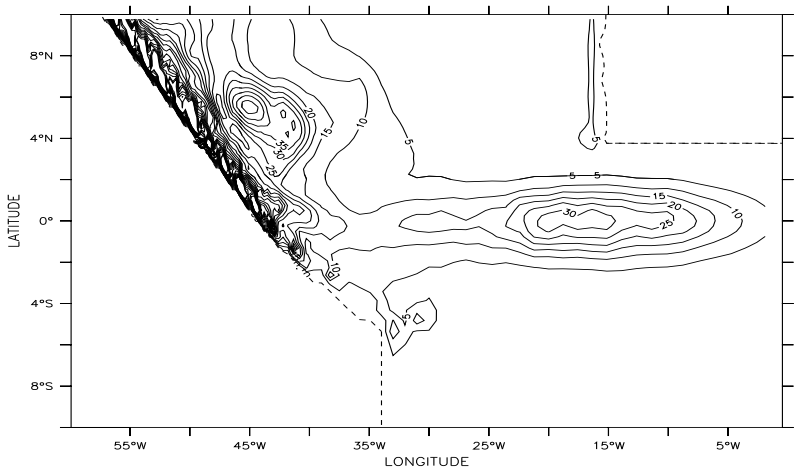


Figure 5.23: The variance of the meridional velocity at 450m depth in $cm^2/s^2$.

will drift towards areas of higher variability and Figure 5.23 shows that in the interior the highest variance of meridional velocity is along the equator. This analysis shows that the Rossby waves generate a secondary circulation with eastward flow off the equator and westward flow at the equator. Tracers will converge towards the equator where they find the highest variance of meridional velocity. These effects are certainly not enough to explain the equatorial tracer distribution in the AAIW but they should be taken into account in the analysis of the observations.

# Chapter 6

# On the dynamics of the Tsuchyia Jets

## 6.1 Introduction

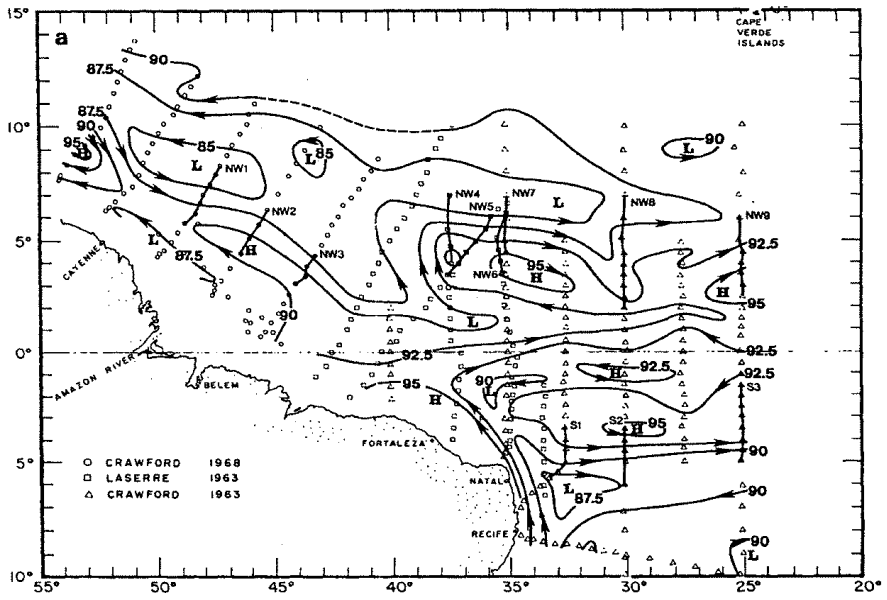


Figure 6.1: Acceleration potential (dyn cm) at 140m depth for February to April (Cochrane et al. (1979). Note the eastward flow at 5S and 5N.

The Atlantic as well as the Pacific ocean feature two narrow subsurface countercurrents that flow eastward several degrees poleward of either side of the equator. As

they cross the basin, their core rises and shifts polewards. They were first reported in the Pacific by Tsuchyia (1975) and later described in the Atlantic by Cochrane et al. (1979, see Figure 6.1). For the reminder of this chapter we will refer to them as Tsuchyia Jets (TJ). Their basic properties in the Pacific have recently been summarized by Rowe et al. (2000) who analyzed an extensive set of hydrographic and ADCP data. They found that the Pacific TJs carry about 14 Sv of water across the basin and that their core densities decrease as they flow east.

Much less observations are available in the Atlantic. In fact, only the flow west of 25W has been investigated in detail. At 30W Cochrane et al. (1979) find for the southern Tsuchyia Jet (sTJ) a transport of 15 Sv (based on three hydrographic sections in February and one section in August). On the other hand, Schott et al. (1998) determine the transport at 35W to be 2 Sv (based on four ADCP sections, two in October, one in March and one in June). These values are hard to reconcile, and, similarly to the previous chapter, it can be expected that the aliasing of the tropical wave field makes it difficult to interpret the observations. Furthermore, Cochrane et al. (1979) face the problem of choosing a level of no motion, and the Schott et al. (1998) measurements are so close to the western boundary that one cannot exclude the possibility that signals from the NBC influence the observations.

In both oceans it can be concluded from the properties of the TJ cores that the source region of the TJ water lies outside the tropics. The final destination of the TJ water is less clear, since in both oceans the eastern basin outside the equatorial wave guide is not very well sampled. Even less understood is their dynamics. Because their core is below the thermocline, it is commonly assumed that they cannot be directly wind-driven. McPhaden's (1984) analytical approach explains the TJs as a balance between vertical diffusion of relative vorticity and advection of planetary vorticity. The limitation of this solution is that the TJs cannot be separated from the EUC. The more recent attempt by Marin et al. (2000) has the drawback that it assumes a priori a density distribution, thereby masking the important question of what determines and maintains the density structure.

More promising seems to be the idea of Johnson and Moore (1997) who assume that the TJs are forced at the western boundary and then continue as an inertial, inviscid flow. As the jets penetrate eastward they compensate for the shallowing of the thermocline with a poleward shift. The forcing mechanism, however, remains

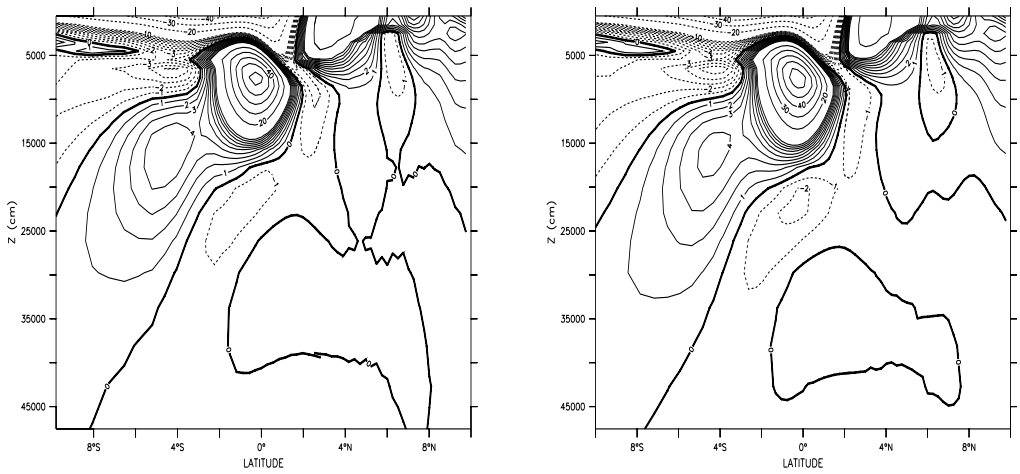


Figure 6.2: The yearly mean of the zonal velocity in the experiment without MOC (left) and the experiment with MOC (right). The contour intervals are only displayed from -10cm/s to 10cm/s to emphasize the subthermocline flow. The core of the TJs is located at 4S/4N in 200m depth.

unclear.

Based on the results of a highly idealized numerical model, McCreary et al. (2001) explains the Pacific TJs as being remotely forced by the Indonesian throughflow. By analogy, the Atlantic TJs are driven by the MOC (McCreary, pers. comm.). In this study it was attempted to verify this by comparing an experiment with MOC to an experiment without MOC (Fig. 6.2). The figure shows the flow field from earlier experiments that used a constant meridional viscosity of $2000 m^2/s$, therefore the TJs are more diffuse than in Exp1 (see next section). However, their cores are clearly separated from the EUC, and the viscosity is the same that is used in the McCreary et al. (2001) study. The figure shows, that the interior flow and specifically the TJs are indistinguishable in both experiments.

The previously described theories all have their shortcomings and none of them is able to fully explain the TJs. In this study we investigate a detail of the TJs that hitherto has not received much attention: the core of the TJs changes density as it flows east, suggesting that diapycnal processes and eddy fluxes might be relevant.

This has already been noticed by Rowe et al. (2000), McCreary et al. (2001) and Suginohara (pers. comm.) but has yet to be explored in detail. In the following section the Tjs are described as they are found in Exp1. The third section investigates the major source of eddy fluxes in the equatorial Atlantic and relates them to friction and ageostrophic velocities.

## 6.2 The structure of the Tsuchyia Jets in the model

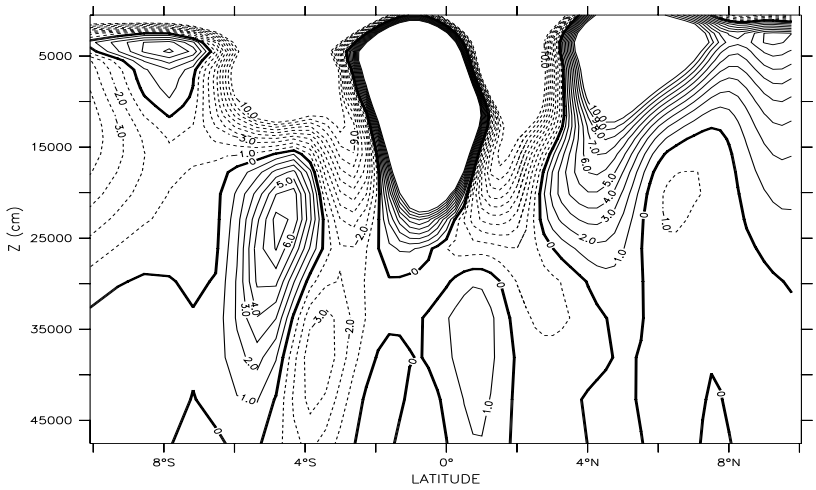


Figure 6.3: The zonal mean velocity at 30W. The TJs are the bands of eastward velocity at 5S and 4N. The northern TJ merges with the lower part of the NECC. Only the contour lines between -10cm/s and 10cm/s are shown to emphasize the TJs.

A vertical section across the modeled field of zonal velocity at 30W is shown in Figure 6.3. The surface jets have been described in Chapter 3, and here the focus is on the zonal flow below the thermocline at 5S and 4N. At 5S the southern TJ (sTJ) can easily be identified as the isolated core of eastward velocity at 5S. The northern TJ cannot be distinguished from the lower part of the NECC, therefore

the following discussion will focus on the sTJ. Figure 6.4 shows the velocity at 150m depth, and one can identify two distinct regions: a zonal flow parallel to the equator that is not connected to the western boundary and extends to about 10W, and a southeastward flow thereafter. Between the EUC and the sTJ there is a westward current that seems to be connected to the sTJ. This becomes more clear by studying the PV distribution (defined as $-(f+\zeta)*T_z$, Figure 6.5) that shows a broad band of low PV water between the equator and the core of the sTJ which suggests strong mixing between 4S and 4N.

A look at the Sverdrup streamfunction in Figure 3.7 (Chapter 3) suggests that

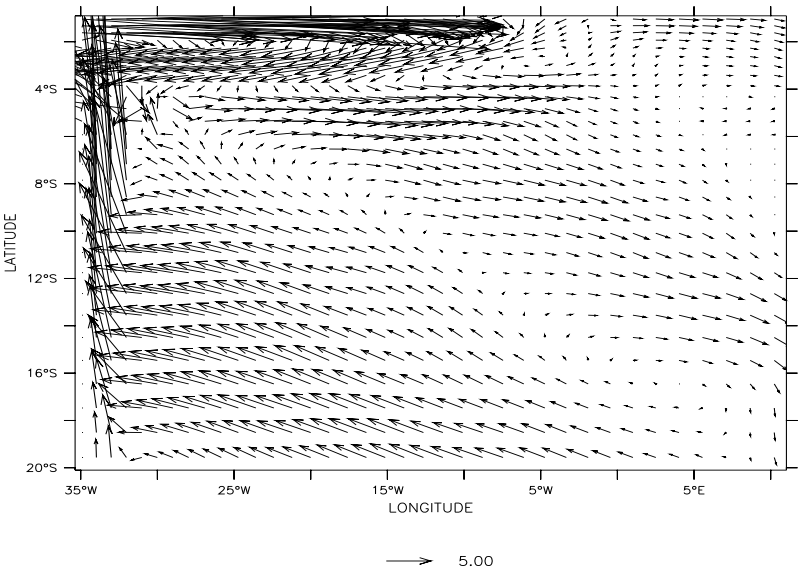


Figure 6.4: The mean velocity in 150m depth between 20S and 2S.

the southeastward extension of the sTJ is part of the equatorial gyre and is directly forced by the wind. To verify this, Exp 1 was repeated but without the nonlinear terms in the momentum equation. This means that the resulting flow must be in Sverdrup balance everywhere, with the exception of regions with strong shear where friction becomes important. Figure 6.6 shows the resulting flow field in 150m depth. Philander (1990) already showed that the EUC in a linear solution is much broader than in a nonlinear solution because the poleward diffusion of momentum is not countered anymore by equatorward advection of momentum in the thermocline.

Further comparison with Figure 6.4 shows that the southeastward flow remains the same. The difference is that in Exp 1 this flow is fed by the sTJ whereas in the linear run it is fed by the broad EUC. This is an important result: The TJs are under two different dynamical regimes, the eastern part being directly wind-driven and in Sverdrup balance, whereas the western part requires nonlinear dynamics. The remainder of this chapter will be devoted to the study of the narrow zonal flow in the western part of the basin.

A section of temperature and zonal velocity along the core of the sTJ is shown in Figure 6.7. Overlying the sTJ is the core of the SEC and adjacent on the sTJ's western end is the NBC. It can be seen that the core water of the sTJ becomes warmer as the sTJ penetrates east. Figure 6.8 shows the mean transport of the sTJ which we defined as the integral over the positive eastward velocity between 6S and 2S, and 50m and 500m. It is not reasonable to compute the seasonal variation of this transport since it will reflect not only transport changes in the sTJ but also the meandering of the EUC and the seasonal Rossby waves (both of which do not contribute to the annual mean transport). The peak in transport and velocity west of 30W suggest that western boundary dynamics are relevant there. Unfortunately

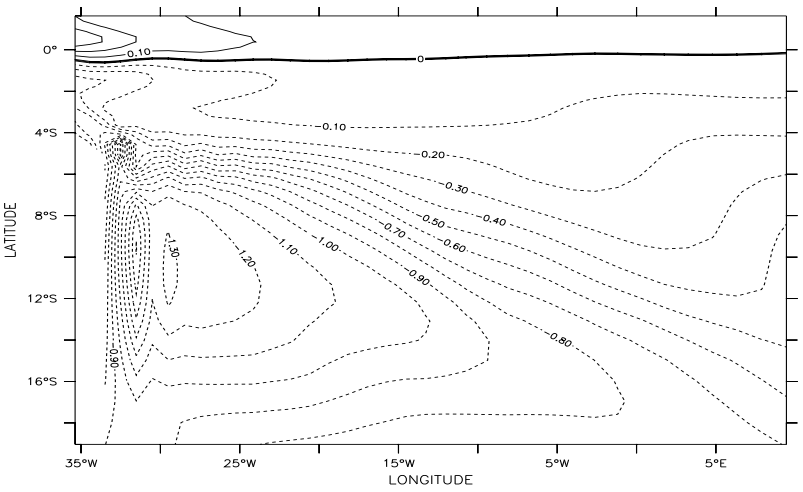


Figure 6.5: The potential vorticity between 20S and 2N in 150m depth.

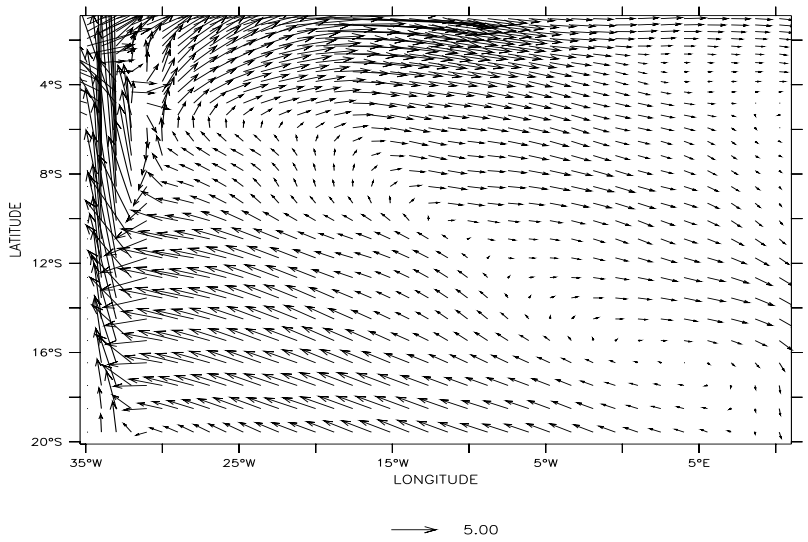


Figure 6.6: The mean velocity in 150m depth between 20S and 2S for the experiment without advection of momentum.

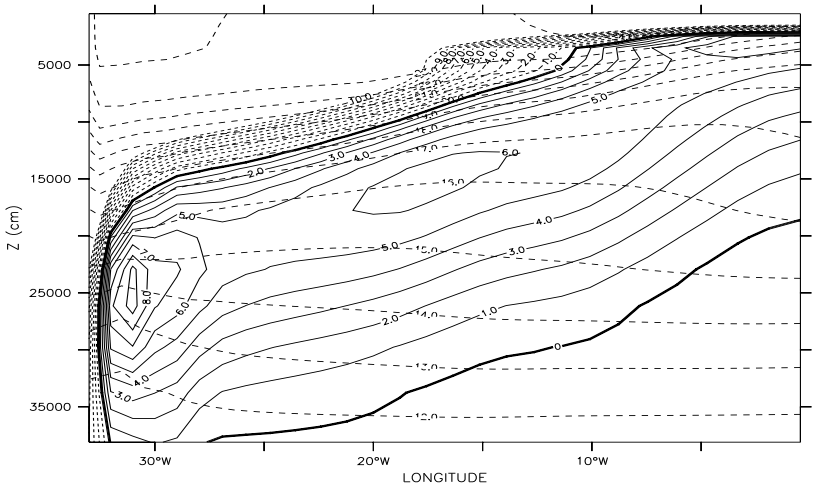


Figure 6.7: The zonal mean velocity along the core of the sTJ at 5S (in cm/s)

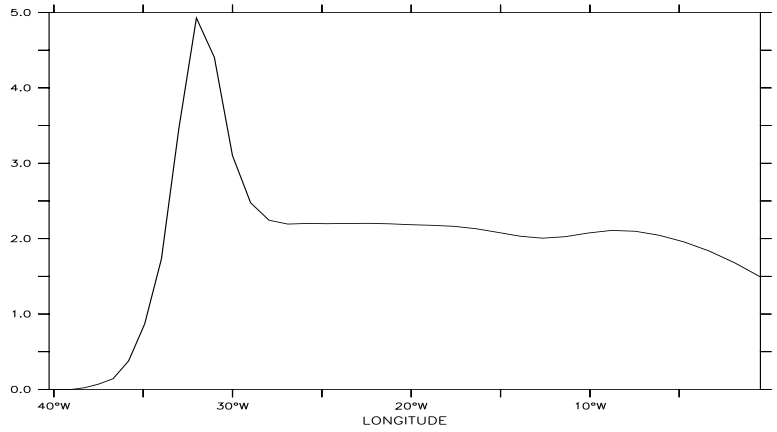


Figure 6.8: The annual mean of the eastward transport between 6S and 2S and between 50m depth and 500m depth (in Sv). The peak west of 30W is due to a strong local recirculation near the western boundary.

the zonal resolution in this area (1 degree) does not allow for a detailed analysis of this flow.

Figures 6.4, 6.6, 6.7 and the analysis of observations by Rowe et al. (2000) suggest that eddy fluxes are relevant to the maintenance of the TJs. The next section will investigate the source and importance of these eddy fluxes.

## 6.3 Wave-zonal flow interaction

In our opinion the theories that were outlined in the introduction are not sufficient to explain the structure of the Tsuchyia Jets, and in the previous section it was shown that eddies or waves might be relevant to the TJs. Waves can have two distinct effects on the mean flow: they accelerate the flow directly via the convergence of eddy momentum flux, and they change the stratification via the flux of heat. It is difficult to estimate the relative contribution of this effects on the mean flow. Only for the case of a zonally averaged flow has it been possible to develop a framework for such a comparison. This framework is called the Transformed Eulerian Mean (TEM) equations (Andrews and McIntyre (1976)) and is discussed here to guide our

understanding of eddy fluxes.

The main purpose of zonally averaging the equation of motion around a latitude circle is that the zonal pressure gradient and the mean advection of tracer and momentum vanish (by continuity $\overline{v}$ has to vanish). The zonal derivatives of the eddy fluxes vanish as well. Furthermore, the vertical advection of momentum is neglected in this quasi-geostrophic framework. This yields the following equation for the zonal momentum:

$$u_t - fv^a = F - \overline{(v'u')}_y, \tag{6.1}$$

with F being the friction and $v_a$ the ageostrophic meridional velocity. The overbars are only retained over the eddy properties and dropped everywhere else ( $\overline{v} \equiv v$). The resulting temperature equation is:

$$T_t + wT_z = -\overline{(v'T')}_y + H, \tag{6.2}$$

with H being the heating. The averaging reduces the continuity equation to:

$$v^a_y + w_z = 0 \tag{6.3}$$

Thus, by zonally averaging it was possible to reduce the system to two dimensions in which it is possible to combine the momentum and the heat effect of eddies into one equation.

Equations 6.1 and 6.2 show that for the steady state in the absence of friction and heating the eddies will induce a meridional overturning circulation. To consider a more general case, $w$ is rewritten as:

$$w^* = w - \frac{1}{T_z}\overline{(v'T')}_y \tag{6.4}$$

and the continuity equation yields:

$$v^* = v^a - (\frac{1}{T_z}\overline{(v'T')})_z \tag{6.5}$$

Equation 6.1 can then be rewritten as:

$$u_t - fv^* = F - \overline{(v'u')}_y + f(\frac{1}{T_z}\overline{(v'T')})_z \tag{6.6}$$

The last two terms on the rhs constitute the divergence of the Eliassen-Palm flux and this formulation makes it possible to compare the relative impact of thermal

and direct momentum forcing.

The application of this theory to the sTJ in the model is not straightforward because it is not reasonable in the ocean to average around a latitude circle. It is, however, possible to make progress if only a special area of the sTJ is analyzed. Figure 6.7 suggests the reformulation of the TEM equations to study the time averaged flow along the axis of maximum velocity. In this model, the axis reaches from 30w/250m to 10W/100m, east of 10W the flow starts to shift poleward. Along this axis $u_x$ is identically zero and Equation 6.3 remains unchanged apart from replacing the zonal average by an temporal average. In the absence of heating and with $\overline{(u'T')_x} << \overline{(v'T')_y}$ (Figure 6.9) the temperature balance becomes:

$$wT_z = -\overline{(v'T')_y} - vT_y - uT_x. \tag{6.7}$$

Again, the overbars are only retained over the eddy terms. The vertical velocity

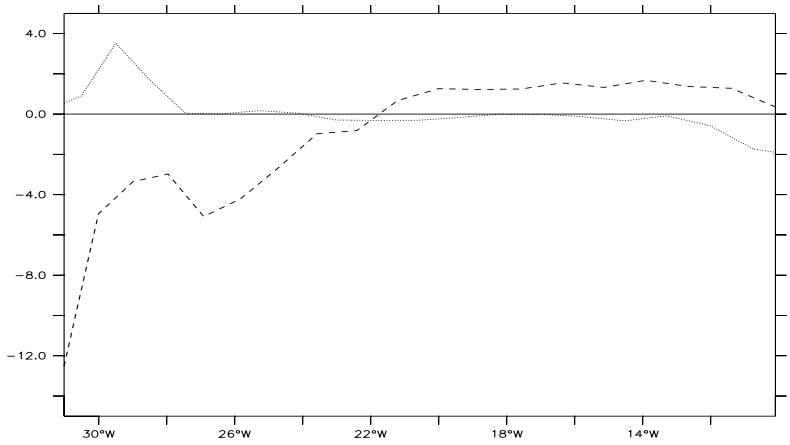


Figure 6.9: This plot shows the comparative strength of meridional (broken line) and zonal (dotted line) eddy temperature flux along the core of the sTJ (in $10^{-7}K/s$). The meridional flux is dominating over most of the core area.

can, as in TEM, be rewritten as:

$$w^* = w - \frac{1}{T_z}\overline{(v'T')_y} \tag{6.8}$$

The reason for only looking at the flow along the axis of maximum velocity is that it is now possible to use (6.3) to determine the meridional residual circulation like in TEM as:

$$v^* = v^a - (\frac{1}{T_z}\overline{(v'T')})_z, \tag{6.9}$$

Along the chosen axis the advection of momentum vanishes because the horizontal derivatives of the zonal flow are identically zero along the core of the jet. With these preparations, and after removing the part of the meridional velocity that is directly controlled by the zonal pressure gradient the resulting equation for the zonal momentum can be written as:

$$fv^* = k_z u_{zz} + k_y u_{yy} - \overline{(u'u')_x} - \overline{(v'u')_y} + f(\frac{1}{T_z}(v'T'))_z \tag{6.10}$$

This equation allows for the calculation of the relative importance of eddy heat flux, eddy momentum flux and dissipation. Figure 6.10 shows the two different eddy flux

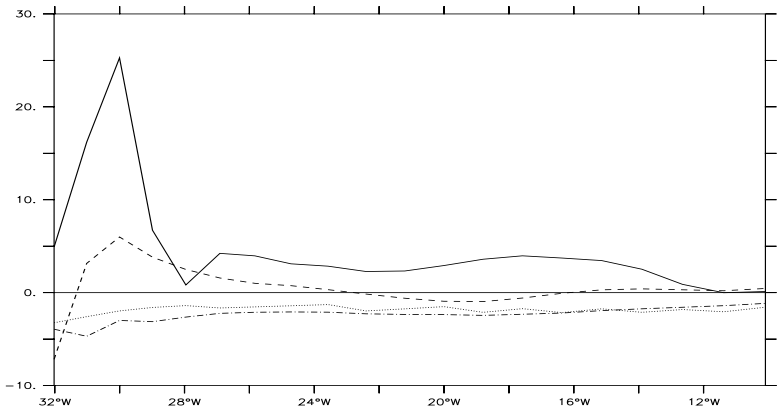


Figure 6.10: The contribution of the different terms in equation (6.10) to the zonal momentum budget (along the core of the sTJ, in $10^{-9}m/s^2$). The solid line shows the contribution of the eddy heat flux, the broken line the sum of the two eddy momentum flux convergence terms, the dotted line the effect of vertical viscosity and the dash-dotted line the effect of meridional viscosity.

contributions and the effect of meridional and vertical viscosity. It can be seen that the effect of the eddy heat flux dominates the convergence of eddy momentum flux

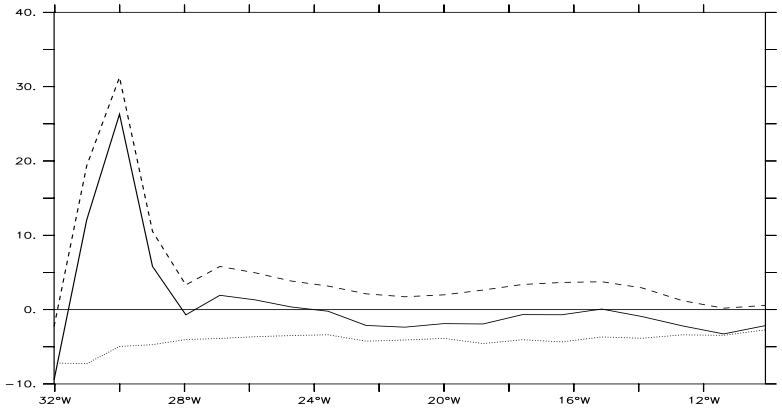


Figure 6.11: Like Figure 6.10, but for the sum of eddy flux contribution (solid line), the friction (broken line) and the sum of friction and eddy flux contribution (dotted line).

and that the meridional and vertical viscosity are of equal importance. The next figure (Fig. 6.11) shows the sum of the eddy fluxes, the sum of the friction terms and the sum of dissipation of momentum and effective eddy momentum flux. The eddy fluxes are roughly balanced by the friction, and the residual is supporting a weak meridional circulation $v^*$ of the order of $10^{-4} m/s$. In principle, it is possible to arrive at an independent estimate of the ageostrophic velocity $v^a$ and the residual $v^*$, but the rigid lid formulation of the model does not require and calculate the surface pressure. It is possible to recover the surface pressure from the equation of motion, but to do this, the very eddy fluxes that were just evaluated would have to be used. Therefore, without the surface pressure there is no independent way to calculate the ageostrophic velocity.

The analysis above suggests that the sTJ is maintained against friction by the eddy heat fluxes which steepen the slope of the isotherms. The remaining problem is to find the source of these eddy fluxes. The fact that the Tjs are of equal strength and structure in the experiment with steady wind and the experiment with seasonally changing wind suggest, as in the case of the NBC rings, that the seasonal Rossby waves are not relevant for the TJs. Another possible source of wave energy is an

unstable equatorial current system. The quasi-geostrophic instability theories break down at the equator, but Masima and Philander (1999) studied the development of instabilities in the equatorial waveguide with an idealized numerical model of the Pacific ocean. They show that instabilities develop along the regions of strong shear between the SEC and EUC. The resulting waves compare well to the observations of Legeckis (1977) and are commonly referred to as Legeckis or Tropical Instability Waves. Figure 6.12 shows a snapshot of the TIW in this model. Apart from the seasonal waves, they are in this model the only other waves that can be detected along the equator. Their zonal wavelength is approximately 1100km and their period is approximately one month (Fig. 6.13). The following figure (Fig. 6.14) shows a vertical section along the equator and it can be seen that the TIW develop near the surface and radiate energy eastward and downward. Their properties compare very well to the observations of Weisberg et al. (1979) who observed at 5W waves with a wavelength of 1220km and a period of 31 days.

The latitude-depth structure of these TIWs can be seen in Figure 6.15 which

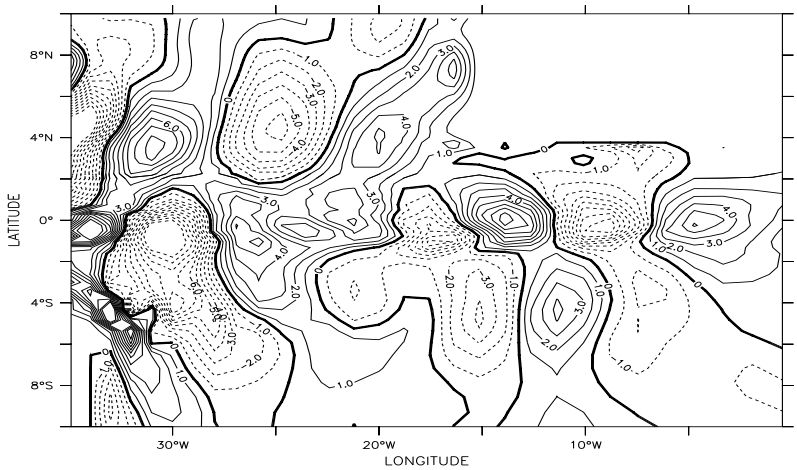


Figure 6.12: A snapshot of meridional velocity anomalies in 200m depth (in cm/s).

shows the first EOF of the meridional velocity anomaly at 25W. Away from the equator, the velocity perturbation of the waves is in geostrophic balance, leading to a correlation between the temperature perturbation (Fig. 6.16) and the velocity

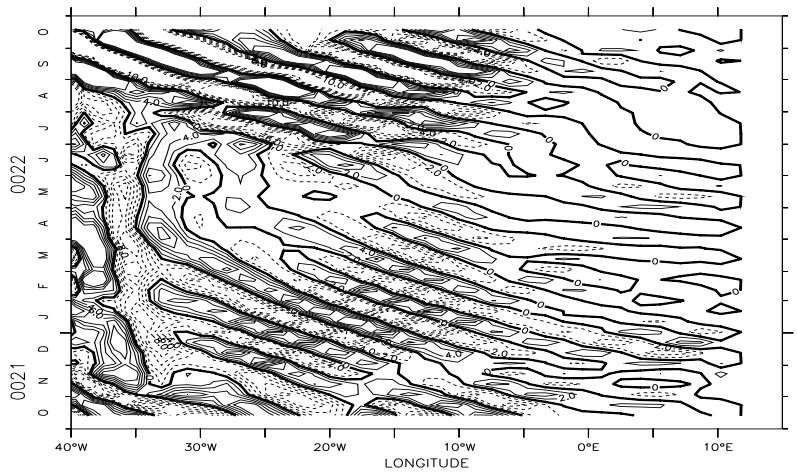


Figure 6.13: A Hovmoeller diagram of meridional velocity anomalies along the equator in 200m depth (in cm/s). Their activity is mostly confined to the area between 35W and 0W.

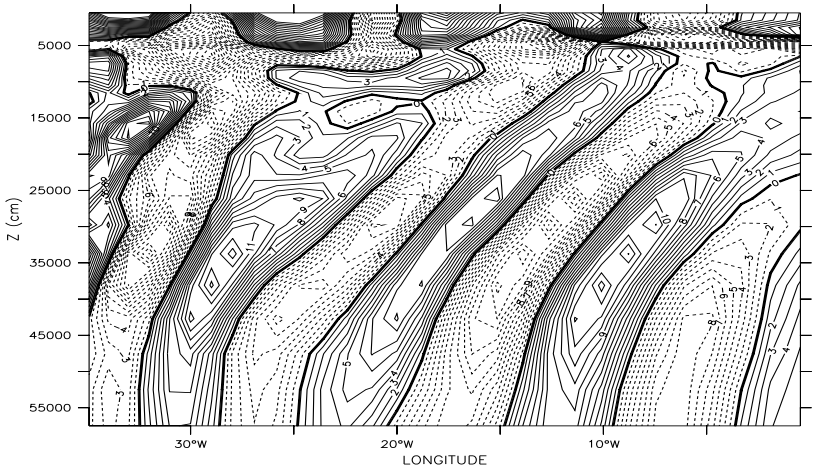


Figure 6.14: A snapshot of meridional velocity anomalies along the equator for the same time as in Figure 6.12.

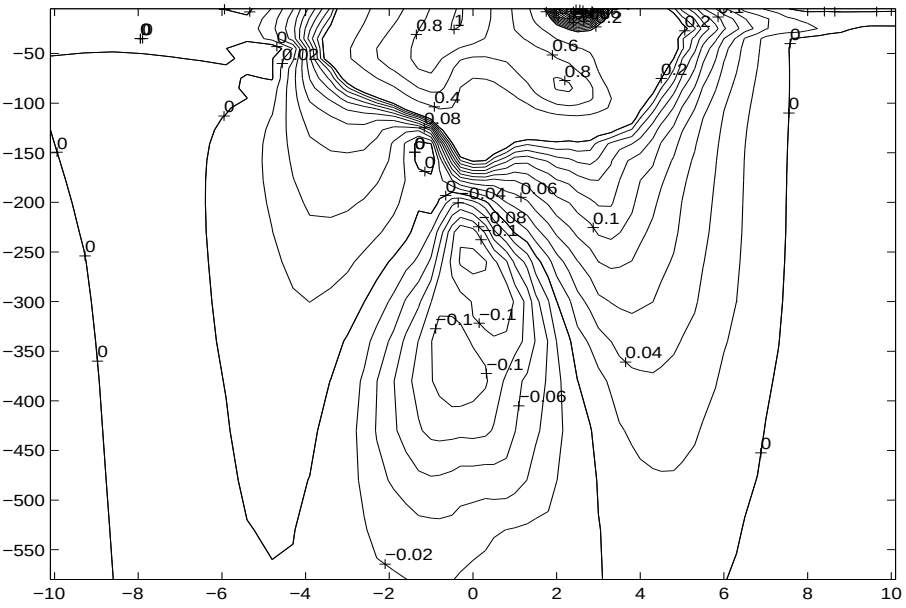

Figure 6.15: The first EOF of the meridional velocity anomalies at 25W. This mode explains 46 % of the variability (the second mode explains 13 %).

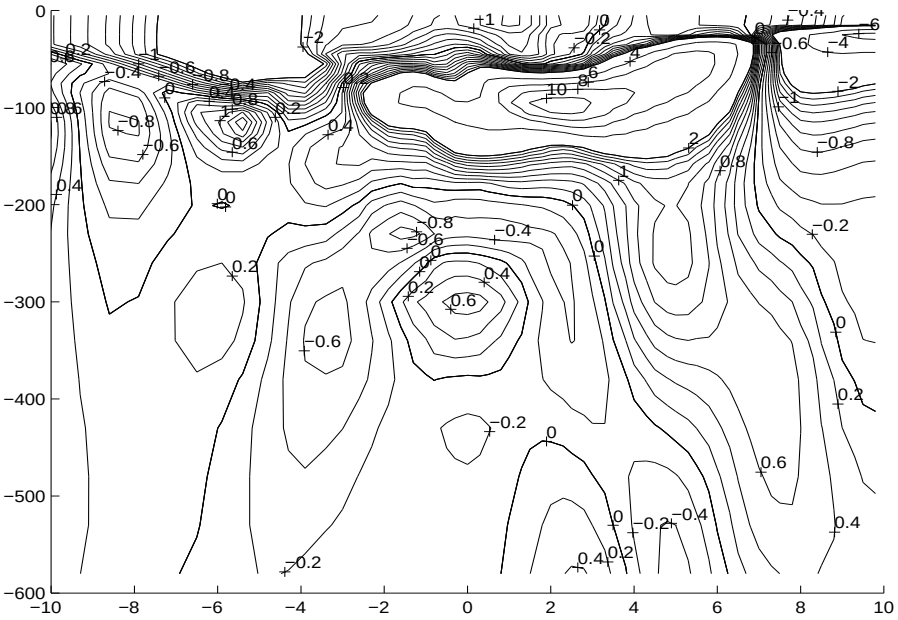

Figure 6.16: The first EOF of the temperature anomalies at 25W. This mode explains 53 % of the variability (the second mode explains 22 %).

perturbation. Thus, the particular structure of the TIW leads to maxima in the heat flux at approximately 5S and 4N which is able to maintain the TJs against dissipation.

We could see that the narrow zonal jet between 30W and 10W is controlled by eddy fluxes and dissipation. The strength of either of these effects depends on surface forcing and subgrid parameterization which is not necessarily well represented in this model. Therefore it can be concluded that, although the model enabled us to understand the dynamics of the TJs, their strength is unlikely to be realistic. Especially below 500m depth where the vertical resolution of the model becomes very coarse the TIWs will not be represented appropriately. For the pathways of the return flow of the MOC, however, this is not expected to be very important, because the amount of water that leaves the topics via the TJs is controlled by the wind-driven interior flow. It can be expected that stronger TJs are the result of stronger mixing between the equator and 5S/4N which will lead to stronger recirculations between the TJs and the westward flow equatorward of it (see Figures 6.4 and 6.5). This, of course, is speculation and would have to be verified with a higher resolution model.

The purpose of this chapter is to investigate the relevance for eddy fluxes for the TJs. It it shown that in this model the sTJ is under three different regimes:
1) West of 30W the sTJ is too close to the western boundary (which is at 34W) to treat it independently from the western boundary flow. Since the zonal resolution at 30W is not sufficient to resolve the strong zonal shear, this area could not be included in this study. It is worth pointing out, however, that above 150m depth the sTJ is not connected to the western boundary and therefore a direct forcing of the sTJ east of 30W by the western boundary flow is unlikely.
2) Between 30W and 10W the model results suggest that the narrow sTJ is maintained against friction by eddy heat and momentum fluxes. The source of these fluxes are the TIW that are generated along the strong shear between EUC and SEC.
3) East of 10W the sTJ bends south and feeds the directly wind-driven circulation of the equatorial gyre.

# Chapter 7

# Summary

A northward flow of warm upper layer water is required to compensate for the export of North Atlantic Deep Water (NADW). This return flow of the MOC has been shown to be important for the northern hemisphere climate. The pathways of this flow form a complex three dimensional pattern that is not well described by observations. Therefore an idealized numerical model of the Atlantic ocean has been used to investigate how the warm water return flow of the MOC crosses the equator and reaches the northern subtropical gyre. This research focused in particular on five different topics:

- Clarification of the interaction between the MOC and the wind-driven circulation.

The equatorial thermocline consists mainly of South Atlantic water (Kawase and Sarmiento (1985)) which can now be explained by the specific shape of the wind field in the tropical Atlantic and the way the MOC interacts with the resulting flow at the western boundary. The wind field in the North Atlantic strongly inhibits an interior pathway and allows only a lower western boundary current as a path from the northern subtropical gyre to the tropics. But at the western boundary the MOC return flow forces this water north and blocks this path. Furthermore, Wilson and Johns (1997) showed during a carefully designed series of cruises, that not more than 8 Sv of South Atlantic water enters the Caribbean Sea through the southern passages. This water arrives there in the surface layer and in the intermediate layer

but no thermocline water from the South Atlantic enters the Caribbean Sea. The experiments show how the thermocline water of the South Atlantic feeds the NBC, which in turn retroflects into the EUC (only the surface part of the NBC flows into the NECC). In the EUC the water is entrained into the mixed layer and continues north in the Ekman layer. This does not only explain why there is no South Atlantic thermocline water found in the North Atlantic. It also explains why only half of the MOC return flow enters the Caribbean Sea through the southern passages. The other half might flow north in the Ekman layer all across the basin and may enter the Caribbean Sea anywhere or not at all.

- A quantitative study of the relative contributions of the different cross hemispheric pathways to the warm water limb of the MOC.

This quantitative study was not the focus of the thesis, it is included to provide a background for the following research. The absolute contribution of each of the pathways is dependent on the uncertain boundary conditions; however, we believe that the model allows to determine the relative importance of the different pathways.

In the model, one can identify four different paths that deliver approximately 17 Sv of warm SA water into the NA to compensate for the outflow of NADW. The most significant of these pathways is a convoluted thermocline-surface path. This path originates in the subtropical SA where water subducts and then approaches the western boundary of the SA. At the western boundary, the water either enters the southward Brazil Current and recirculates in the southern subtropical gyre, or it joins the NBC which will carry the water north towards the equator. On the thermocline level, most of the NBC deflects to the east and feeds the EUC. On its way to the east, the EUC's core rises and gradually loses its water to the equatorial mixed layer due to the equatorial Ekman divergence. The SEC then returns this upwelled SA thermocline water to the NBC as warm surface water. The NBC delivers this new surface water to the NECC, where it continues east to feed the northward flowing Ekman layer of the tropical gyre. Based on the model results, this pathway contributes between 6 Sv and 9 Sv to the MOC return flow (see Figures 7.1 and 7.2). This value depends on how much NA water can be mixed across the NECC front and reach the equatorial upwelling region. Most, but not all, of the SA

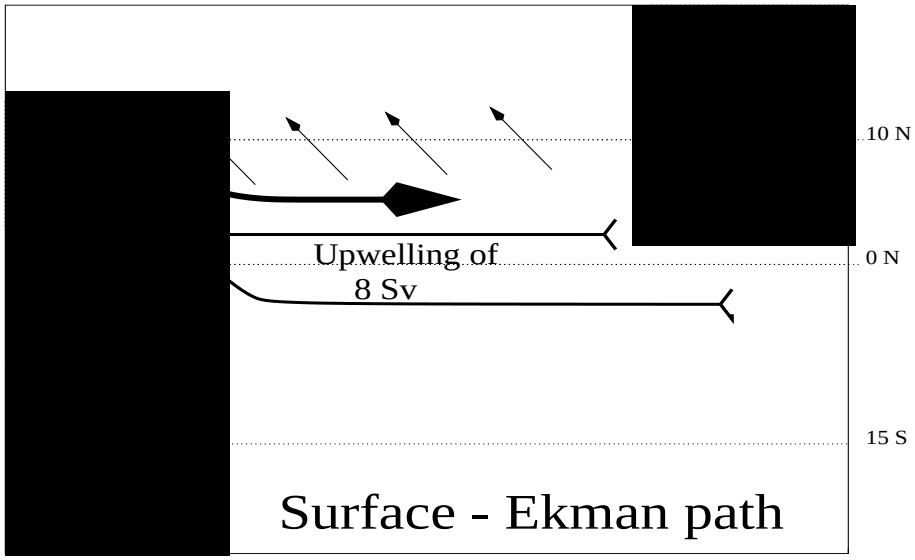


Figure 7.1: The surface part of the MOC return flow. The water upwells into the equatorial mixed layer and is returned to the NBC by the two equatorial branches of the SEC. From there it enters the NECC and eventually flows north in the Ekman layer of the tropical gyre. A small fraction of the water is trapped in the NBC rings. The transport values shown here and in the following figures serve merely to indicate the relative strength of the pathways, by no means should they be interpreted as actual transports because neither the model configuration nor the methodology allow for a more accurate estimation.

thermocline water enters the EUC and follows the path described above, while some of it continues north in the NBC. Of this continuing thermocline water, the largest portion enters the NECC and the northern Tsuchyia Jet and flows east below the NECC. From there it gradually feeds the northward Sverdrup flow of the tropical gyre. Between 1 Sv and 4 Sv of SA thermocline water takes this adiabatic path, the second path to the north. Surprisingly, the NBC rings, which in the literature were described as a major pathway, were not found to contribute more than 1 Sv to the MOC return flow. In their core they trap the rest of the NBC water that is not deflecting into the NECC or the northern TJ. After their generation, the NBC rings continue as independent vortices northwest along the coast of South America and carry the SA water across the tropical gyre into the Caribbean Sea (see Figures 7.1 and 7.2).

Whereas the TJ-path has not been described yet, the thermocline-upwelling path,

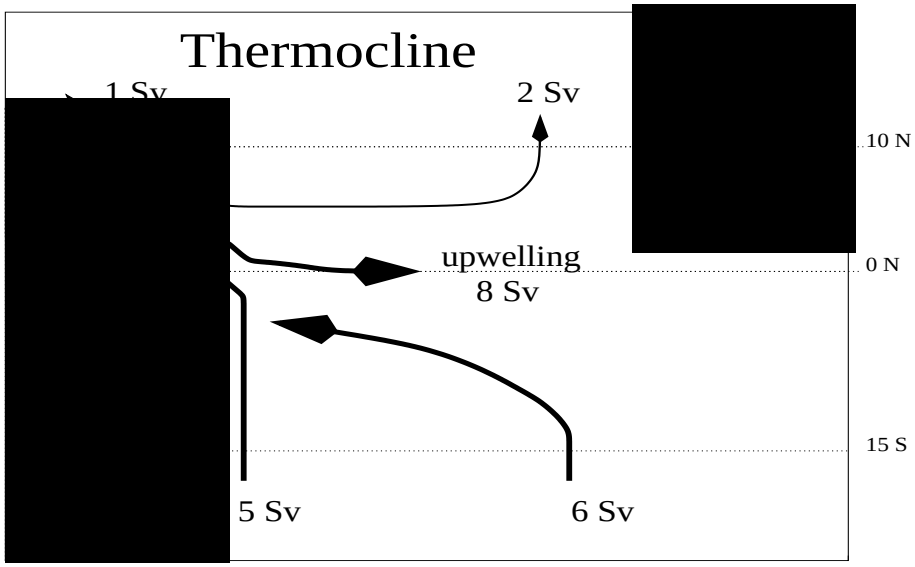


Figure 7.2: The thermocline part of the MOC return flow. After subduction in the southern subtropical gyre the SA water joins the NBC. From there, most of it retroflects into the EUC and eventually upwells into the equatorial mixed layer. Smaller fractions of it cross the tropical gyre in the NBC rings or enter the Sverdrup flow of the tropical gyre via the NECC and the northern Tsuchyia jet.

which is the most important crosshemispheric path, has been described extensively in idealized and in more complex model studies. However, for the purpose of climate studies and coupled ocean-atmosphere models it should be pointed out that there is no direct connection between the equatorial upwelling region and the northward Ekman flow in the tropical gyre. The asymmetry in the wind field forces the upwelled water to the western boundary where it reaches the NECC via the NBC. Only from there does the upwelled thermocline water reach the tropical Ekman layer. This makes it difficult to construct simple two dimensional climate models or scenarios which rely on a simple relation between surface wind stress and sea surface temperature in the tropical gyre.

The remaining 6 Sv of the MOC return flow is carried north in the IWBC, the fourth pathway. The intermediate water has its source and sink outside the model domain, and in the model the strength of its flow is determined by the open boundary conditions of the model. The open boundary conditions were constructed to be consistent with the observed AAIW flow along the western boundary. As in the more idealized work of Edwards and Pedlosky (1998), the laminar IWBC breaks up into

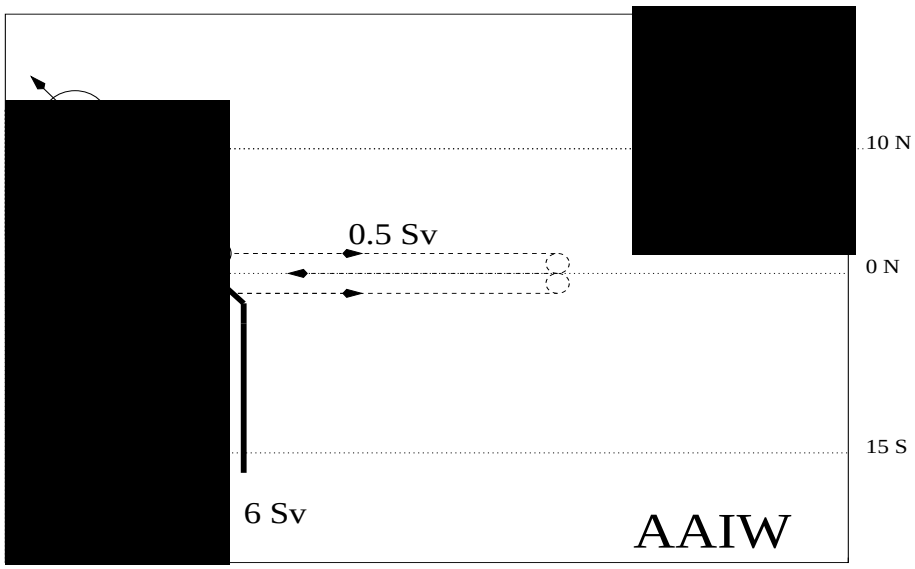


Figure 7.3: The intermediate path of the MOC return flow. The water flows north along the western boundary in the IWBC which breaks up into eddies upon crossing the equator. The weak recirculation cell along the equator is caused by the Rossby wave induced Stokes drift.

intermediate eddies after crossing the equator. This leads to a turbulent IWBC in the northern hemisphere that carries the SA further north in eddies, rather than in a laminar boundary current (see Figure 7.3). The wave induced Lagrangian interior circulation of the equatorial AAIW layer was found to be less than 0.5 Sv.

- A dynamical explanation for the generation and structure of the NBC rings.

The model results suggest that the NBC rings are the result of first baroclinc mode Rossby waves that grow on a barotropically unstable NECC. The waves propagate west and reflect at the South American coast towards the northwest. The anticyclones of the waves become amplified by the steady NBC/NECC retroflection eddy and continue along the coast as NBC rings. Even in the experiment with seasonally changing winds, the NBC rings are generated fairly regularly every 50 days. The further fate of the NBC rings depends on the position of the ITCZ, the seasonal changes of which cause the circulation of tropical gyre to spin up or to spin down. This will accelerate the rings in the spring and slow them down or even stall and

dissipate them in the fall. Thus, some of the NBC rings can be blocked from a propagation towards the Caribbean Sea and dissipate close to their origin.

Recent observations showed that some NBC rings are reaching down well below the thermocline into the intermediate layer. The simple wave reflection alone as it is discussed above cannot explain this deep structure. A close inspection of the modeled intermediate layer showed that the IWBC generates eddies as it flows north and crosses the equator. Its shear increases due to the conservation of potential vorticity until it becomes unstable and breaks up into eddies. These eddies continue north until they either dissipate or merge with the shallow NBC/NECC retroflection eddy. The result are NBC rings than can easily reach beyond 1000m depth. Furthermore it was found that the NBC rings do not contribute significantly to the MOC return flow.

- A new interpretation for the observed flow fields in the intermediate layer of the equatorial Atlantic.

The model reproduces four out of six available velocity observations in the equatorial intermediate layer, all of which are all explainable by the velocity field of seasonal Rossby waves. According to our model results, there is no need to invoke the existence of strong zonal currents (as proposed by Schott et al. (1998)) to explain the observations. There is, however, a weak Rossby wave induced Stokes drift along the equator. This Stokes drift has a magnitude of several mm/s and it points to the west on the equator and to the east at 2S and 2N. Furthermore, the equatorial maximum of meridional velocity variance leads to a convergence of particles at the equator.

- A theory for the Tsuchyia Jets.

The Tsuchyia Jets consist of two components, the first one of which is directly driven by the wind. The second component is a strictly nonlinear feature of the flow: the strong horizontal and vertical shear between the EUC and the SEC leads to instabilities. The resulting instability waves cause a flux of zonal eddy momentum and heat from the equator to the Tsuchyia Jets at 5S/5N. There, the jets are maintained against meridional and vertical viscosity mainly by the meridional heat flux which steepens the isotherms.

Although the model reproduces the circulation of the tropical Atlantic remarkably well and explains several hitherto not understood processes of the tropical circulation, several problems were encountered that could not be answered within the limits of the model configuration. Furthermore, we believe that the good model performance is only in part due to our physical understanding. Certainly, a fortunate choice of empirical parameters and boundary conditions was important as well. Some of the uncertain, less understood processes became obvious during the analysis of the models results and the study of the relevant literature. The most important of these processes is probably the upwelling induced by the equatorial Ekman divergence. Because of the small scales that are involved, the viscosity that together with the wind field determines the upwelling rate, must be parameterized. Although there are several published attempts towards a more physically based parameterization for the viscosity, there is a lack of small- and mesoscale observations to validate them.

Another surprisingly little understood phenomenon is the NECC. The NECC as a zonal current exists only as a long time mean, snapshots show it as an accumulation of eddies which to our knowledge is not sufficiently appreciated in the literature. Satellite based observations should make it possible to evaluate the space and time scales of the NECC variability. A thereby validated numerical model could then be used to study the details of the strong vertical and horizontal recirculations in the western tropical Atlantic.

The intermediate layer poses a range of questions, the obvious one being: Are there strong zonal intermediate currents or not? Here we proposed an alternative, more appealing explanation of the observations in the intermediate layer. However, only a current meter mooring on the equator will provide a definite answer. An deep reaching equatorial current meter mooring will also provide information about the waves that connect the eastern basin with the western basin and the structure of the tropical instability waves that drive the Tsuchyia Jets. In this context, it is worthwhile to study the impact of the Midatlantic Ridge on the properties of planetary waves. Furthermore it is desirable to explain the model's lack of variability along the western boundary to exclude the possibility that there is an important part of the tropical Atlantic's dynamics which is overlooked or not understood.

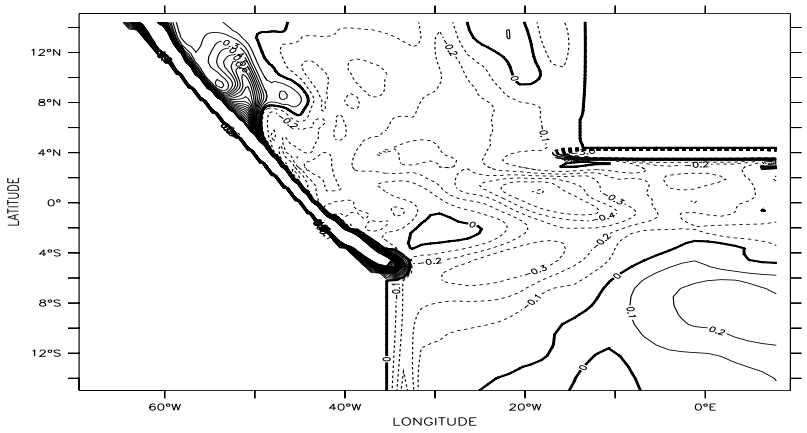


Figure 7.4: The SST difference between the annual mean temperature in the experiment with MOC and the annual mean temperature in the experiment without MOC (in $^oC$). After including the MOC, the central equatorial SST becomes colder and the western boundary water becomes warmer. This is a result based on very simple boundary conditions which has to be validated with a more realistic model setup.

The initial motivation for this thesis was that the MOC might be as important for the climatic relevant SST as the atmospheric forcing, because the MOC determines the water mass structure of the tropical Atlantic. The present analysis of the MOC pathways is a first step towards understanding the MOC's impact on the SST. The model that is used in this study is very idealized and we focused on the dynamics of the pathways. However, even in this idealized study there is a SST difference between the experiment with and the experiment without MOC (Fig. 7.4). The MOC changes the source waters of the equatorial thermocline which leads to a cooling of the equatorial thermocline and a warming of the western boundary (due to a strengthened NBC). A logical next step from this thesis towards an understanding of the climatic impact of the MOC is to study the effect of MOC variability in a more realistic setting. Especially the thermal forcing, which in the present study is simple restoring, needs to become more realistic. Within such a study one can compare the MOC induced SST variability with the observed SST variability.

# References


Anderson, D. L. T., and Corry, R. A. 1985. Seasonal transport variations in the Florida straits: a model study. *J.Phys.Oceanogr.*, **15**, 773–786.

Andrews, D.G., and McIntyre, M.E. 1976. Planetary waves in horizontal and vertical shear: The generalized Eliassen-Palm relation and the mean zonal acceleration. *J.Atmos.Sci.*, **33**, 2031–2048.

Arhan, M., Mercier, H., Bourles, B., and Gouriou, Y. 1998. Two hydrographic sections across the Atlantic at $7^o30N$ and $4^o30S$ . *Deep-Sea Res.*, **45**, 829–872.

Beckmann, A. 1988. Vertical structure of midlatitude mesoscale instabiity. *J.Phys.Oceanogr.*, **18**, 1354–1371.

Blanke, B., and Delecluse, P. 1993. Variability of the tropical Atlantic ocean simulated by a general circulation model with two different mixed-layer physics. *J.Phys.Oceanogr.*, **23**, 1363–1388.

Blanke, B., Arhan, M., Madec, G., and Roche, S. 1999. Warm water paths in the equatorial Atlantic as diagnosed with a general circulation model. *J.Phys.Oceanogr.*, **29**, 2753–2768.

Boebel, O., Schmid, C., and Zenk, W. 1999a. Kinematic elements of Antarctic Intermediate Water in the south Atlantic. *Deep Sea Res.*, **46**, 355–392.

Boebel, O., Davis, R.E., Ollitrault, M., Peterson, R.G., Richardson, P.L., Schmid, C., and Zenk, W. 1999b. The intermediate depth circulation of the western south Atlantic. *Geophys. Res. Let.*, **26**, 3329–3332.

Boening, C.W., and Cox, M.D. 1988. Particle dispersion and mixing of conservative properties in an eddy-resolving model. *J.Phys.Oceanogr.*, **18**, 320–338.

Bourles, B., Gouriou, Y., Chuchla, R., and Johns, W.E. 1999. On the circulation in the upper layer of the western equatorial Atlantic. *J.Geophys.Res.*, **104**, 21151–21170.

Bryan, F.O., Wainer, I., and Holland, W.R. 1995. Sensitivity of the tropical Atlantic circulation to specification of wind stress climatology. *J.Geophys.Res.*, **100**, 24729–24744.

Busalacchi, A. J., and O'Brien, J.J. 1980. The seasonal variability in a model of the tropical Pacific. *J.Phys.Oceanogr.*, **10**, 1929–1951.

Busalacchi, A. J., and Picault, J. 1983. The seasonal variability from a model of the tropical Atlantic. *J.Phys.Oceanogr.*, **13**, 1564–1588.

Cane, M.A., Dolan, S.C., and Zebiak, S.E. 1986. Experimental forecasts of the 1982/83 El Nino. *Nature*, **321**, 827–832.

Carton, J.A., and Huang, B.H. 1994. Warm events in the tropical Atlantic. *J.Phys.Oceanogr.*, **24**, 888–903.

Chen, D.K., Cane, M.A., and Zebiak, S.E. 1999. The impact of NSCAT winds on predicting the 1997/1998 El Nino: A case study with the Lamont-Doherty Earth Observatory model. *J.Geophys.Res.*, **104**, 11321–11327.

Cochrane, J. D., Kelly, F.J., and Olling, C.R. 1979. Subthermocline countercurrents in the western equatorial Atlantic ocean. *J.Phys.Oceanogr.*, **9**, 724–738.

Cox, M.D. 1989. An idealized model of the world ocean. Part I: The global-scale water masses. *J.Phys.Oceanogr.*, **19**, 1730–1752.

Davis, R.E. 1998. Preliminary results from directly measuring middepth circulation in the tropical and south Pacific. *J.Geophys.Res*, **103**, 24619–24639.

Delecluse, P., Servain, J., Levy, C., Arpe, K., and Bengtsson, L. 1994. On the connection between the 1984 Atlantic event and the 1982-1983 ENSO. *Tellus*, **46**, 448–464.

Didden, N., and Schott, F. 1993. Eddies in the North Brazil Current retroflection region as observed by GEOSAT altimetry. *J.Geophys.Res.*, **98**, 20121–20131.

Edwards, C.A., and Pedlosky, J. 1998. Dynamics of nonlinear cross-equatorial flow. Part I: potential vorticity transformation. *J.Phys.Oceanogr.*, **28**, 2382–2406.

Fine, R.A. 1987. The penetration of tritium into the tropical Pacific. *J.Phys.Oceanogr.*, **17**, 553–564.

Fine, R.A., Reid, J.L., and Ostlund, H.G. 1981. Circulation of tritium in the Pacific. *J.Phys.Oceanogr.*, **11**, 3–14.

Fratantoni, D. 1996. *On the pathways and mechanisms of upper ocean mass transport across the atlantic equator.* Ph.D thesis at the University of Miami.

Fratantoni, D.M., and Glickson, D.A. 2001. North Brazil Current ring generation and evolution observed with SeaW iFS. *submitted to J.Phys.Oceanogr.*

Fratantoni, D.M., Johns, W.E., and Townsend, T.L. 1995. Rings of the North Brazil Current. *J.Geophys.Res.*, **100**, 10633–10654.

Fratantoni, D.M., Richardson, P.L., Johns, W.E., a nd R.H.Smith, C.I. Fleurant, Garzoli, S.L., Wilson, W.D., and Goni, G.J. 1999. The North Brazil Current Rings Experiment. *EOS*, **80**.

Fratantoni, D.M., Johns, W.E., Townsend, T.L., and Hurlburt, H.E. 2000. Low-latitude circulation and mass transport in a model of the tropical Atlantic ocean. *J.Phys.Oceanogr.*, **30**, 1944–1966.

Ganachaud, A., and Wunsch, C. 2001. Improved estimates of global ocean circulation, heat transport and mixing from hydrographic data. *Nature*, **410**, 240–240.

Garzoli, S.L., and Katz, E.J. 1983. The forced annual reversal of the Atlantic North Equatorial Countercurrent. *J.Phys.Oceanogr.*, **13**, 2082–2090.

Goni, G.J., and Johns, W.E. 2000. A census of North Brazil Current rings observed from TOPEX/POSEIDON Altimetry: 1992-1998. *accepted in Geophys.Res.Let.*

Gordon, A.L. 1986. Interocean exchange of thermocline water. *J.Geophy.Res.*, **91**, 5037–5046.

Greatbach, R.J., and Lu, J. 2000. The relationship between the meridional overturning and the zonally averaged north-south pressure gradient in an abyssal circulation model. *submitted to J.Phys.Oceanogr.*

Harper, S. 2000. Thermocline ventilation and pathways of tropical-subtropical water mass exchange. *Tellus*, **52**.

Hellerman, S., and Rosenstein, M. 1983. Normal monthly wind stress over the world ocean with error estimates. *J.Phys.Oceanogr.*, **13**, 1093–1104.

Huang, R.X., and Yang, J. 1996. Deep-Water upwelling in the frictional western boundary layer. *J.Phys.Oceanogr.*, **26**, 2243–2250.

Inui, T., Lazar, A., Malanotte-Rizzoli, P., and Busalacchi, A. 2001. Wind stress effects on the Atlantic tropical-subtropical circulation. *accepted in J.Phys.Oceanogr.*

Jochum, M., and Malanotte-Rizzoli, P. 2001. On the influence of the meridional overturn-

ing circulation on the tropical-subtropical pathways. *J.Phys.Oceanogr.*, **31**, 1313–1323.

Johns, W.E., Lee, T.N., Schott, F., Zantropp, R.J., and Evans, R.H. 1990. North Brazil Current retroflection: seasonal structure and eddy variability. *J.Geophys.Res.*, **95**, 22103–22120.

Johns, W.E., Lee, T.N., Beardsley, R.C., Candela, J., Limeburner, R., and Castro, B. 1998. Annual cycle and variability of the North Brazil Current. *J.Phys.Oceanogr.*, **28**, 103–128.

Johnson, G.C., and Moore, D.W. 1997. The pacific subsurface countercurrents and an inertial model. *J.Phys.Oceanogr.*, **27**, 2448–2459.

Johnson, G.C., McPhaden, M.J., and Firing, E. 2001. Equatorial Pacific ocean horizontal velocity, divergence and upwelling. *J.Phys.Oceanogr.*, **31**, 839–849.

Kawase, M. 1987. Establishment of deep ocean circulation driven by deep-water production. *J.Phys.Ocean.*, **17**, 2294–2317.

Killworth, P. 1991. Cross-equatorial geostrophic adjustment. *J.Phys.Oceanogr.*, **21**, 1581–1601.

Kroeger, J. 2001. Mechanismen meridionaler Transportprozesse im tropischen Atlantik. *Dissertation at the IfM Kiel.*

LeBlond, P.H., and Mysak, L.A. 1978. *Waves in the ocean.* Elsevier.

Leetmaa, A., Jr., J.P. McCreary, and Moore, D.W. 1981. Equatorial currents: Observations and theory. In: Evolution of Physical Oceanography. *MIT press.*

Leeuwenburgh, O., and Stammer, D. 2001. The effect of ocean currents on sea surface temperature anomalies. *J.Phys.Oceanogr.*, **31**, 2340–2358.

Legeckis, R. 1977. Long waves in the eastern equatorial Pacific ocean: A view from a geostationary satellite. *Science*, **197**, 1179–1181.

Li, X., Chang, P., and Pacanowski, R.C. 1996. A wave-induced stirring mechanism in the mid-depth equatorial ocean. *J.Mar.Res.*, **54**, 487–520.

Liu, Z. 1994. A simple model of the mass exchange between the subtropical and the tropical ocean. *J.Phys.Oceanogr.*, **24**, 1153–1165.

Liu, Z., and Philander, S.G.H. 1995. How different wind stress patterns affect the tropical-subtropical circulations of the upper ocean. *J.Phys.Oceanogr.*, **25**, 449–462.

Liu, Z., Philander, S.G.H., and Pacanowski, R.C. 1994. A GCM study of tropical-subtropical upper-ocean exchange. *J.Phys.Oceanogr.*, **24**, 2606–2623.

Luyten, J.R., Pedlosky, J., and Stommel, H. 1983. The ventilated thermocline. *J.Phys.Oceanogr.*, **13**, 292–309.

Ma, H. 1996. The dynamics of the North Brazil Current retroflection eddies. *J.Mar.Res.*, **54**, 35–53.

Malanotte-Rizzoli, P., Young, R.E., Hedstrom, K., Arango, H., and Haidvogel, D.B. 2000. Water mass pathways between the subtropical and tropical ocean in a climatological simulation of the North Atlantic ocean circulation. *Dynam. Atmos. Oceans*, **32**, 331–371.

Marin, F., Hua, B.L., and Wacogne, S. 2000. The equatorial thermostad and subsurface countercurrents in the light of atmospheric Hadley cell dynamics. *J.Mar.Res.*, **58**.

Masima, S., and Philander, S.G.H. 1999. An analysis of tropical instability waves in a numerical model of the Pacific Ocean - 1.Spatial variability of the waves. *J.Geophys.Res*,

**104**, 29613–29635.

Masima, S., Philander, S.G.H., and Bush, A.B.G. 1999. An analysis of tropical instability waves in a numerical model of the Pacific Ocean - 2. Generation and energetics of the waves. *J.Geophys.Res*, **104**, 29613–29635.

McClean, J.L., and Klinck, J.M. 1995. Description and vorticity analysis of 50-day oscillations in the western tropical region of the CME Model. *J.Phys.Oceanogr.*, **25**, 2498–2517.

McCreary, J.P., and Lu, P. 1994. Interaction between the subtropical and equatorial ocean circulations: the subtropical cell. *J.Phys.Oceanogr.*, **24**, 466–497.

McCreary, J.P.Jr. 1981. A linear stratified ocean model of the equatorial undercurrent. *Phil.Tran. Royal Soc. London*, **298**, 603–645.

McCreary, J.P.Jr, Lu, P., and Yu, Z. 2001. Dynamics of the Pacific subsurface countercurrents. *submitted to J.Phys.Oceanogr.*

McPhaden, M.J. 1984. On the dynamics of equatorial subsurface countercurrents. *J.Phys.Oceanogr.*, **13**, 1216–1225.

Mueller-Krager, F.E., McClain, C.R., and Richardson, P.L. 1988. The dispersal of the Amazon's water. *Nature*, **333**, 57–59.

Munk, W.H. 1966. Abyssal Recipes. *Deep-Sea Res.*, **13**, 707–730.

Oliger, O., and Sundstrom, A. 1978. Theoretical and practical aspects of some initial boundary value problems in fluid dynamics. *J. Appl. Math.*, **35**, 419–446.

Pedlosky, J. 1979. *Geophysical Fluid Dynamics.* Springer.

Pedlosky, J. 1987. An inertial theory for the equatorial undercurrent. *J.Phys.Oceanogr.*, **17**, 1978–1985.

Pedlosky, J. 1996. *Ocean Circulation Theory.* Springer.

Philander, S.G. 1990. *El Nino, La Nina and the Southern Oscillation.* Academic Press.

Pond, S., and Pickard, G.L. 1983. *Introductory Dynamical Oceanography.* Pergamon Press.

Richardson, P.L., and Schmitz, W.J. 1993. Deep cross-equatorial flow in the Atlantic measured with SOFAR floats. *J.Geophys.Res*, **98**, 8371–8387.

Roemmich, D. 1983. The balance of geostrophic and Ekman transports in the tropcial Atlantic ocean. *J.Phys.Oceanogr.*, **13**, 1534–1539.

Rowe, P.B., Firing, E., and Johnson, G.C. 2000. Pacific equatorial subsurface countercurrent velocity, transport and vorticity. *J.Phys.Oceanogr.*, **30**, 1172–1187.

Schmitz, W.J., and McCartney, M.S. 1993. On the North Atlantic circulation. *Rev. Geophys.*, **31**.

Schmitz, W.J., and Richardson, P.L. 1991. On the sources of the Florida Current. *Deep Sea Research*, **38**, S379–S408.

Schott, F.A., Fischer, J., Reppin, J., and Send, U. 1993. On mean and seasonal currents and transports at the western boundary of the equatorial Atlantic. *J.Geophys.Res.*, **98**, 14353–14368.

Schott, F.A., Stramma, L., and Fischer, J. 1998. Transports and pathways of the upper-layer circulation in the western tropical Atlantic. *J.Phys.Oceanogr.*, **28**, 1904–1928.

Seager, R., Kushnir, Y., Chang, P., Naik, N., Miller, J., and Hazeleger, W. 2001. Looking for the role of the ocean in the tropical Atlantic decadal climate variability. *J.Climate*, **14**, 638–655.

Servain, J. 1991. Simple climatic indexes for the tropical Atlantic ocean and some applications. *J.Geophys.Res.*, **96**, 15137–15146.

Silveira, I. C. A. da, Brown, W., and Flierl, G. 2000. Dynamics of the North Brazil Current Retroflection region from the WESTRAX Observations. *submitted to J.Geophys.Res.*

Spall, M.A. 1992. Rossby wave radiation in the Cape Verde Fronal Zone. *J.Phys.Oceanogr.*, **22**, 796–807.

Spall, M.A., and Robinson, A.R. 1989. A new open ocean, hybrid coordinate primitive equation model. *Mathematics and Computers in Simulation*, **31**, 241–269.

Stevens, D.P. 1990. On open boundary conditions for three dimensional primitive equation oceancirculation models. *Geophys. Astrophys. Fluid Dynamics*, **51**, 103–133.

Stommel, H.M. 1961. Thermohaline convection with two stable regimes of flow. *Tellus*, **13**, 224–230.

Suga, T., and Talley, L.D. 1995. Antarctic Intermediate Water circulation in the tropical and subtropical Atlantic. *J.Geophys.Res*, **100**, 13441–13453.

Sverdrup, H.U. 1947. Winddriven currents in a baroclinic ocean with application to the equatorial currents in the eastern Pacific. *Proc.Natl.Acad.Sci.,USA*, **33**, 318–326.

Toggweiler, J.R., and Samuels, B. 1995. Effect of the Drake Passage on the global thermohaline circulation. *Deep-Sea Res.*, **42**, 477–500.

Tsuchiya, M. 1975. Subsurface countercurrents in the eastern equatorial Pacific Ocean. *J.Mar.Res.(Suppl.)*, **33**, 145–175.

Tsuchiya, M., Lukas, R., Fine, R.A., Firing, E., and Lindstrom, E. 1989. Source waters of the Pacific Equatorial Undercurrent. *Progress in Oceanography*, **23**, 101–147.

Veronis, G. 1975. *The role of models in tracer studies. In: Numerical models of ocean circulation.* National Academy of Sciences, Washington D.C.

Wacogne, S. 1990. Dynamical regimes of a fully nonlinear stratified model of the Atlantic equatorial undercurrent. *J.Geophy.Res.*, **94**, 4801–4815.

Warren, B.A. 1981. *Deep circulation in the world ocean. In: Evolution of Physical Oceanography.*

Weaver, J.A., and Sarachik, E.S. 1990. On the importance of vertical resolution in certain ocean general circulation models. *J.Phys.Oceanogr.*, **20**, 600–609.

Weisberg, R.H., A.Horigan, and Colin, C. 1979. Equatorially trapped Rossby-gravity wave propagation in the Gulf of Guinea. *J.Mar.Res.*, **37**, 67–86.

Wilson, W.D., Johns, E., and Molinari, R.L. 1994. Upper layer circulation in the western tropical North Atlantic ocean during August 1989. *J.Geophys.Res.*, **99**, 22513–22523.

Xie, S.P., and Tanimoto, Y. 1998. A pan-Atlantic decadal oscillation. *Geophys.Res.Lett.*, **25**, 2185–2188.

Yoshida, K. 1959. A theory of the Cromwell current and equatorial upwelling. *J.Oceanogr.Soc.Jpn.*, **15**, 154–170.